

TWO-DIMENSIONAL ELECTRICAL RESISTIVITY IMAGING OF KAOLIN DEPOSIT
AT DAJIN GWAMNA, KANKARA LOCAL GOVERNMENT, KATSINA STATE,
NIGERIA

By

Hussaini ABUBAKAR, B.Sc. PHYSICS (UMYU 2011),
P13SCP8005

A THESIS SUBMITTED TO THE SCHOOL OF POSTGRADUATE STUDIES,
AHMADU BELLO UNIVERSITY, ZARIA

IN PARTIAL FULFILLMENT OF THE REQUIREMENTS FOR THE AWARD
OF A
MASTER OF SCIENCE DEGREE IN APPLIED GEOPHYSICS.

DEPARTMENT OF PHYSICS,
FACULTY OF PHYSICAL SCIENCES
AHMADU BELLO UNIVERSITY, ZARIA
NIGERIA

MAY, 2018

DECLARATION

I declare that the work in this dissertation entitled “TWO-DIMENSIONAL ELECTRICAL RESISTIVITY IMAGING OF KAOLIN DEPOSIT AT DAJIN GWAMNA, KANKARA LOCAL GOVERNMENT, KATSINA STATE, NIGERIA” has been carried out by me in the Department of Physics under the supervision of Dr. P. O. Sule and Dr. A. L. Ahmed.

The information derived from other literatures has been duly acknowledged in the text and a list of references provided. No part of this dissertation was previously presented for another degree or diploma at this or any other institution.

Hussaini ABUBAKAR

Name of student

Date

Signature

DEDICATION

I dedicate this research work to my father Alhaji Abubakar Garba and to my late mother.

CERTIFICATION

This thesis entitled “TWO-DIMENSIONAL ELECTRICAL RESISTIVITY IMAGING OF KAOLIN DEPOSIT AT DAJIN GWAMNA, KANKARA LOCAL GOVERNMENT, KATSINA STATE, NIGERIA” by Hussaini, ABUBAKAR has met the regulations governing the award of the degree of Master of Science in Applied Geophysics of Ahmadu Bello University, and is approved for its contributions to knowledge and literary presentation.

Dr. P. O. Sule
Chairman, Supervisory Committee

Signature

Date

Dr. A. L. Ahmed
Member, Supervisory Committee

Signature

Date

Prof. N. Rabi
Head of Department

Signature

Date

Prof. S. Z. Abubakar
Dean, School of Postgraduate studies

Signature

Date

ACKNOWLEDGEMENT

In the name of Allah, the most Beneficent, the most Merciful, may his peace and blessing be upon his Messenger Muhammad (S. A. W.), his household, companions and all those who follow the straight path to the day of judgment, for granting me this opportunity to carry out this dissertation successfully for the completion of my M. Sc. Applied Geophysics programme.

I would like to use this opportunity to express my profound appreciation for the purposeful enlightenment, correctness and guidance provided by my supervisors Dr. P. O. Sule and Dr. A. L. Ahmed. I wish to also express my appreciation and gratitude to Prof. K. M. Lawal for his useful advice that led to the success of this work. I must express my appreciation to my wonderful Lecturers, Mr. J. O. Osumeje, Dr. R. Jimoh and Malam Sani for their academic and moral support.

I would like to express my profound appreciation to my parent for their help financially and moral support, my appreciation goes to all my uncles, aunties and to my entire relatives for their support and prayers, I appreciate all your assistance in whatever way, may Allah have mercy, blessing and reward you abundantly.

I wish to bestow my special indebtedness to my brothers and sisters; Nafi'u, Usman, Hassan, Abdullahi, Abba, Aliyu, Aminu, Ahmad, Fuzaimatu, Rashida, Maimunatu, Sa'adatu, Fadimatu, Sa'adiyya, Zainab and Aisha. For your care love and prayers, may Allah have mercy, blessing and reward you abundantly. I also wish to state my deep appreciation to my friends; Abdurrahman I., Kamal, Salisu, Anas, Abdurrahman A., Jamilu, Tukur and so many others too numerous to mention for their support and prayers to the success of this programme.

Finally, I appreciate the contributions made by my course mates; Ahmad M. Idris, Alhassan Idris, Daniel Eshemiake, Sani Garba, Zainab Musa and Hajarah I. Isah, those whom we undergo M. Sc. Applied Geophysics programme. May Allah grant all of us a fruitful best of luck.

ABSTRACT

Two-dimensional Electrical Resistivity Imaging (ERI) technique was applied to delineate Kaolin deposit at Dajin Gwamna, Kankara Local Government, Katsina State, Nigeria. Wenner-Schlumberger configuration was utilized for this ERI field survey along seven profiles. The data obtained using ABEM Terrameter SAS4000 with electrode selector ES 464 were processed using the RES2DINV software. Seven Vertical Electrical Sounding points were distributed within the study area. The data were obtained using Ohmega Ω Resistivity meter and were processed using IPI2Win software. The results of the seven 2-D Electrical Resistivity Imaging profiles in correlation with the Vertical Electrical Sounding results and borehole log data have revealed three distinct layers; these layers range from top layer with resistivity values between $5\Omega\text{m}$ to $490\Omega\text{m}$, it is made up of mainly dark brown sandy clay, clay, Kaolin and mottled Kaolin; the thickness varies from the surface to 35m depth in profile 1, 34m in profiles 2 and 4, 26m in profile 3, 20m in profiles 5 and 6, and also 30m in profile 7. The result indicates that Kaolin deposit within the study area has range of resistivity values between $11\Omega\text{m}$ to $97\Omega\text{m}$. The study also revealed that, the delineated layers of Kaolin were extending from east to west and in the north direction, whereby layers of Kaolin were absent in profile 1 which is located in the southern part of the survey area. It was observed that the exploration of Kaolin mineral should be targeted trending east, west and also in the northern part of the site. The weathered basement rock emerges from the depth of 27.00m to 39.40m in profile 1, 14.00m to 39.4m in profile 2, 26.00m depth to 39.4m in profile 3, and from the depth of 34.00m to 39.40m in profiles 4, 5, 6 and 7; consisting of biotite-mica, feldspar and quartz which has resistivity values between $56\Omega\text{m}$ to $608\Omega\text{m}$, with fresh basement rock from a depth of 33.80m downwards in profile 1, 35.00m downwards in profiles 4 and 5, and from the depth of 36.5 downwards in profiles 6 and 7, whereby in profile 2 and 3 fresh basement is absent. The fresh basement has resistivity values ranging between $200\Omega\text{m}$ to above $6000\Omega\text{m}$.

TABLE OF CONTENTS

	Page
Title page -----	i
Declaration -----	-ii
Dedication -----	-iii
Certification -----	-iv
Acknowledgment -----	v
Abstract -----	vi
Table of Contents -----	vii
List of Figures -----	xi
List of Tables -----	xiii
List of Plates -----	xiv
CHAPTER ONE: INTRODUCTION -----	1
1.1 General Overview -----	1
1.2 Statement of the Problem -----	5
1.3 Justification of the Research -----	5
1.4 Aim and Objectives of the Study -----	-6
1.5 Location of the Study Area -----	6
1.6 Climate and Vegetation -----	8
1.7 General Geology of the Area -----	9
CHAPTER TWO: LITERATURE REVIEW AND THEORITICAL BACKGROUND -----	10
2.1 General Overview of Geophysical and Geological Investigations of Kaolin -----	-10
2.2 Kankara Kaolin Deposits -----	14
2.3 Origin of Clay -----	-14
2.4 The Clay Mineral Kaolin and its Formation-----	15

2.5	Uses of Kaolin Clay - - - - -	17
2.6	Electrical Resistivity Methods - - - - -	18
2.6.1	Theory of the Resistivity methods - - - - -	20
2.7	Vertical Electrical Sounding (VES) - - - - -	26
2.8	Constant Separation Traversing (CST) - - - - -	27
2.9	Electrode Arrays- - - - -	27
2.9.1	Wenner Array - - - - -	28
2.9.2	Dipole-Dipole Array - - - - -	29
2.9.3	Wenner-Schlumberger Array- - - - -	31
2.9.4	Pole-Pole Array -- - - - -	31
2.9.5	Pole-Dipole Array- - - - -	32
2.10	Factors affecting Electrical Resistivity- - - - -	33
2.10.1	Water Salinity- - - - -	34
2.10.2	Porosity of Rock- - - - -	34
2.10.3	Effect of Temperature- - - - -	35
2.10.4	Effects of Geological Processes- - - - -	35
2.11	The Concept of Apparent Resistivity- - - - -	36
2.12	Typical Resistivity Values of Earth Materials - - - - -	37
	CHAPTER THREE: METHODOLOGY AND INSTRUMENTATION - - - - -	42
3.1	Electrical Resistivity Imaging - - - - -	42
3.1.1	Choice of the Array - - - - -	44
3.2	Vertical Electrical Sounding Technique- - - - -	44
3.3	Reconnaissance Survey- - - - -	45
3.4	Instrumentation- - - - -	45

3.4.1	List of instruments used for Resistivity Imaging survey- - - - -	46
3.4.2	List of instruments used for Vertical Electrical Sounding survey - - - - -	46
3.4.3	The ABEM Lund Imaging System- - - - -	47
3.4.4	OHMEGA Ω Resistivity meter - - - - -	49
3.5	Field Measurement Procedure - - - - -	50
3.6	Field Problems- - - - -	53
CHAPTER FOUR: FIELD RESULTS AND INTERPRETATION - - - - -		54
4.1	Introduction - - - - -	54
4.2	Data Processing Procedure- - - - -	54
4.3	Interpretation Technique - - - - -	58
4.4	Geological Control - - - - -	59
4.5	Geologic Section from Borehole Data - - - - -	59
4.6	Typical Resistivity Values from Previous Works- - - - -	61
4.7	Field Results - - - - -	62
4.7.1	Result of Profile One - - - - -	64
4.7.2	Result of Profile Two - - - - -	66
4.7.3	Result of Profile Three - - - - -	68
4.7.4	Result of Profile Four - - - - -	70
4.7.5	Result of Profile Five - - - - -	73
4.7.6	Result of Profile Six - - - - -	76
4.7.7	Result of Profile Seven - - - - -	79
4.7.8	Merging of the profiles for the detection of continuity of the subsurface structures- 81	
4.7.8.1	Continuity of structures - - - - -	81
4.8.	Vertical Electrical Sounding Results and Discussions- - - - -	86

4.8.1	Result of VES I - - - - -	-86
4.8.2	Result of VES II- - - - -	-87
4.8.3	Result of VES III - - - - -	-88
4.8.4	Result of VES IV - - - - -	-89
4.8.5	Result of VES V- - - - -	-90
4.8.6	Result of VES VI - - - - -	-91
4.8.7	Result of VES VII- - - - -	-92
4.9	Geoelectric section along profile AA'- - - - -	-94
4.10	Geoelectric section along profile BB' - - - - -	-95
CHAPTER FIVE: CONCLUSION AND RECOMMENDATIONS - - - - -		96
5.1	Conclusion - - - - -	96
5.2	Recommendations - - - - -	97
REFERENCES- - - - -		-98

LIST OF FIGURES

Figure 1.1: Accessibility map of the study area -----	7
Figure 1.2: Google earth map of study area -----	7
Figure 1.3: Geological map of Kankara area and its environs -----	9
Figure 2.1: Major Kaolin deposits of Kanakara area, Kankara I (Tsaunin Boda), Kankara II (Dajin Gwamna, The study area), Kankara III (Anguwan Liman), Kankara IV and Kankara V -----	11
Figure 2.2: Current (C_1 , C_2) and Potential (P_1 , P_2) Distributions within Homogeneous Isotropic ground. -----	19
Figure 2.3: Schematic diagram showing the basic principle of D.C. Resistivity measurements- -----	20
Figure 2.4: A Conventional four Electrode Array usually used to measure Subsurface Resistivity -----	24
Figure 2.5: Common Arrays used in Resistivity Surveys and their Geometric factors-----	30
Figure 2.6: Resistivities of Rocks, Soils and Minerals -----	39
Figure 3.1: A map illustrating the 2-D profiles 1-7 layout and VES points VES I – VII (Profiles AA' and BB') -----	53
Figure 4.1: Two possible arrangements of the blocks used in a 2-D model together with the data points in the pseudosection -----	57
Figure 4.2: An example of a profile showing data set with a few bad data points -----	58
Figure 4.3 Geological Well-Log of Garagi (Kankara Local Government Area) obtained from RUWASSA, Katsina (2014) -----	60
Figure 4.4 Geological Well-Log of Unguwar Nagamda (Kankara Local Government Area) obtained from RUWASSA, Katsina (2014) -----	61

Figure 4.5: Types of colors used in the interpretation of 2-D results - - - - -	63
Figure 4.6: Result of 2-D inversion of the Wenner-Schlumberger array data along profile 1-	65
Figure 4.7: Result of 2-D inversion of the Wenner-Schlumberger array data along profile 2 -	67
Figure 4.8: Result of 2-D inversion of the Wenner-Schlumberger array data along profile 3 -	69
Figure 4.9: Result of 2-D inversion of the Wenner-Schlumberger array data along profile 4 -	71
Figure 4.10: Result of 2-D inversion of the Wenner-Schlumberger array data along profile5-	74
Figure 4.11: Result of 2-D inversion of the Wenner-Schlumberger array data along profile6-	77
Figure 4.12: Result of 2-D inversion of the Wenner-Schlumberger array data along profile7-	80
Figure 4.13: Inverse resistivity model of profile 2- - - - -	82
Figure 4.14: Inverse resistivity model of profile 3- - - - -	83
Figure 4.15: Inverse resistivity model of profile 4- - - - -	83
Figure 4.16: Inverse resistivity model of profile 5- - - - -	84
Figure 4.17: Inverse resistivity model of profile 6- - - - -	84
Figure 4.18: Inverse resistivity model of profile 1- - - - -	85
Figure 4.19: Inverse resistivity model of profile 7- - - - -	85
Figure 4.20: Computer iterated curve of VES I- - - - -	87
Figure 4.21: Computer iterated curve of VES II- - - - -	88
Figure 4.22: Computer iterated curve of VES III- - - - -	89
Figure 4.23: Computer iterated curve of VES IV- - - - -	90
Figure 4.24: Computer iterated curve of VES V- - - - -	91
Figure 4.25: Computer iterated curve of VES VI- - - - -	92
Figure 4.26: Computer iterated curve of VES VII- - - - -	93
Figure 4.27: Geoelectric section of Profile AA' beneath VES II, III, (VES IV) ' and V - - - -	94
Figure 4.28: Geoelectric section of Profile BB' beneath VES I, (VES IV) ' and VII - - - - -	95

LIST OF TABLES

Table 2.1: Typical Resistivity values of Rocks, Soils and Minerals,* -10°C to -60°C respectively; strongly temperature –dependent. Based on Telford et al. (1990) with additional data from McGinnis and Jensen (1971), Reynolds (1987). Reynolds and Paren (1980, 1984) and many commercial projects. - - - - -	40
Table 3.1: Coordinates of points along the profiles- - - - -	52
Table 4.1 Typical Resistivity values compiled from previous work (Michael, 1977) - - - - -	62
Table 4.2: VES I result and interpretation- - - - -	86
Table 4.3: VES II result and interpretation - - - - -	87
Table 4.4: VES III result and interpretation - - - - -	88
Table 4.5: VES IV result and interpretation - - - - -	90
Table 4.6: VES V result and interpretation - - - - -	91
Table 4.7: VES VI result and interpretation - - - - -	92
Table 4.8: VES VII result and interpretation - - - - -	93

LIST OF PLATES

- Plate I: Layers of Kaolin clay reached by local miners while digging in vertical (A) and in horizontal directions (B)-----5
- Plate II: ABEM LUND Imaging system together with Terrameter SAS 4000 and ES 464-- -49
- Plate III: OHMEGA Ohm Resistivity meter system with its accessories - - - - - 50

CHAPTER ONE:

INTRODUCTION

1.1 General Overview

Minerals are the foundation for economic and industrial development of any nation. Machinery for manufacturing and other applications, production of chemicals for various industrial and domestic uses, energy generation, drugs for medical applications, research into new possibilities; in fact all aspect of human living is affected by minerals (Vogley, 1985 and Runge, 1996). Clay minerals have been mined since the Stone Age and have been indispensable in architecture, in industry and agriculture. Today they are among the most important minerals used by manufacturing and environmental studies. Clay has a wide spread occurrence in the world. In Nigeria, clay is widely distributed and is found in sufficient quantity or suitable quality for modern industrial purposes. Clay as one of the major Nigerian deposits covers an estimated proven reserve of billions of tons. More than 80 clay deposits have been reported from all parts of the country (Akhirevbulu and Ogunbajo, 2011).

Deposits of clay in mineable quantities occur in almost all the States of the Federation. Major deposits occur in Kankara in Katsina State, Naraguta (Jos) in Plateau State, Alkaleri in Bauchi State, Shabu and Lafia areas of Nasarawa State and at Ahoko near Lokoja in Kogi State (Obaje, 2009). Clay is one of the earliest mineral substances utilized by man. It played an extremely important part in ancient civilizations, records of which were preserved in brick buildings, in monuments and in pottery, and as inscriptions upon claytablets. Clay is still an indispensable raw material today. The present uses of clay and clay products are too numerous to list completely. In domestic life, clay is used extensively in pottery, earthenware, china ware, cooking ware, vases, plumbing fixtures, tiles, porcelain wares and ornaments. In

building, it is used for building bricks, vitrified and enameled bricks, tiles for floors, roofs, walls and drains, sewer pipes and as an ingredient of cement. In the electrical industry, it is used for conduits, sockets, insulators and switches. It is used on a large scale in making refractory ware, such as fire bricks, furnace linings, chemical stone ware, crucibles, retorts and saggars. From the practical point of view, the most important physical properties of clay are plasticity, shrinkage, fusibility and colour (Obaje, 2009).

Electrical resistivity (ρ) is an inherent property of all earth materials. Resistivity is the reciprocal of electrical conductivity and thus is a measurement of a material resistance to the flow of an electrical current. In most porous rock systems, ionic conduction by interstitial fluids and surface conduction at the interface between the solid rock matrix and the electrolyte solution are responsible for the major part of electrical current flowing through a formation (Pfannkuch, 1969). Clay minerals, however are capable of conducting current both electronically and through the electric double layer at the mineral-electrolyte interface, due to high cation exchange properties. Clay minerals typically have lower resistivities than other silicate minerals or carbonate minerals.

Resistivity surveys determine the variation in the electrical resistivity of the subsurface by applying electric current across arrays of surface electrodes (Loke, 1999). Electrical resistivity is a function of porosity, fluid saturation, resistivity of the pore fluid and the solid, and the material texture among others. The survey data are processed to produce graphic depth sections of the thickness and resistivity of the subsurface electrical layers. All resistivity methods employ an artificial source of current, which is introduced into the ground through point electrodes or long line contacts; the latter arrangement is rarely used nowadays. The procedure is to measure potentials at other electrodes in the vicinity of the current flow.

Because the current is measured as well, it is possible to determine an effective or apparent resistivity of the subsurface (Telford *et al.*, 1990).

Geophysical techniques have been found very useful in many areas such as mineral exploration, groundwater investigation and some environmental studies. It involves studying the physical properties of the earth to provide vital information on subsurface material conditions for numerous practical applications. These are done by taking measurements at or near the earth's surface that are influenced by the internal distribution of physical properties. Consequently, analysis of these measurements can reveal how the physical properties of the earth's interior vary vertically and laterally that reflect the subsurface geology. Another method of investigating subsurface geology is of course by drilling and pitting which provide information only at discrete locations and are expensive.

2-D electrical resistivity imaging/tomography survey are usually carried out using a large number of electrodes, 25 or more, connected to a multi-core cable. Resistivity imaging is particularly useful in clayey ground where methods such as the ground penetrating radar GPR are less effective and helps define translational boundaries that are difficult to detect using other geophysical methods.

At the present time, two-dimensional electrical resistivity imaging surveys are widely implemented for mapping areas with complex geological structures where the traditional 1-D resistivity sounding surveys (which subdivide the subsurface into horizontal layers) are not sufficiently accurate. It has become a standard geophysical technique (Dahlin, 1996). Two-dimensional electrical resistivity imaging models are more accurate than 1-D resistivity

sounding models as they allow the determination of horizontal as well as vertical resistivity variations (Loke, 2004).

Typical 1-D resistivity sounding surveys usually involve approximately 10 to 20 readings, while the 2-D imaging surveys contain 100 to 1000 measurements. The 2-D electrical resistivity imaging method has many applications such as mapping freshwater aquifers, mapping of groundwater contamination, investigating landslides and mapping unconsolidated sediments (Acworth, 1987; Christensen and Sorensen, 1994; Barker, 1996; Johansson and Dahlin, 1996; Dahlin and Owen, 1998; Ritz et al., 1999).

Electrical resistivity survey is a non-destructive and cost effective method and has the advantage of rapid data collection and interpretation. Two or three people could conveniently achieve 5 – 7 long electrical profiling lines each day, at a normal production rate. Thus, the use of multi-electrode systems for the data acquisition allows a dramatic increase in field productivity. The method adopted for this research dissertation was the 2-D Electrical Resistivity Tomography using the ABEM LUND Imaging System SAS4000 with electrode selector ES 464. The ABEM LUND Imaging System is a multi-electrode system for cost effective and high resolution 2-D and 3-D resistivity surveys. The included data acquisition software supports 2-D and 3-D surveys with surface arrays which may also be used for borehole measurements. The data can be inverted automatically to provide an image of true resistivity. It is the automatic nature of this process of interpretation which enables it to be termed “imaging”.

1.2 Statement of the Problem

There was a report from the study area that in the course of digging hand-dug wells by local miners more than 40 years ago, Kaolin were detected at variable depths from the earth's surface. Hence, there is need to determine the depth and lateral extent to which the Kaolin strata are intercepted.



Plate I: Layers of Kaolin clay reached by local miners while digging in vertical (A) and in horizontal directions (B).

1.3 Justification of the Research

Kaolin clay has important uses worldwide. The most significant uses are in building where it is used for building bricks, vitrified and enameled bricks, tiles for floors, roofs, walls and drains, sewer pipes and as an ingredient of cement. In the electrical industry, it is used for conduits, sockets, insulators and switches. It is used on a large scale in making refractory ware, such as fire bricks, furnace linings, chemical stone ware, crucibles, retorts and saggars. As a result of the aforementioned uses, the report of the occurrence of Kaolin deposit within the study area necessitates a geophysical investigation to ascertain the probable lateral extent

of the Kaolin deposit in the area of study which will serve as a guide for an in-depth survey to ascertain the Kaolin reserve of the area.

1.4 Aim and Objectives of the Study

Since Electrical Resistivity Imaging provides a more detailed view of the subsurface structure, the aim of this research is to apply two-dimensional electrical resistivity imaging technique and vertical electrical sounding to delineate Kaolin deposit within the study area.

The objectives of this study are;

- i. to determine the subsurface geoelectric formations
- ii. to determine the resistivity value associated with the Kaolin
- iii. to delineate the Kaolin bearing layers and
- iv. to determine the probable vertical and lateral extent of the Kaolin deposit within the area of the survey;

1.5 Location of the Study Area

The study area Dajin Gwamna, is in Kankara Local Government area of Katsina State and is situated 5.6km from Kankara and 1.4km from Danmarke Village, which is about 2 hours 2 minutes drive from Zaria (about 123km, see Figure 1.1). The study area falls within latitude $11^{\circ} 53' 00''\text{N}$ to $11^{\circ} 54' 00''\text{N}$ and longitude $7^{\circ} 26' 00''\text{E}$ to $7^{\circ}27'00''\text{E}$, (see Figure 1.2). The figure is the Google earth map of the study area. The study area is however easily accessible through some federal roads, such as Zaria, Hunkuyi, Danja, Tsigu, Marabar Kankara roads and also through Zaria, Hunkuyi, Danja, Bakori marabar Kankara, Kankara roads.




 Study Area
 (Dajin Gwamna)

Figure 1.1: Accessibility map of the study area (Courtesy Google earth).

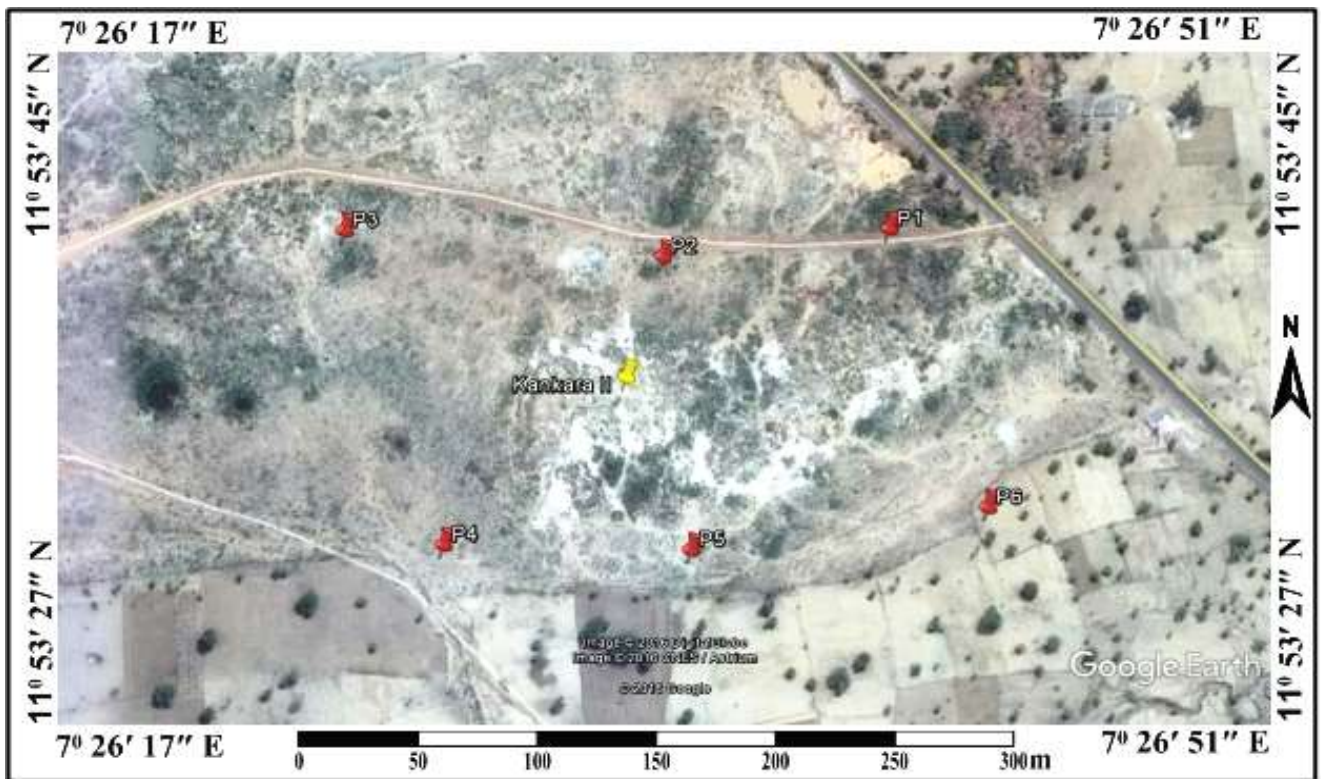


Figure 1.2: Google earth map of study area (Courtesy Google earth).

1.6 Climate and Vegetation

The study area is part of the tropical intercontinental north where the annual rainfall ranges between 50 cm to 100 cm. It enjoys some four months of rainfall and has some eight months of aridity. Also, the relative humidity is always low about 40 percent in January and rise to about 60 percent in July. There are two principal winds that govern the climate of the area namely, the Tropical Maritime air mass (Tm) and the Continental air mass (Tc), (Ayoade, 2004). While the former air mass brings rain to the entire study area during the wet season, the latter air mass brings aridity, since it originates from the desert area it is always cold, dry and dusty locally known as harmattan wind (Udo, 2001). Soils in this area are formed under condition of aridity and deposition of sand by the wind. The soils are fine sandy loam, relatively easy to cultivate with little leaching hence, it is generally good for cultivation of groundnuts, grains and cotton especially areas around Funtua.

Both vegetation and soils are somehow related since they are affected by the climate, geology and relief of the area. The soil determines to a large extent the type of plants that grow and in like manner, the soil helps to enrich the plant cover. The study area shares some characteristics of a sudan type of savanna vegetation. The trees are scattered with poor grassland. Some of the tree species include shear-butter tree, locust bean and date palms (Adefila, 2014).

Regarding people, the most predominant tribes are the Fulanis and Hausas. However, there are Yorubas, Igbos and other tribes occupying some pocket areas. The Fulanis are noted for their animal husbandry and do engage in seasonal migration with their cattle, goats, sheep and donkey. The Hausas also engage in animal rearing but mostly occupied with sedentary agriculture. The major crops grown by the farmers include maize, guinea-corn, millet, soya-beans and groundnuts at both commercial and subsistence levels (Udo, 2001). In addition,

horticulture is practiced mostly along the main streams and rivers where vegetables like okro, tomatoes, onion, sugar-cane, lettuce and spinach are cultivated.

1.7 General Geology of the Area

Generally, the survey area lies in the Northwestern part of Nigeria, underlain by rocks of the Basement Complex, consisting mainly of migmatites, granite gneiss, biotite gneiss, metasediments of generally amphibolite facies metamorphism and granitic rocks of the older granite suite (Ajibade, 1976). Augen gneiss and mica schist were present with mica schist dipping generally SE at angles varying from 27° to 43° . The geological formation in the vicinity strikes generally EW and outcrops of the host mica schist can be found along the river channels (Oyeka, 1976). The area considered in this research (Dajin Gwamna) is underlain by granite gneiss (Figure 1.3).

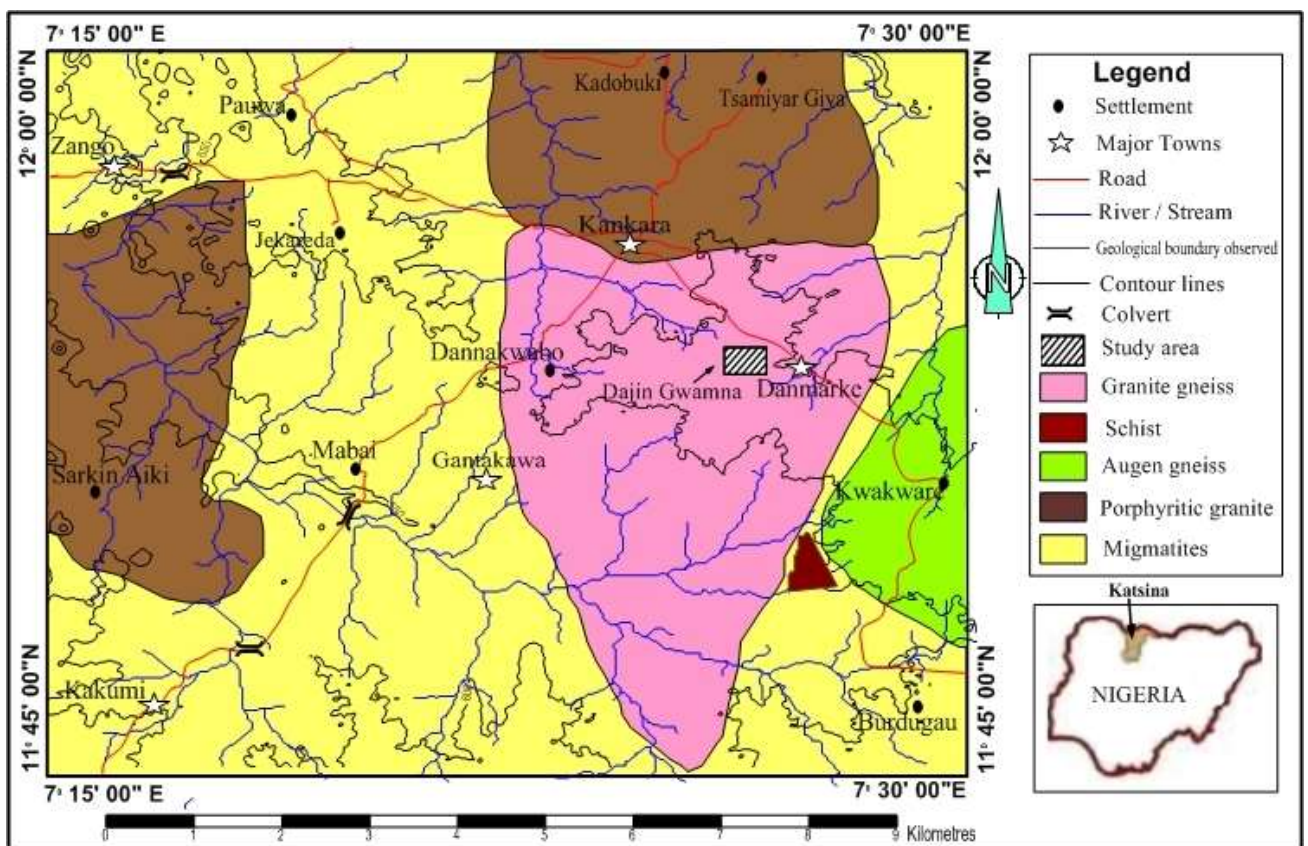


Figure 1.3: Geological map of Kankara area and its environs (Modified from Kankara and Farouk, 2015).

CHAPTER TWO:

LITERATURE REVIEW AND THEORITICAL BACKGROUND

2.1 General Overview of Geophysical and Geological Investigations of Kaolin

There is no record of any geophysical survey carried out to the best of my knowledge in the present study area Dajin Gwamna.

Michael (1977) carried out Geophysical exploration of Kaolin mineral near Kankara (Kankara 1, see Figure 2.1). His results showed that, resistivity sounding technique proved the most efficient field system in delineating the buried Kaolin mineral deposit. He proved that gravity method as a useful tool in mirroring the anomalous zones and in the assessment of the reserves of the concealed Kaolin deposit, which is of the order of $1.7 \pm 0.4 \times 10^6$ metric tonnes. He also showed that the top layer structure was best delineated by the seismic refraction method.

Aggarwai (1983) applied three different geophysical methods namely; resistivity, self potential (S.P.) and Very Low Frequency (V.L.F.) to delineate the extent of Kaolin deposit and explore possible places for groundwater aquifers in the vicinity of Minjibir, Kano State. The resistivity survey indicated three layer sub-strata with resistivities of 600 Ωm to 1,175 Ωm for the first layer, 100 Ωm to 235 Ωm for the middle layer and 2,400 Ωm and above for the third layer. It showed a thickness varying from 1.1 m to 1.7 m for the top layer and 11.4 ± 2.4 m to 21.7 ± 1.3 m for the second layer. The results were in agreement with those deduced from the V.L.F. detailed survey and the available borehole data of the survey area. Using resistivity profiling and S.P. methods, the extent of the Kaolin deposit was delineated and its total mass was estimated to be around 1.7 ± 0.2 million tonnes. He also suggested two prospective places to drill boreholes for water supply based on the results of the V.L.F., S.P., and resistivity surveys.

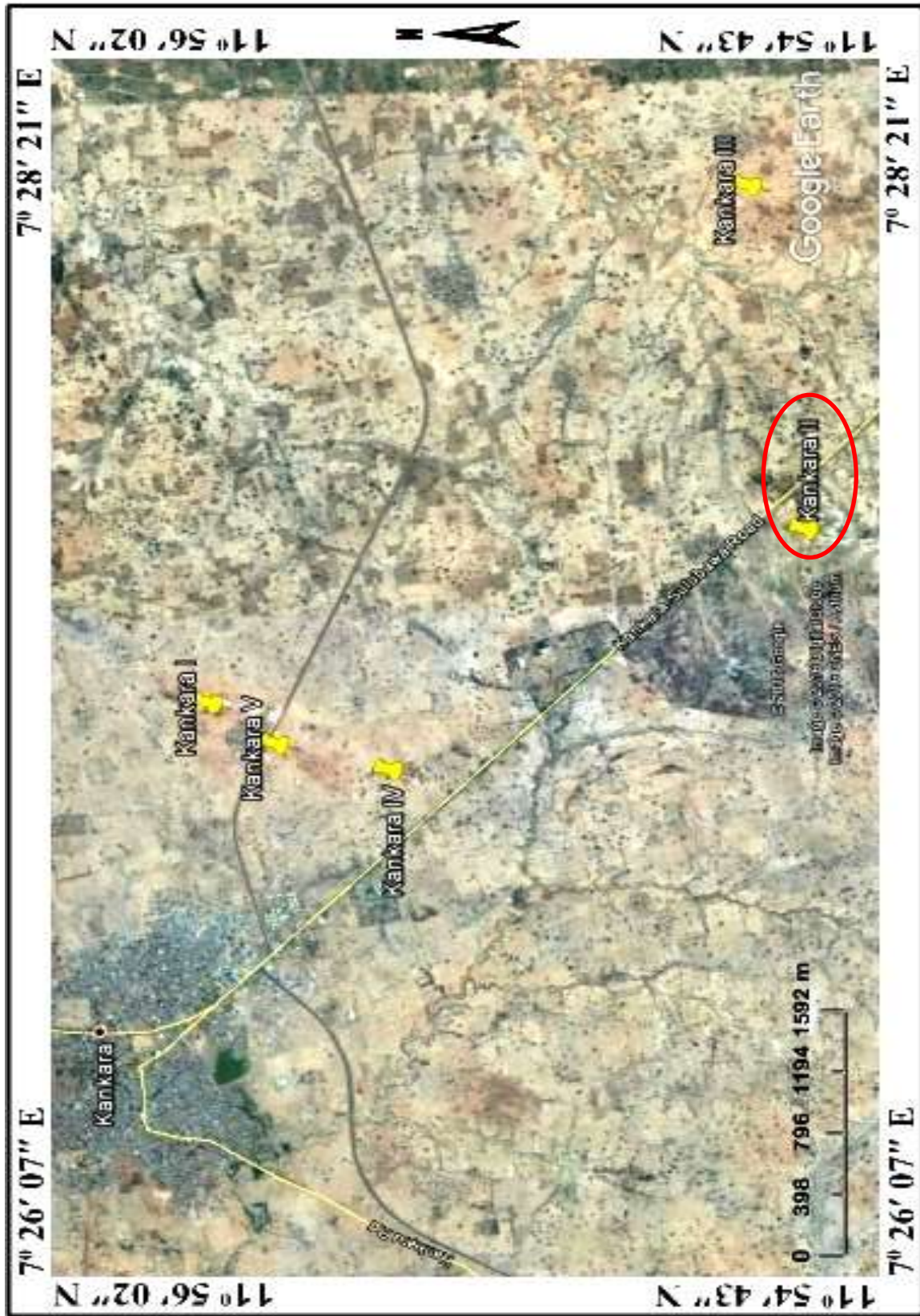


Figure 2.1: Major Kaolin deposits of Kankara area, Kankara I (Tsaunin Boda), Kankara II (Dajin Gwamna, **The study area**), Kankara III (Anguwan Liman), Kankara IV and Kankara V. (Courtesy Google earth).

Adeoye (2000) carried out Geotechnical analysis in combination with vertical electrical soundings at Taranji in Udubu area of Bauchi State, Northeastern Nigeria. The Geotechnical analysis indicates that the Clay has tough tensile strength with liquid limit of 29.25% and plastic limit of 13.04% and average linear shrinkage of 5.75%. Vertical electrical soundings of twenty (20) hand-dug pits of average depth of one thousand metres (1,000 m) were examined and sampled along the profiles. Geological mapping of the area, geochemical studies of the clay and the ironstone were also determined.

Elueze *et al.* (2004) worked on residual clay occurrences in the Precambrian complex of Iwo and Ijebu districts of Southwestern Nigeria using mineralogical and chemical analyses (X-ray diffraction, XRD; Atomic absorption spectrometry, AAS; wet sieve analysis and attenberg limits) to examine their mineralogy, chemical composition and geotechnical properties in order to evaluate their economic values. The X-ray diffraction studies showed Kaolinite as the dominant clay with Illite and Montmorillonite in trace amounts; also Quartz, Feldspar and Goethite were found as the main non clay constituents.

Geophysical methods (Airborne Electromagnetic, AEM and Airborne Magnetic, AM surveys) in combination with regional gravity surveys and ground geophysical measurements have also proved to be effective in the exploration of Kaolin and Ilmenite in Finland to delineate boundaries and properties of the deposits (Lohva and Lehtimaki, 2005).

The Geoelectric investigation in Lakiri village, Southwestern Nigeria was carried out using Schlumberger configuration of geophysical prospecting by Badmus and Olatinsu (2009) which revealed the occurrence of vast deposit of Kaolin that can serve as raw materials for industries e.g. building and porcelain, the results also revealed the quality of the Kaolin both chemical

and physical properties as additives for both industrial and mining purposes and the ground water potential of this area has been affected by the presence of this solid mineral as most aquifers are overlain by thick overburden material of fresh deposit of clay and Kaolin.

Geophysical and geostatistical methods were combined to quantify the clay deposits in Idofe, Imope, Iganran, Aparaki and Falafanmu in Southwestern Nigeria. The vertical electrical sounding (VES) geophysical method determined the resistivity and thicknesses of the clay at 80 points, while the geostatistical method estimated the volume of clay to be 35,062,528.03 m³ (Mosuro *et al.*, 2011).

Egbai (2011, 2013) carried out geophysical investigation on Kaolin deposits in the sedimentary terrain using a geophysical method (Vertical electrical sounding VES) to determine the thickness, existence and quantity of Kaolin stating that the large quantity found in Ozanogogo, Delta State, can be mined commercially, he also carried out the same survey at Ukwu-Nzu and Ubulu-Uku in Aniocha North, Delta State and established the reserve to be 401,235.84 tonnes and 69,535.44 tonnes respectively, stating that the reserve might not be enough for commercial purposes because of its low quantity but could be mined at a local level.

Talabi *et al.* (2012) have used geochemical methods (x-ray fluorescence analytical technique and granulometric analysis) to evaluate the compositional features and industrial application of Ikere Kaolin. Based on its mineralogy, chemical composition and physical characteristics they have found it suitable to be an industrial raw material in refractory, pottery and paint industries.

The characteristic properties of the Kaolin within Ise-Orun and Emure LGA of Ekiti State were examined using geochemical methods (x-ray diffraction XRD, differential thermal analysis DTA, atomic absorption spectrometry AAS, and x-ray fluorescence XRF), beneficiated and processed for ceramic automobile parts, friction lining materials and other related industries because of their thermal shock, wear, resistance and material cost (Aderiye, 2014).

Geophysical investigation of Kaolin deposit was carried out in Ikere, Southwestern Nigeria using vertical electrical soundings and horizontal electrical profiling involving Dipole-dipole and Schlumberger configurations has revealed the lateral continuity of the Kaolin deposit within the study area (Ogundana *et al.*, 2015).

2.2 Kankara Kaolin Deposits

Kankara Kaolin deposits lies within an area bounded by latitude 11°53' and 11°55'N and longitude 7°26' and 7°28'E and extends over an area bordering Elgoje, Danmarke, Anguwan Liman, and Yargoje villages. The three major deposits are completely buried under variable thickness of overburden and occur in sporadic lenses of varying sizes and geometry (Oyeka, 1976).

2.3 Origin of Clay

Clay is a product of decomposition of rocks, particularly granite that is abundant all over the earth surface. Granite, which is also known as feldspathic rock, is decomposed through time in many different physical actions such as wind, rains, erosion, earth movement: earth-quake, volcanic eruption, etc. and eventually becomes clay as we know it. Bowers *et al.* (1984) in Mode and Amobi (2006) have reported that, there are four geological processes which give rise to clay minerals formation:

- i. Weathering
- ii. Precipitation from concentrated solutions (saline lakes and closed marine basins)
- iii. Burial diagenesis (effects of chemical and thermal change) and
- iv. Hydrothermal alteration (water rock interaction at higher temperature due to thermal effects of magnetic intrusion).

The water-rock ratio, the rock composition and the temperature at which the reactions take place, are the variables that control the four processes in the various clay minerals formed. They range from conditions at the earth-air or earth-water interface which give minimum temperatures of 40°C for ocean bottom formation and around 150°C average for land occurrence to the upper limit at which clay minerals occur, which heat is 2000°C in young rocks. Burial depths are usually not greater than 6-7km (Mode and Amobi, 2006).

2.4 The Clay Mineral Kaolin and its Formation

Kaolin (china clay) is a hydrated aluminum silicate crystalline mineral (kaolinite) formed over many millions of years by the hydrothermal decomposition of granite rocks. It belongs to the group of clay minerals that contain atoms of silicon, aluminum, oxygen, ferrous and ferric iron, and hydroxyl groups as the main constituents. It also has other elements such as phosphorus, potassium, calcium, sodium, magnesium, etc., in minute quantities (Badmus *et al.*, 2013). It is hydrated because it contains silica of aluminum with a composition of silica of aluminum with an approximately 46% SiO₂, 40% Al₂ O₃ and 14% H₂O. Hydrous kaolin is characterized by its fine particle size, plate like or lamellar particle shape with chemical inertness. It is named after the hill in China (Kao-Ling) where it was first mined, for many years before its discovery in Europe in 1745. The iron content in each type of Kaolin clay determines its colour. It is usually white to near white in colour. Other colours such as purple,

bleach brown, sometimes red, blue or brown tints, etc., are due to the impurities in the material. Kaolinite is a clay mineral, part of the group of industrial minerals, with the chemical composition $\text{Al}_2\text{Si}_2\text{O}_5(\text{OH})_4$. It is a layered silicate mineral, with one tetrahedral sheet linked through oxygen atoms to one octahedral sheet of alumina octahedral. It is a soft, earthy, usually white mineral (dioctahedral phyllosilicate clay), produced by the chemical weathering of aluminum silicate minerals like feldspar. Chemical analysis carried out on Kaolin clay showed that it is acidic and contains high concentration of alkaline metals. The physical analyses also revealed Kaolin clay to have an average porosity of 0.46 and bulk density of 1.4 g cm^{-3} (Badmus and Olatinsu, 2009). Members of the Kaolin family include dickite, nacrite, allophane, and hallosite (Kaolinitic clays), (Brindley, 1951). That is, they all have the same chemical composition but different internal structures (Zoltan *et al.*, 2005). The flat particle shape that increases opacity, its chemical inertness, soft and non-abrasive texture due to the absence of coarse impurities are the distinguishing properties of Kaolin from other Kaolinitic clays (Atanda *et al.*, 2012).

There are *two types* of Kaolin in sedimentary rock based on their geological origin. These are the primary kaolin and secondary kaolin. The *primary kaolin* is found and originated from parent rock and have not been transferred by the force of nature. This class of Kaolin is purer in nature. The *secondary kaolin* are Kaolin that have been removed or eroded, transported and deposited as sediment from the site of their parent rock by the force of nature such as water, wind, or glacial action. As transportation and deposition were going on, the Kaolins become contaminated with materials of different origin. Kaolin formation results from the alteration of the feldspar of granites. This alteration may be caused by the process of ordinary weathering of feldspar first, into clay mineral to kaolin with less water. It is also formed by the action of

gases on the feldspar deposit formed as a result of intrusion of granite associated with some special set of minerals such as cassiterites and other minerals of pneumatolytic origin. Kaolin as a mineral is described technically as a white alumina-silicate. It does not react with other materials and is insoluble in water.

2.5 Uses of Kaolin Clay

Kaolin is used in making fire bricks which can withstand very high temperatures usually above 1500°C and are used to line blast furnaces and kilns in iron and steel industries, glass, ceramics, aluminum and petroleum industries (Adindu *et al.*, 2014) since they can resist all types of stresses (thermal, mechanical, chemical) such as erosion, creeping deformation, corrosion and thermal shocks, i.e, ability to retain their original forms without cracking or flaking under sudden temperature changes (Commission, 2007). The mixture of kaolin and sawdust in the ratio of 1:1 by volume produces quality insulating fire bricks (Malu and Babson, 2007). The Ajokuta steel complex of Nigeria uses kaolin and river sand from the Niger River. Kaolin is largely used in the paper industry as a coating pigment and fillers (Adindu *et al.*, 2014); they increase brightness, opacity, give the desired finish, make the paper whiter and enhance printing properties of the paper. Properties possessed by Kaolin which are of great interest to the paper industry include whiteness, low viscosity, non-abrasiveness, controlled particle size and flat hexagonal plates (Murray, 2010). Kaolin is also preferred in this sector because of its optical properties, chemical inertness and it is inexpensive compared to other minerals.

Kaolin is a traditional raw material in the ceramic industry in the production of white ware (sanitary ware, household utensils amongst others) since it gives the ware a smooth surface finish, and electrical insulation (Benea and Gorea, 2004). It is also used as an extender

pigment that provides colour or whiteness. Kaolin is used in rubber and plastic industry, also in pharmaceutical industries as a protectant for the temporary relief of ano-rectal itching and diaper rash (Kaolin Uses, Benefits and Dosage, 2000). Kaolin has been used as an insecticide against various arthropods that affect crops.

The earth sciences use the clay minerals in the earth crust:

(i) as indicators of the environment during weathering and authi-genesis in the sediments and in the study of source area of the detrital supply and

(ii) as pH indicators and indicators of processes in micro- and mega-environments and of changes in the course diagenesis and metamorphosis, mineralogical, petrological, geological and geochemical investigations of clay minerals serve as one of the correlation methods, in the recognition of processes in the petroleum-bearing sediments, coal-bearing formations, origin of riverine, lacustrine, marine, oceanic sediments, climatic, geodynamic, paleogeographical, stratigraphic and weathering rate interpretations (Konta, 1995).

2.6 Electrical Resistivity Method

The resistivity methods are based on measuring the electrical potentials between one electrode pair while transmitting direct current (D.C.) between another electrode pair. The depth of penetration is proportional to the separation between the electrodes in a homogeneous ground. Varying the electrode separation provides information about the stratification of the ground. The measured quantity is called apparent resistivity. Interpreting the apparent resistivity data consists of two steps: a physical interpretation of measured data, resulting in a physical model, and a geological interpretation of the resulting physical parameters. Figure 2.2 showed the current and potential distributions within a homogeneous isotropic ground in a vertical plane

through the current electrodes C_1 and C_2 . When an external voltage is applied across them, there will be a flow of current through the earth from one electrode C_1 to the other, C_2 . The resistivity method is based on measuring the potential difference between one electrode pair (P_1 and P_2 , called potential electrodes) while transmitting D.C. between another electrode pair (C_1 and C_2) and r_1 , r_2 , r_3 and r_4 are the electrode separations. The rheostat varies the current I which is measured by the ammeter (A) while the voltmeter (U) measures the potential difference ΔU .

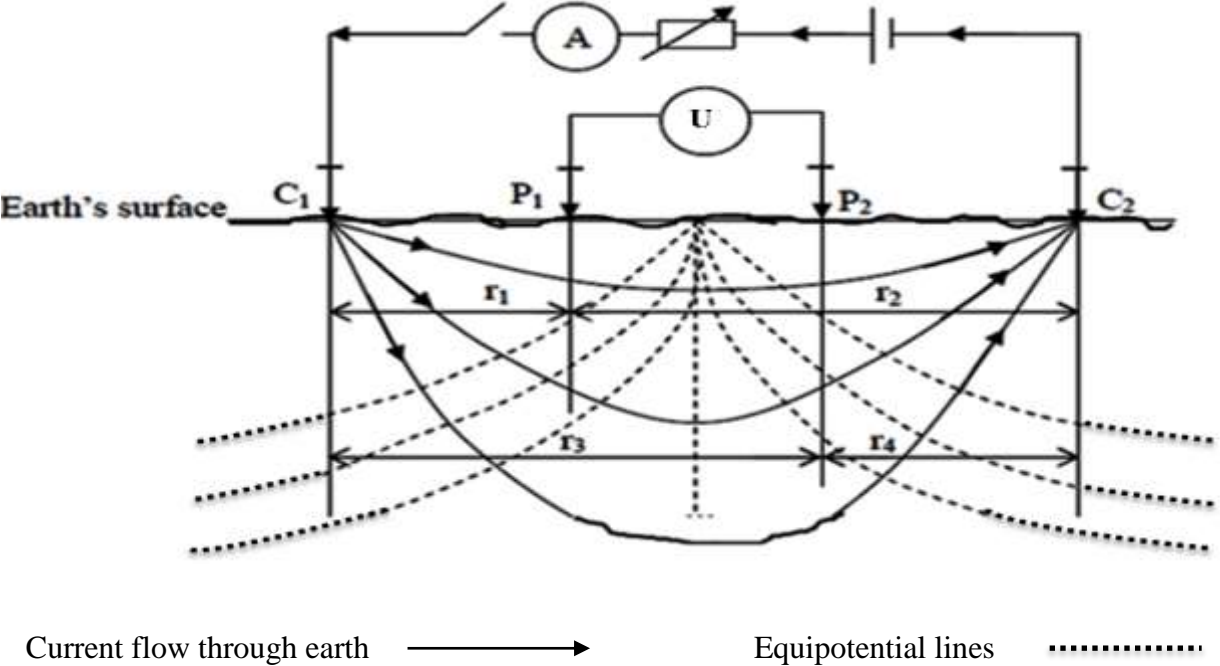


Figure 2.2: Current (C_1 , C_2) and Potential (P_1 , P_2) Distributions within Homogeneous Isotropic ground.

The electrical resistivity surveys are used routinely in geothermal, mining, coal, groundwater and engineering applications (Keller and Frischknecht, 1966). In engineering application, electrical surveys are used for dam stability studies, bedrock strength, mapping overburden, faults and fracture.

There are three basic modes of operation for any resistivity method: sounding, profiling and sounding – profiling (called imaging).

2.6.1 Theory of the Resistivity methods

The resistivity method is based on measuring the potentials between one electrode pair while transmitting direct current (D.C.) between another electrode pair (Figure 2.3). The depth of penetration is proportional to the separation between the current electrodes, in a homogeneous ground, and varying these electrode separation provides information about the stratification of the ground.

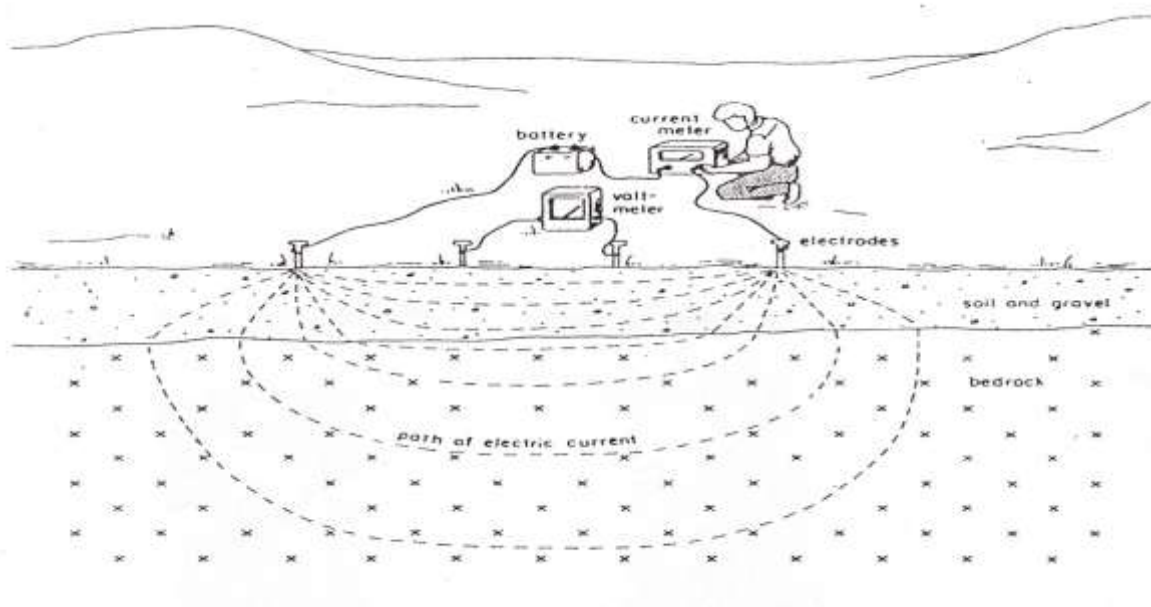


Figure 2.3: Schematic diagram showing the basic principle of DC Resistivity measurements.

The principle underlying the resistivity method is embodied in Ohm's law, which states that the current density at a given point is proportional to the electric field intensity at that point. Thus, Ohm's law gives the relationship between current density J (amperes/m²) and electric field intensity E (volts/m) as:

$$\vec{J} = \sigma \vec{E} \quad (2.1)$$

where σ is the conductivity of the medium and E is the gradient of a scalar potential U (volts),
i.e.

$$\vec{E} = -\nabla U \quad (2.2)$$

Putting equation (2.2) into Equation (2.1)

$$\vec{J} = -\sigma \nabla U \quad (2.3)$$

From divergence condition,

$$\nabla \cdot \vec{J} = 0 \quad (2.4)$$

Thus, from Equation (2.3)

$$\nabla \cdot \vec{J} = -\nabla \cdot (\sigma \nabla U) = 0 \quad (2.5)$$

$$\nabla \sigma \cdot \nabla U + \sigma \nabla^2 U = 0 \quad (2.6)$$

For a homogeneous earth, σ is a constant and since the derivative of a constant is equal to zero, then the first term in Equation (2.6) vanishes hence,

$$\nabla^2 U = 0 \quad (2.7)$$

Equation (2.7) is called Laplace Equation.

Applying boundary conditions, Equation (2.7) can be solved for specific cases. For instance, for a single current electrode deeply buried inside a homogeneous ground, Equation (2.7) is expressed in spherical polar coordinates as:

$$\nabla^2 U = \frac{1}{r^2} \frac{\partial}{\partial r} \left(r^2 \frac{\partial U}{\partial r} \right) + \frac{1}{r^2 \sin \theta} \frac{\partial}{\partial \theta} \left(\sin \theta \frac{\partial U}{\partial \theta} \right) + \frac{1}{r^2 \sin^2 \theta} \left(\frac{\partial^2 U}{\partial \phi^2} \right) = 0 \quad (2.8)$$

For point current source, there is complete symmetry of current flow with respect to the θ and ϕ directions and the derivatives with respect to these directions are zero. Thus, Equation (2.8) becomes

$$\nabla^2 U = \frac{\partial}{\partial r} \left(r^2 \frac{\partial U}{\partial r} \right) = 0 = \frac{d}{dr} \left(r^2 \frac{dU}{dr} \right) \quad (2.9)$$

From the symmetry of the system, the potential will be a function of r only, where r is the distance from the first electrode. Under these conditions Laplace's equation, in spherical coordinates, simplifies to this by differentiating Equation (2.9), which becomes

$$\nabla^2 U = \left(\frac{\partial^2 U}{\partial r^2} \right) + \frac{2}{r} \left(\frac{\partial U}{\partial r} \right) = 0 \quad (2.10)$$

Multiplying by r^2 and integrating, we get

$$\frac{\partial U}{\partial r} = \frac{a}{r^2}$$

Integrating again, we have

$$U = -\frac{a}{r} + b$$

where a and b are constants, U is the electric potential at the measuring point and r is the distance from that point to the single current electrode. Since $U = 0$ as $r \rightarrow \infty$ then $b = 0$ and

$$U = -\frac{a}{r} \quad (2.11)$$

The current flows radially outwards in all directions from the deeply buried point current electrode and the total current crossing a sphere of radius r is

$$I = 4\pi r^2 J = -4\pi r^2 \sigma \frac{dU}{dr} = -4\pi \sigma a = -\frac{4\pi a}{\rho} \quad (2.12a)$$

after using Equation (2.3) and Equation (3.10). Thus,

$$a = -\frac{I\rho}{4\pi} \quad (2.12b)$$

putting Equation (2.12b) into Equation (2.11) we have

$$U = \frac{I\rho}{4\pi} \frac{1}{r}, \quad \rho = 4\pi r \left(\frac{U}{I} \right) \quad (2.13)$$

The equipotentials which are everywhere perpendicular to the current flow lines will be spherical surfaces given by r is equal to a constant.

The point current electrode of the three-point-system is located at the surface of the homogeneous isotropic medium with the air above having zero conductivity, the return current electrode is at a great distance. As in the previous case $b=0$ since $U=0$ as $r \rightarrow \infty$

$$\text{In addition } \frac{\partial U}{\partial z} = 0 \text{ at } z = 0$$

since $\sigma_{air} = 0$. In the present case, all the current flows through a hemispherical surface in the lower subsurface region.

Hence

$$a = -\frac{I\rho}{2\pi} \quad \text{and} \quad U = \frac{I\rho}{2\pi} \frac{1}{r} \quad \text{or} \quad \rho = 2\pi r \left(\frac{U}{I} \right) \quad (2.14)$$

When two current point electrodes are used and placed linearly with two potential electrodes on the surface of an isotropic homogeneous ground of constant resistivity, as shown in the in Figure 2.4, a potential difference can be derived through the following expressions:-

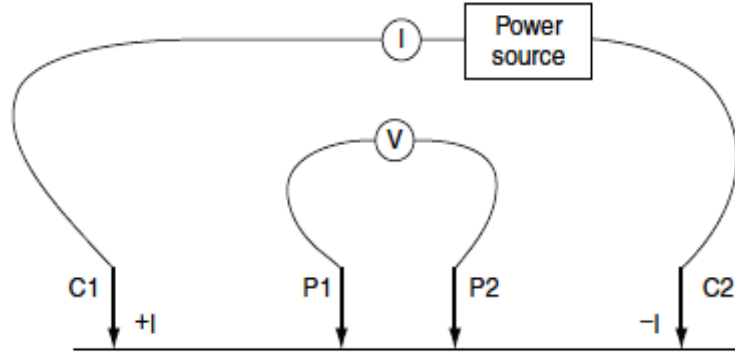


Figure 2.4: A conventional four electrode array usually used to measure subsurface Resistivity

Given that,

$$r_1 = C1 P1, r_2 = C2 P1, r_3 = C1 P2 \text{ and } r_4 = C2 P2$$

As before, the potential due to C1 at P1 is

$$U_1 = -\frac{a_1}{r_1} \quad \text{Where,} \quad a_1 = -\frac{I\rho}{2\pi}$$

Similarly, the potential due to C2 at P1 is

$$U_2 = -\frac{a_2}{r_2} \quad \text{Where,} \quad a_2 = \frac{I\rho}{2\pi} = -a_1 \quad (\text{since the current at the two electrodes are equal and opposite in direction})$$

Therefore, the potential at P1 due to both current electrodes is,

$$U = U_1 + U_2 = -\frac{a_1}{r_1} - \frac{a_2}{r_2} \quad (2.15)$$

Substituting the expression of a_1 and a_2 into equation (2.15),

$$U = \frac{I\rho}{2\pi} \left[\frac{1}{r_1} - \frac{1}{r_2} \right] \quad (2.16)$$

Similarly, when the second potential electrode is introduced at P2, the potential at P2 due to both current electrodes is

$$U = \frac{I\rho}{2\pi} \left[\frac{1}{r_3} - \frac{1}{r_4} \right] \quad (2.17)$$

The potential difference between P1 and P2 is,

$$\Delta U = \frac{I\rho}{2\pi} \left(\frac{1}{r_1} - \frac{1}{r_2} - \frac{1}{r_3} + \frac{1}{r_4} \right) \quad (2.18)$$

where ρ is the homogeneous resistivity, I is the current and r_1 , r_2 , r_3 , and r_4 , are the inter-electrode distances and this is the general four-electrode configuration.

For a non-homogeneous earth, ρ becomes apparent resistivity ρ_a . From Equation (2.18) the apparent resistivity can be solved for as;

$$\rho = \rho_a = \frac{\Delta U}{I} \frac{2\pi}{\left(\frac{1}{r_1} - \frac{1}{r_2} - \frac{1}{r_3} + \frac{1}{r_4} \right)} \quad (2.19)$$

The result is independent of the position of the electrodes and is not affected when the current and the potential electrodes are interchanged.

The resistance is calculated using Ohm's law:

$$R = \frac{\Delta U}{I} \quad (2.20)$$

where R is the resistance in ohms; ΔU is the potential difference in volts; and I is the current in amperes. The material parameter ρ which is the inverse of electrical conductivity σ is related to the resistance via a geometric factor K' that is a function of the electrode configuration. The resistivity of the homogeneous ground can be calculated using the relation

$$\rho_a = \rho = K' \frac{\Delta U}{I} \quad (2.21)$$

$$\text{where } K' = \left(\frac{2\pi}{\frac{1}{r_1} - \frac{1}{r_2} - \frac{1}{r_3} + \frac{1}{r_4}} \right) \quad (2.22)$$

K' is the geometric factor.

The electrical resistivity methods have been widely used for shallow and deep investigations, routinely in geothermal, mining, coal, groundwater and engineering applications (Keller and Frischknecht, 1966). In engineering application, electrical surveys are used for dam stability studies, bedrock strength, mapping of overburden, faults and fractures. Resistivity studies are often effective because the resistivity of porous earth materials is primarily a function of the amount of fluid which fills the pores, the conductivity of fluid and the clay content of the matrix (Kean *et al.*, 1987).

2.7 Vertical Electrical Sounding (VES)

This is also known as electrical drilling or expanding probe. It is used mainly in the study of horizontal or near horizontal interfaces. Consequently, readings are taken as the current reaches progressively greater depth. The measured apparent resistivity values are normally plotted against electrode spacing values on a log–log graph paper. To interpret the data from such a survey, it is normally assumed that the subsurface consists of horizontal layers. In this

case, the subsurface resistivity changes only with depth, but does not change in the horizontal direction. In many engineering and environmental studies, the subsurface geology is very complex where the resistivity can change rapidly over short distances. The resistivity sounding method might not be sufficiently accurate for such situations. However, the technique is extensively used in geotechnical surveys to determine overburden thickness and also in hydrogeology to define horizontal zones of porous strata.

2.8 Constant Separation Traversing (CST)

This is also known as electrical profiling. It is used to determine lateral variations of resistivity. The current and potential electrodes are maintained at a fixed separation and the array is progressively moved along different profiles. This gives some information about lateral changes in the subsurface resistivity, but cannot detect vertical changes in the resistivity. This method is employed in mineral prospecting to locate faults or shear zones and to detect localized bodies of anomalous conductivity. It is also used in geotechnical surveys to determine variations in bedrock depth and the presence of steep discontinuities. Results from a series of CST traverses with fixed electrode spacing can be employed in the production of resistivity contour maps.

The most useful method is a combination of sounding and profiling which delineates both lateral and vertical variations in resistivity. This is the method employed in electrical resistivity imaging.

2.9 Electrode Arrays

Many configuration of electrodes have been designed (Loke, 1999). The choice of the best array for a field survey depends on the type of structure to be mapped, the sensitivity of the

resistivity meter and the background noise level. In practice, the arrays that are most commonly used for 2-D imaging surveys are:

i) Wenner

ii) Dipole-Dipole

iii) Wenner-Schlumberger

iv) Pole-Pole

v) Pole-Dipole

Some of the characteristics of array that are considered for field survey are:

(i) The sensitivity of the array to vertical and horizontal changes in the subsurface resistivity.

(ii) The depth of investigation

(iii) The horizontal data coverage

(iv) The signal strength

(v) Sensitivity to surficial inhomogeneties

(vi) Electromagnetic coupling

2.9.1 Wenner Array

In the Wenner array the separation a between adjacent electrodes is constant and the apparent resistivity ρ_a is given by:

$$\rho_a = 2\pi a \cdot \frac{\Delta V}{I} \quad (2.23)$$

where “ a ” is the uniform separation called electrode spacing and $2\pi a$ is the geometric factor.

The Wenner array is relatively sensitive to vertical changes in the subsurface resistivity below the centre of the array. However, it is less sensitive to horizontal changes in the subsurface resistivity. In general, the Wenner array is good in resolving vertical changes (i.e., horizontal structure), but relatively poor in detecting horizontal changes (i.e., narrow vertical structures). Among the common arrays, the Wenner array has the strongest signal strength. This can be an important factor if the survey is carried out in areas with high background noise. One disadvantage of this array for 2-D surveys is the relatively poor horizontal coverage as the electrode spacing is increased.

2.9.2 Dipole-Dipole Array

This array is widely used in resistivity and IP surveys because of the low electromagnetic coupling between the current and potential circuits. The spacing between the current electrode pair, C2 - C1, is given as “ a ” which is the same as the distance between the potential electrode pair, P1 - P2. The factor “ n ” is the ratio of the distance between the C1 and P1 electrodes to the C2 - C1 or P1 - P2 dipole separation “ a ”. For surveys with this array, the “ a ” spacing is initially kept fixed and the “ n ” factor is increased from 1 to 2 to 3 until up to about 6 in order to increase the depth of investigation.

The dipole-dipole array is very sensitive to horizontal changes in resistivity, but relatively insensitive to vertical changes in the resistivity. It is good in mapping vertical structures, such as dykes and cavities, but relatively poor in mapping horizontal structures such as sedimentary layers.

The apparent resistivity ρ_a is given by:

$$\rho_a = n\pi(n+1)(n+2)a \cdot \frac{\Delta V}{I} \quad (2.24)$$

where “ na ” is the distance between the two innermost electrodes (one current electrode and the next is potential electrode).

In general, this array has a shallower depth of investigation compared to the Wenner array. However, for 2-D surveys, this array has better horizontal data coverage than the Wenner. Another possible disadvantage of this array is the very small signal strength for large values of the “ n ” factor. Figure 2.5 shows the common arrays used in resistivity surveys and their geometric factors.

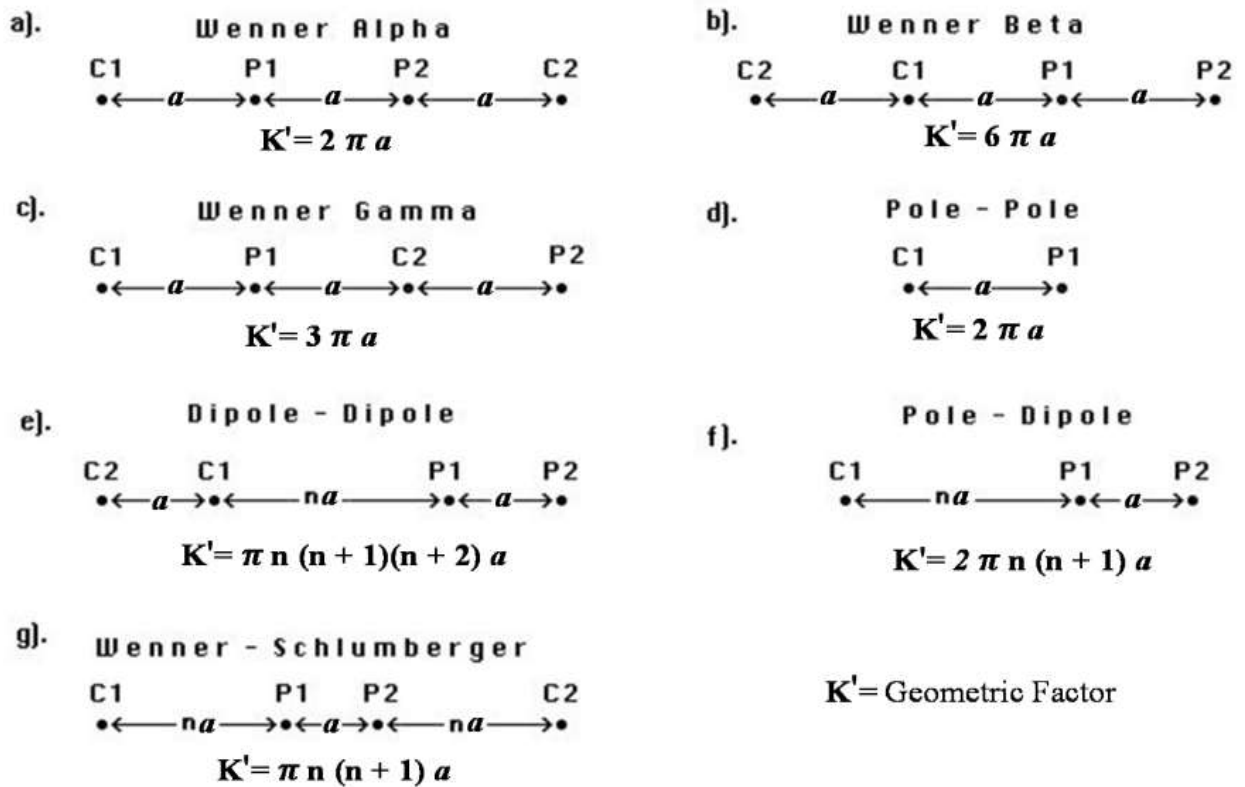


Figure 2.5: Common Arrays used in Resistivity Surveys and their Geometric Factors.

2.9.3 Wenner-Schlumberger Array

This is a hybrid between the Wenner and Schlumberger arrays (Pazdirek and Blaha, 1996) arising out of relatively recent work with electrical imaging surveys. The array is moderately sensitive to both horizontal and vertical structures. In areas where both types of geological structures are expected, this array might be a good compromise between the Wenner and the dipole-dipole arrays. The signal strength for this array is smaller than that of the Wenner array but higher than the dipole-dipole array.

The Wenner-Schlumberger array has a slightly wider horizontal data coverage than the Wenner array, but narrower than that obtained with the dipole-dipole array. The apparent resistivity ρ_a is given by:

$$\rho_a = n\pi(n + 1)a \cdot \frac{\Delta V}{I} \quad (2.25)$$

where “ na ” is the distance between the C1 - P1 or P2 - C2 electrodes. The “ n ” factor is the ratio of the distance between the C1 - P1 or P2 - C2 electrodes to the spacing between the P1-P2 potential pair and a is the electrode spacing, P1 - P2.

2.9.4 Pole-Pole Array

This array is not as commonly used as the Wenner, dipole-dipole and Schlumberger arrays. In practice the ideal pole-pole array, with one current and one potential electrode does not exist. To approximate the pole-pole array, the second current and potential electrodes (C2 and P2) must be placed at a distance which is more than 20 times the maximum separation between C1 and P1 electrodes used in the survey. The effect of the C2 or P2 electrode is approximately proportional to the ratio of the C1 - P1 distance to the C2 - P1 distance. If the effects of the C2 and P2 electrodes are not taken into account, the distance of these electrodes from the survey

line must be at least 20 times the largest C1 - P1 spacing used to ensure that the error is less than 5%. In surveys where the inter-electrode spacing along the survey line is more than a few metres, there might be practical problems in finding suitable locations for the C2 and P2 electrodes to satisfy this requirement.

Pole-pole array is popular in some applications such as archaeological surveys where small electrode spacings are used. It has the widest horizontal coverage and the deepest depth of investigation. However, it has the poorest resolution. Another disadvantage of this array is that because of the large distance between the P1 and P2 electrodes, it can pick up a large amount of telluric noise which can severely degrade the quality of the measurement.

The apparent resistivity ρ_a is given by:

$$\rho_a = 2\pi a \cdot \frac{\Delta V}{I} \quad (2.26)$$

where “ a ” is the distance between C1 and P1 electrodes.

2.9.5 Pole-Dipole Array

The pole-dipole array also has relatively good horizontal coverage. It has a significantly higher signal compared with the dipole-dipole array and it is not as sensitive to telluric noise as the pole-pole array. The pole-dipole array also requires a remote electrode, the C2 electrode, which must be placed sufficiently far from the survey line. For the pole-dipole arrays, the effect of the C2 electrode is approximately proportional to the square of ratio of the C1 – P1 distance to the C2- P1 distance. Thus the pole-dipole array is less affected by the C2 remote electrode compared with the pole-pole array. If the distance of the C2 electrode is more than 5 times the largest C1 - P1 distance used, the error caused by neglecting the effect of the C2

electrode is less than 5%. The exact error also depends on the location of the P2 electrode for the particular measurement and the subsurface resistivity distribution.

The signal strength is lower compared with the Wenner and Wenner-Schlumberger arrays but higher than the dipole-dipole array. For IP surveys, the higher signal strength (compared with the dipole-dipole array) combined with the lower EM coupling (compared with the Wenner and Wenner-Schlumberger Arrays) due to the separation of the circuitry of the current and potential electrodes makes this array an attractive alternative.

The apparent resistivity ρ_a is given by:

$$\rho_a = 2\pi n(n + 1)a \cdot \frac{\Delta V}{I} \quad (2.27)$$

where “ na ” is the distance between C1 and P1 electrodes and “ a ” the distance between P1 and P2 electrodes.

2.10 Factors affecting Electrical Resistivity

The electrical resistivity of rocks and minerals is an extremely variable property and depends on a number of factors. Bulk resistivities from the surface to more than 15km depth in a normal crust are controlled by aqueous electrolytic conduction by way of pores, fractures, faults, and shear zones. The resistivity of crystalline rock formations such as granulites, granite, and diorite in-situ is largely dependent upon the water in the fissures and fractures. Similarly, the porosity, degree of saturation and the nature of pore-electrolytes govern the resistivity of rocks like sandstone and limestone. A slight increase in resistivity with depth is the result of decreasing pore, fracture, fault and shear-zone porosity due to increased lithostatic load.

2.10.1 Water Salinity

Conduction in near-surface rocks is largely electrolytic, taking place in connected pore spaces, along grain boundaries, in fractures, faults and shear zones but negligibly through the silicate framework. The ions which conduct the current result from the dissociation of salts, such dissociation occurring when salts are dissolved in water. Since each ion is able to carry only a definite quantity of charge, it follows that the more ions that are available in a solution the greater will be the charge that can be carried. Hence, the solution with the larger number of ions will have the higher conductivity. In general, for a given porosity, a rock which contains saline water within its pores will have a greater conductivity when the salinity of the water is high than when it is low. Resistivity decreases with increase in salinity.

2.10.2 Porosity of Rock

Porosity can be defined as the ratio of the percentage of the volume of void space to the total volume of the rock. Porosity arises from the fact that the particles do not occupy all the possible space. It provides a direct measure of the total void space available for the storage of fluids.

Resistivity and porosity in sedimentary rocks can be related by the general form of Archie's law, which for rocks devoid of clay is written as

$$F = \frac{\rho_r}{\rho_s} = a\phi^{-m} \quad (2.28)$$

Where F is the formation resistivity factor, ρ_r is the resistivity of the rock, ρ_s is the resistivity of the solution in the pores of the rock, ϕ is porosity, while “ a ” and “ m ” are constants peculiar to the rock type. The constant “ m ” is usually referred to as the cementation factor while the

constant “ a ” is referred to as the coefficient of saturation. The most common mineral forming soils and rocks have very high resistivity in a dry condition, and the resistivity of soils and rocks is therefore normally a function of the amount and quality of water in pore spaces and fractures. The degree of connection between the cavities is also important.

2.10.3 Effect of Temperature

An increase in temperature lowers the viscosity of water, with the result that ions in the water become more mobile. The increased mobility of the ions results in an observed resistivity decrease with increase in temperature according to the formula (Keller and Frischknecht, 1966):

$$\rho_t = \frac{\rho_{18^0}}{1 + \alpha(t - 18^0)} \quad (2.29)$$

where ρ_{18^0} is the resistivity measured at a reference temperature of 18°C, α is the temperature coefficient of resistivity (about 0.025 per degree centigrade for most electrolytes) and t is the ambient temperature.

2.10.4 Effects of Geological Processes

General, weathering or hydrothermal alteration of granite significantly lowers its resistivity. Dissolution, faulting and shearing usually increase porosity and fluid permeability, and hence lower resistivity. Precipitation of calcium carbonate and silica reduces porosity and hence reduces fluid permeability and increases resistivity. Induration by compaction or metamorphism reduces porosity, permeability and hence increases resistivity. Salt water intrusion provides more ions for conduction and therefore reduces resistivity.

2.11 The Concept of Apparent Resistivity

Most resistivity techniques define a response function called apparent resistivity, ρ_a which can be calculated from the surface measurements. These apparent resistivities are usually functions of a variable that is related to the depth of current penetration.

The apparent resistivity is equal to the true resistivity only when the subsurface is homogeneous. In practice, this condition is difficult to obtain. However, the subsurface is assumed to be divided into thin strata with each stratum regarded as completely homogeneous and isotropic (Koefoed, 1979). This is a convenient way of representing a response of the actual distribution of lateral resistivity in the surface on the basis of subsurface measurements. If the electrodes are laid out along a profile and their separations are increased systematically, the change in the apparent resistivity will be a function of electrode spacing. Subsurface resistivity is measured by applying an electric current through two current electrodes and measuring the resulting voltage difference between potential electrodes. For the general four electrode spread, the potential difference ΔU between the potential electrodes is given by (Equation 2.18).

By measuring ΔU and I and knowing the electrode configuration, the resistivity can be calculated. Over uniform earth or homogeneous isotropic medium this calculated resistivity is constant for different electrode separation and any current. However, if the ground is inhomogeneous, the calculated resistivity varies as the electrode spacing is varied or the array is moved about. This calculated resistivity is called “apparent resistivity ρ_a ”, which is diagnostic of the real resistivities of the subsurface in the vicinity of the electrode array. The apparent resistivity may be smaller or larger than the real resistivities or in rare cases identical with one of the real resistivity values. The apparent resistivity is the same as the real resistivity

in a homogeneous subsurface, but normally a combination of contributing strata of an inhomogeneous subsurface. The value of the apparent resistivity obtained with small electrode spacing is called the surface resistivity. In any layout, the potential and current electrodes can be interchanged and from the principle of reciprocity, the apparent resistivity should be the same (unchanged) in either case.

2.12 Typical Resistivity Values of Earth Materials

The physical properties of the earth materials (rocks and minerals), electrical resistivity has the widest range of variations. Resistivity of metallic minerals may be as small as $10^{-5}\Omega\text{m}$. That of dry close-grained rocks like gabbro could be as large as $10^7\Omega\text{m}$. The maximum possible range is even greater, from native silver, $1.6 \times 10^{-8}\Omega\text{m}$ to pure sulphur $10^{16}\Omega\text{m}$. A good conductor is usually defined as a material of resistivity less than $10^{-5}\Omega\text{m}$ while an insulator is one having resistivity greater than $10^7\Omega\text{m}$, between this limit laid the semi-conductors (Telford *et al.*, 1990). The common minerals forming rocks and soils have very high resistivity values in dry condition and the resistivity of rocks and soils is therefore normally a function of the amount and quantity of water in pores and fractures. The degree of connection between cavities is also important; consequently the resistivity of a rock type or soil type may vary widely. The electrical resistivity varies between different geological materials depending mainly on variations in water content and dissolved ions in the water. Resistivity investigations can thus be used to identify zones with different electrical properties, which can then be referred to different geological strata. However, the variation may be limited within confined geological area and variations in resistivity within certain soil or rock type will reflect variations in physical properties. For example the lowest resistivities encountered for sandstones and limestone means that the pore spaces in the rock are saturated with water, whereas the highest

values represent strongly consolidated sedimentary rock or dry rock above the groundwater surface. Sand, gravel and sedimentary rocks may also have very low resistivities provided the pores in the rocks are saturated with saline water. Fresh crystalline rock is highly resistive apart from certain ore minerals, but weathering commonly produces highly conductive clay rich saprolite. The variation in characteristics within one type of geological material makes it necessary to calibrate resistivity data against geologic documentation for instance, surface mapping, test pits or drilling. Typical ranges of resistivities of geologic materials are shown in Figure 2.6 and Table 2.1. The amount of water in a material depends on the porosity, which may be divided into primary porosity and secondary porosity. Primary porosity consists of pore spaces between the mineral particles and occurs in soils and sedimentary rocks. Secondary porosity consists of fractures and weathered zones, and this is the most important porosity in crystalline rocks such as granites and gneisses. Secondary porosity may also be important in certain sedimentary rocks such as limestone. Even if the porosity is rather low, the electrical conduction taking place through water filled pore spaces may reduce the resistivity of the material drastically. The degree of water saturation will of course affect the resistivity, thus the resistivity above the groundwater level will be higher than below if the material is the same. Consequently, the resistivity method can be used to find the depth to groundwater in materials where a distinct groundwater table exists. However, if the content of fine grained material is significant, the water content above the groundwater surface, held by hygroscopic and capillary forces may be large enough to dominate the electrical behaviour of the material. The resistivity of pore water is dominated by the concentration of ions in solution, the type of ions and the temperature. The presence of clay minerals strongly affects the resistivity of sediments and weathered rocks. The clay minerals may be regarded as electrically conductive particles which can absorb and release ions and water molecules on its

surface through an ion exchange process. Very roughly, igneous rocks have the highest resistivity, sedimentary rocks the lowest and metamorphic rocks intermediate. However, there is a considerable overlapping. Resistivities of particular rock types vary with age and lithology, since the porosity of the rock and the salinity of the contained water are affected by both.

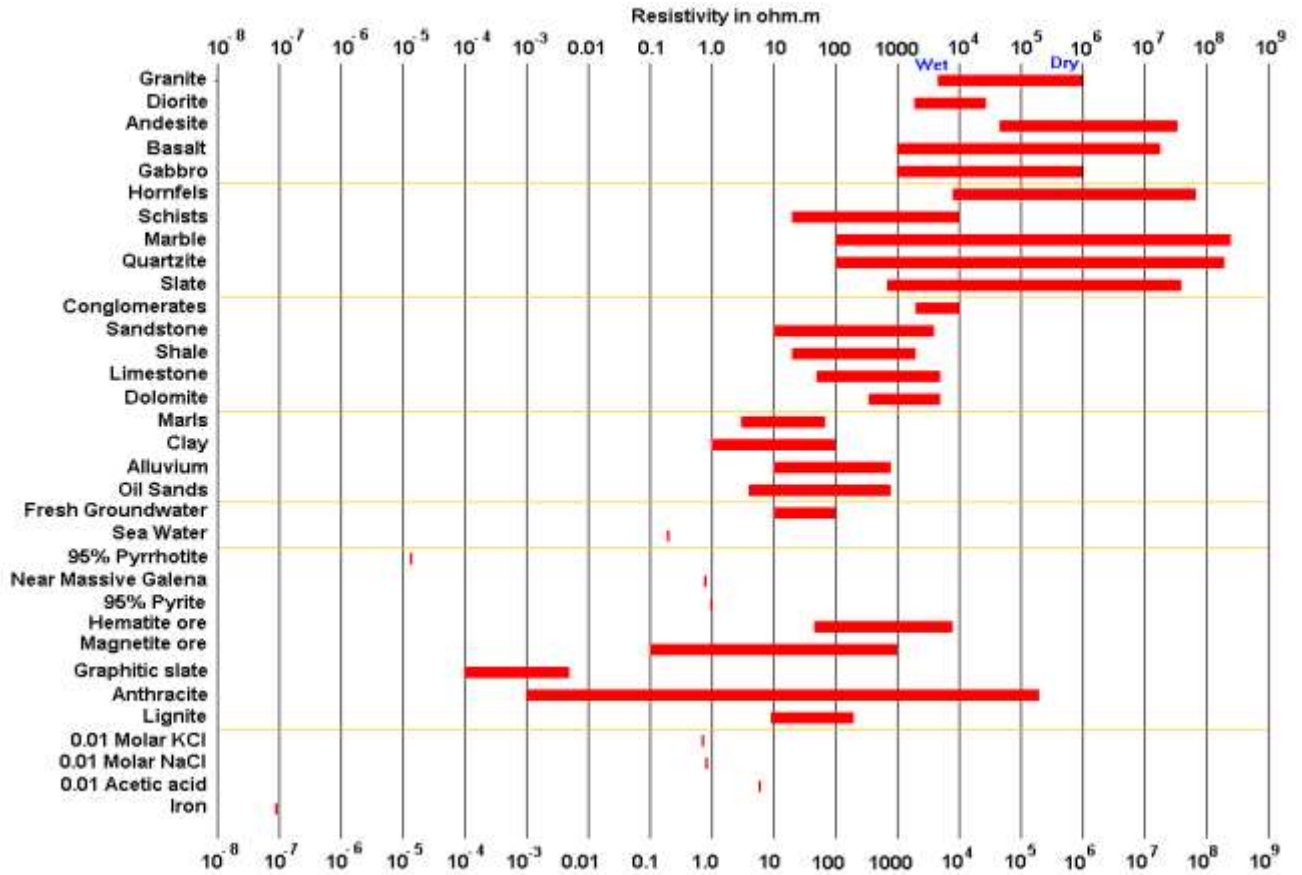


Figure 2.6: Resistivities of Rocks, Soils and Minerals (Loke, 2001).

Table 2.1: Typical Resistivity values of Rocks, Soils and Minerals, * -10°C to -60°C respectively; strongly temperature –dependent. Based on Telford et al. (1990) with additional data from McGinnis and Jensen (1971), Reynolds (1987). Reynolds and Paren (1980, 1984) and many commercial projects.

S/N	Materials	Normal Resistivity (Ωm)
1	Ash	4
2	Colliery spoil	10 – 20
3	Pulverised fuel ash	50 – 100
4	Laterite	800 – 1500
5	Lateritic soil	120 – 750
6	Dry sandy soil	80 – 1050
7	Sandy clay / clayey sand	30 – 215
8	Unsaturated landfill	30 – 225
9	Saturated landfill	15 – 30
10	Acid peat waters	100
11	Acid mine waters	20
12	Rainfall runoff	20 – 100
13	Landfill runoff	< 10 – 50
14	Glacier ice (temperate)	$2 \times 10^6 - 1.2 \times 10^8$
15	Glacier ice (polar)	$5 \times 10^4 - 3 \times 10^5$ *
16	permafrost	$10^3 - > 10^4$
	<i>Sulphides</i>	
17	Chalcopyrite	$1.2 \times 10^{-5} - 3 \times 10^{-1}$
18	Pyrite	$2.9 \times 10^{-5} - 1.5$
19	Pyrrhotite	$7.5 \times 10^{-6} - 5 \times 10^{-2}$
20	Galena	$3 \times 10^{-5} - 3 \times 10^2$
21	Sphalerite	1.5×10^7
	<i>Oxides</i>	
22	Hematite	$3.5 \times 10^{-2} - 10^7$
23	Limonite	$10^3 - 10^7$
24	Magnetite	$5 \times 10^{-5} - 5.7 \times 10^3$
25	Ilmenite	$10^3 - 5 \times 10$
26	Quartz	$3 \times 10^2 - 10^6$
27	Rock salt	$3 \times 10 - 10^{13}$
28	Anthracite	$10^{-3} - 2 \times 10^5$
29	Lignite	$9 - 2 \times 10^2$
30	Granite	$3 \times 10^2 - x 10^6$
31	Granite (weathered)	$3 \times 10 - 5 \times 10^2$
32	Syenite	$10^2 - 10^6$
33	Diorite	$10^4 - 10^5$
34	Gabbro	$10^3 - 10^6$
35	Basalt	$10 - 1.3 \times 10^7$
36	Schists (calcareous and mica)	$20 - 10^4$
37	Schists (graphite)	$10 - 10^2$
38	Slates	$6 \times 10^2 - 4 \times 10^7$
39	Marble	$10^2 - 2.5 \times 10^8$

40	Consolidated shales	$20 - 2 \times 10^3$
41	Conglomerates	$2 \times 10^3 - 10^4$
42	Sandstones	$1 - 7.4 \times 10^8$
43	Limestones	$5 \times 10 - 10^7$
44	Dolomite	$3.5 \times 10^2 - 5 \times 10^3$
45	Marls	$3 - 7 \times 10$
46	Clays	$1 - 10^2$
47	Alluvium and sand	$10 - 8 \times 10^2$
48	Moraine	$10 - 5 \times 10^3$
49	Sherwood sandstone	100 - 400
50	Soil (40 % clay)	8
51	Soil (20 % clay)	33
52	Top soil	250 - 1700
53	London clay	4 - 20
54	Lias clay	10 - 15
55	Boulder clay	15 - 35
56	Clay (very dry)	50 - 150
57	Mercia mudstone	20 - 60
58	Coal measures clay	50
59	Middle coal measures	>100
60	Chalk	50 - 150
61	Coke	0.2 - 8
62	Gravel (dry)	1400
63	Gravel (saturated)	100
64	Quaternary / Recent sands	500 - 100

CHAPTER THREE:

METHODOLOGY AND INSTRUMENTATION

3.1 Electrical Resistivity Imaging

Tomography is defined as an imaging technique which generates a cross sectional picture (tomogram) of an object by utilising the object's response to the nondestructive, probing energy of an external source. Electrical resistivity tomography is a method by which 2-D images of subsurface resistivity distribution are generated (Batayneh, 2006). Electrical resistivity imaging (tomography) involves measuring a series of constant separation traverses with the electrode spacing being increased with each successive traverse. Thus, 2-D resistivity imaging requires data to be recorded with many different electrode separations along a line.

It is important to have a dense enough data to cover laterally and in terms of electrode separations to recover complex structures in the ground; this demands the use of automated multi-electrode data acquisition systems. The Wenner-Schlumberger spread was used for this survey. The basis of the LUND Resistivity Imaging technique follows from that of the normal resistivity technique, in which case when a current is driven into the earth, any variation of the subsurface resistivity will alter the current flow, which will in turn affect the distribution of the electrical potential. Buried bodies distort the regular pattern of current flow.

A conductive body concentrates electric current flow lines towards itself while a resistive body causes the current to flow around itself. The electrical potential fields are hence deflected and their deflections can be detected using potential electrodes at the surface of the earth. Thus, from the measurements on the earth's surface of the electrical potential and the current, it is usually possible to obtain information about the variation of the subsurface resistivity.

Because sand, fine grained sediments and bedrock are expected to exhibit large contrasts in electrical resistivity, the electrical resistivity method should be well suited to resolving them. When the resistivity values are correlated with differing types of geologic materials, they can provide useful information for interpretation.

The electrical resistivity imaging is a survey technique developed for the investigation of areas of complex geology where the use of resistivity soundings and other techniques is unsuitable (Griffiths and Barker, 1993). It involves measuring a series of constant separation traverses with the electrode spacing being increased with each successive traverse. Since increasing separation leads to greater depth penetration, the measured apparent resistivities may be used to construct a vertical contoured section displaying the variation of resistivity both laterally and vertically over the section.

The major limitation of the resistivity sounding method is that it does not take into account horizontal changes in the subsurface resistivity. A more accurate model of the subsurface is a two-dimensional (2-D) model where the resistivity changes in the vertical direction, as well as in the horizontal direction along the survey line. However, at the present time, 2-D surveys are the most practical economic compromise between obtaining very accurate results and keeping the survey costs down. Typical 1-D resistivity sounding surveys usually involve about 10 to 20 soundings, while 2-D imaging surveys involve about 100 to 1000 measurements. In comparison, 3-D surveys usually involve several thousand measurements.

The cost of a typical 2-D survey could be several times the cost of a 1-D sounding survey, and is probably comparable with a seismic survey. In many geological situations, 2-D electrical resistivity imaging surveys can give useful results that are complementary to the information

obtained by other geophysical methods. For example, seismic methods can map undulating interfaces well, but will have difficulty (without using advanced data processing techniques) in mapping discrete bodies such as boulders, cavities and pollution plumes. Ground radar surveys can provide more detailed pictures but have very limited depth penetration in areas with conductive unconsolidated sediments, such as clayey soils.

3.1.1 Choice of the Array

In this work, Wenner-Schlumberger array was used. The Wenner-Schlumberger is a new hybrid between the Wenner and Schlumberger array arising out of more recent work with electrical imaging survey (Pazdirek and Blaha, 1996). This method was used for the following reasons:

1. It has a slightly better horizontal coverage compared with the Wenner array.
2. It is moderately sensitive to both horizontal and vertical structures. In area where both types of geological structures are expected, this array is a good compromise between the Wenner array and dipole-dipole array.
3. The median depth of investigation for this array is about 10% larger than that for the Wenner array for the same electrode spread.
4. The signal strength for this array is weaker than that for the Wenner array, but it is higher than the dipole-dipole array and twice that of the pole-dipole (Loke, 2014).

3.2 Vertical Electrical Sounding Technique

Seven vertical electrical soundings were acquired across the study area. Schlumberger array with a maximum current electrode spacing of 200 m was used for this survey. OHMEGA Ω

Resistivity Meter was used to measure and record the resistance of the subsurface. For each electrode combination for which a sounding was made and reading of resistance R of the volume of earth material within the electrical space of the electrode configuration was obtained. The product of configuration factor K and R was then made to obtain the apparent resistivity of the said earth material. This was subsequently done on all the point data obtained for each VES station to give the set of apparent resistivity values supplied for computer modelling using *IPI2Win* programme for the iteration to obtain the geoelectrical parameters. How the apparent resistivity values increase or decrease with each electrode separation form the basis for quantitative interpretation of the electrical resistivity data.

Qualitative interpretation of the subsurface resistivity distribution can be performed by observing the shape of the field sounding curve. In the curve matching method, a curve is drawn by plotting apparent resistivity against electrode spacing, and this is interpreted by matching the field curve with master curve. Four curve types have been identified within the study area. These are HH, HK, KAK and KKH with HH as the predominant curve type.

3.3 Reconnaissance Survey

Topographical maps and geological maps were obtained. A walk around the entire area to be surveyed with these maps was made, to consider whether resistivity surveying was suitable for the current problem. It was discovered that the method was suitable. So possible profile lines were selected and the entire length of the planed profile lines inspected to ensure their practicability before returning to the area for the detailed survey.

3.4 Instrumentation

In resistivity measurement nowadays, there is a range of instrumentation from very simple to highly sophisticated equipment with the latter including the computer for infield data

processing. The basic parts of any resistivity instrumentation are a portable power source which is either a D.C. or a low frequency A.C., electrodes, preferably stainless steel electrodes, cables and reels, Global Positioning System (G.P.S.), meters for measuring current and voltage both of which may be combined in a single meter reading resistance or apparent resistivity. With the development of computer-controlled data collection and automatic data inversion, the use of computer-controlled multi-electrode systems with automatic measurement for the data acquisition became very relevant. This is because it gives a dramatic increase in field productivity. Such is the ABEM LUND Imaging System.

3.4.1 List of instruments used for Resistivity Imaging survey

- i. ABEM Terrameter SAS 4000
- ii. Electrode Selector ES 464
- iii. 2 Reel of wire
- iv. 41 stainless steel electrodes
- v. 41 cable jumpers
- vi. External 12 volt source (a car battery)
- vii. Field hammers and
- viii. Global positioning system (GPS)

3.4.2 List of instruments used for Vertical Electrical Sounding survey

- i. OHMEGA Ohm Resistivity meter
- ii. Four steel electrodes
- iii. Field hammers
- iv. Measuring tape and

- v. Reels of wire

3.4.3 The ABEM Lund Imaging System

The LUND Imaging System is a multi-electrode system for cost effective and high resolution 2-D and 3-D resistivity surveys. It is an automatic electric imaging system suited for automatic resistivity profiling and drilling. The LUND Resistivity imaging System consists of a basic unit, a standard resistivity meter (ABEM Terrameter SAS 4000) and a (4x64) multi-channel relay matrix switch unit called Electrode Selector ES 464. The system also has four multi-conductor electrode cables wound on reels each with 21 take outs, stainless steel electrodes and cable jumpers and various connectors. The system is compatible with a portable PC-type computer or note book (Laptop). Operating power comes from an internal 12 volts rechargeable NiCd battery pack. Model section plotting of 1-D and 2-D model interpretation sections in colour or gray scale including topography, reference data and reference levels, utility software for extraction of VES, data manipulation and conversion, graphical output in PCX-file format *etc.* are also available (ABEM instruction manual, 2010).

The Lund ES 464 basic system consists of one ES 464 field unit with clip-on NiCd rechargeable battery pack and one communication cable from electrode selector to Terrameter. It is light weight and has waterproof, rugged cast aluminium casing. The Terrameter SAS system consists of a basic unit called the Terrameter SAS 4000 and accessories like ES 464. It is a method whereby consecutive readings are taken automatically and the results are averaged continuously. Signal Averaging System (SAS) results are more reliable than those obtained from single-short systems. The SAS 4000 can operate in different modes, e.g., resistivity, self potential and induced polarization. In all its modes it is capable of measuring simultaneously in four channels thus making it suitable in all sorts of resistivity surveys.

The SAS 1000 is powered by a clip-on NiCd battery pack or by an external 12 volt source, which clips conveniently onto the bottom of the instrument. The SAS-EBA external 12 volt adapter allows the terrameter to utilize an external 12 volt D.C. source, e.g., a car battery. Stainless steel electrodes establish electric contact through long cables, to an ionic conductor which is the ground. All sorts of electrodes generate “noise”. Noise is the fluctuating voltage that appears between a pair of electrodes placed so close that no other natural voltages appear. But stainless steel electrodes create less noise than electrodes made of ordinary steel. Current electrodes and potential electrodes make good contact with the ground to ensure low contact resistance and stability respectively (ABEM LUND Instruction Manual, 2010).

The cables incorporate heavy gauge conductors with excellent insulation to ensure good survey results. The cables are expandable for deeper penetration by connecting them in series with a cable joint. The cables have take-outs at 5m intervals along its length from which the cables are connected to the electrodes using cable jumpers having crocodile clips at both ends. The cables are wound on reels. Plate II, shows the basic instrumentation of the ABEM LUND Imaging System and accessories.



Plate II: ABEM LUND Imaging system together with Terrameter SAS 4000 and ES 464.

3.4.4 OHMEGA Ω Resistivity meter

The instruments used for Vertical Electrical Sounding survey consist of the OHMEGA Ω Resistivity meter, four steel electrodes, field hammers, measuring tape and reels of wire. The OHMEGA Ω resistivity meter measures the resistance and displays on its screen board, depending on its magnitude, it may be in kilo ohms, ohm or milliohms. The OHMEGA Ω Resistivity contains three basic sub-units; a microprocessor for monitoring, control and computation; an electrically isolated transmitter for the supply of defined regulated signal current. It can operate at frequency as low as 4 cycles per second; this property makes it suitable for greater depth of investigation. It is portable, it carries out signal averaging by taking consecutive readings automatically and displaying the average result. This makes it possible for the OHMEGA Ω resistivity meter to extract the signal from any noise. Plate III,

displays the basic instrumentation of OHMEGA Ω Resistivity meter system with its accessories.



Plate III: OHMEGA Ω Resistivity meter with its accessories

3.5 Field Measurement Procedure

Electrical Resistivity Imaging (tomography) is a method by which 2-D images of subsurface resistivity distribution are generated (Batayneh, 2006). Using this method, features with electrical properties differing from those of the surrounding material may be located and characterized in terms of electrical resistivity, geometry and depth of burial. The electrical resistivity tomography data are collected using computer-controlled measurement systems connected to multi-electrode arrays. The data acquisition process is completely controlled by the computer software which checks that all the electrodes are connected and properly grounded before measurement starts. After adequate grounding is achieved the software scans through the measurement protocol selected. The Wenner-Schlumberger array was chosen for

this survey. The field measurement usually started with laying out the cables and electrodes along the chosen profile. Each cable has 21 take-outs. The Terrameter SAS 4000 and the ES 464 were placed in the centre of the layout. The two cables were connected to the electrode selector (ES 464) at the centre of the layout. Take-out 1 and take-out 21 were made to overlap at the cable ends and in the layout centre. The serial port of the Terrameter was connected to the electrode selector. The electrodes were connected to all the take-outs at intervals of 5m on the electrode cables using cable jumpers. For a moist or soft ground, electrodes were just pushed into the ground by hand and then connected. However, hammering and wetting were done on dry and hard ground. The Terrameter was then connected to an external 12 volt battery and switched on, which automatically switches on the electrode selector and the system set-up which was echoed to the screen. The instrument was set to resistivity mode and LUND Imaging System was selected. Electrode test commenced immediately, and grounding improved for the electrodes with bad ground contact. The connectors were also checked for unsatisfactory electrode positions. Electrodes were tested pair-wise against each other starting from the outermost electrodes going towards the centre. The electrode test checks if it is possible to transmit current through all electrodes. This test takes a couple of minutes but saves time afterwards; because programme may stop depending on poor electrode contact. Measurement may also stop if the batteries for either the Terrameter or the electrode selector are low. The programme automatically continues to measure using the two electrode cables when the contact is satisfactory. It was ensured that measurements did not stop during the measurement period. As measurement continued apparent resistivity values were echoed on the screen. When measurement on each layout was finished, the programme was stopped and the Terrameter switched off. The cables were disconnected, wound up, and the electrodes and jumpers were all collected together. The instrument was then transferred to a new profile and

the entire process repeated until all the profiles were completed. While measuring the profiles, the positions of reference points along the lines were noted. The coordinates of the starting points, midpoints and end points along the profiles were noted to facilitate identification of points for further investigation (Table 3.1). Seven profiles were taken for the survey and seven VES points (Figure 3.2).

Table 3.1: Coordinates of points along the profiles.

Profile	Start point	Mid point	End point
1	N11 ⁰ 53' 32.9" E07 ⁰ 26' 41.2"	N11 ⁰ 53' 35.5" E07 ⁰ 26' 39.1"	N11 ⁰ 53' 31.1" E07 ⁰ 26' 34.9"
2	N11 ⁰ 53' 32.9" E07 ⁰ 26' 39.2"	N11 ⁰ 53' 35.3" E07 ⁰ 26' 29.5"	N11 ⁰ 53' 38.4" E07 ⁰ 26' 38.5"
3	N11 ⁰ 53' 32.4" E07 ⁰ 26' 38.5"	N11 ⁰ 53' 35.1" E07 ⁰ 26' 29.9"	N11 ⁰ 53' 38.0" E07 ⁰ 26' 36.4"
4	N11 ⁰ 53' 31.7" E07 ⁰ 26' 37.7"	N11 ⁰ 53' 34.9" E07 ⁰ 26' 37.2"	N11 ⁰ 53' 37.8" E07 ⁰ 26' 36.3"
5	N11 ⁰ 53' 31.3" E07 ⁰ 26' 37.5"	N11 ⁰ 53' 34.5" E07 ⁰ 26' 36.6"	N11 ⁰ 53' 37.4" E07 ⁰ 26' 35.5"
6	N11 ⁰ 53' 31.0" E07 ⁰ 26' 37.0"	N11 ⁰ 53' 34.2" E07 ⁰ 26' 36.1"	N11 ⁰ 53' 37.1" E07 ⁰ 26' 35.0"
7	N11 ⁰ 53' 38.5" E07 ⁰ 26' 38.6"	N11 ⁰ 53' 37.5" E07 ⁰ 26' 35.5"	N11 ⁰ 53' 36.7" E07 ⁰ 26' 32.4"

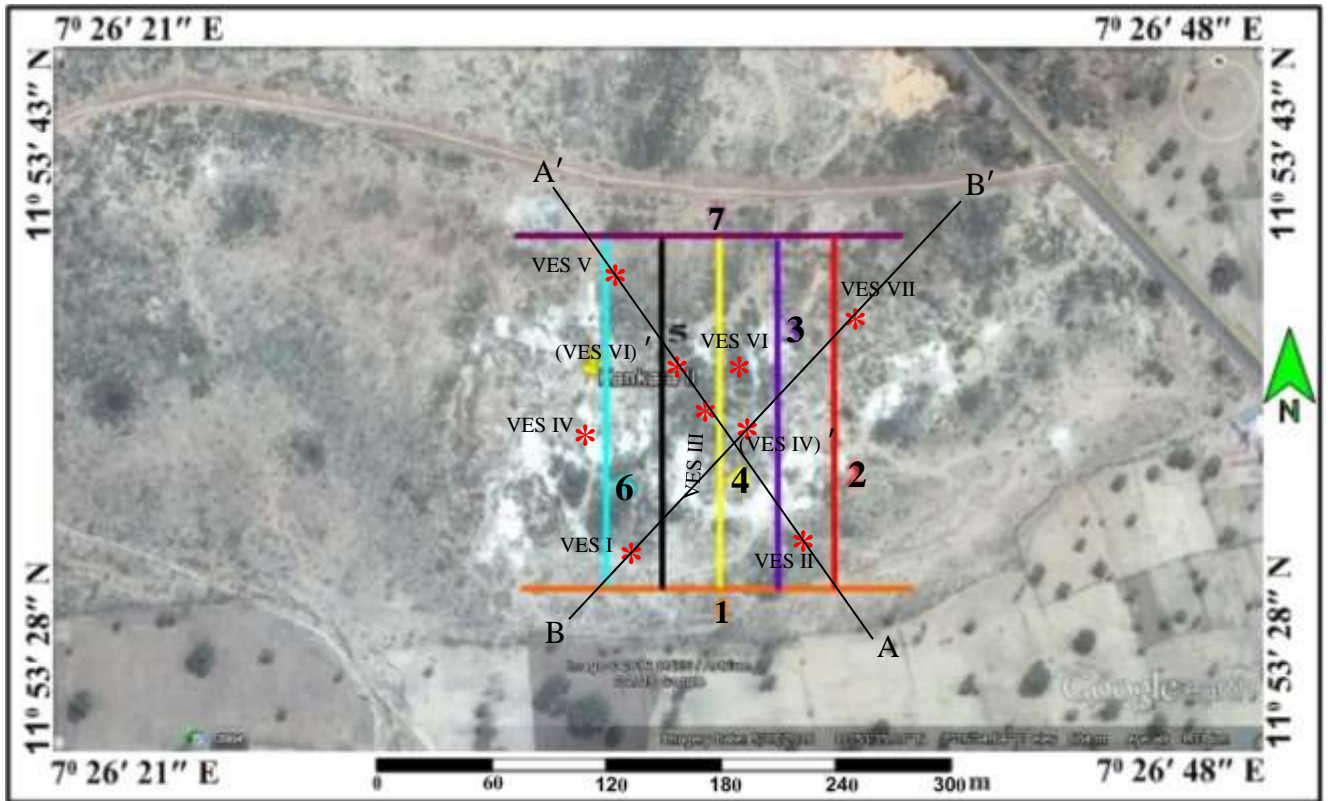


Figure 3.2: A map illustrating the 2-D profiles 1-7 layout and VES points VES 1-VII (Profiles AA' and BB'). Where VES point (VES VI)' were projected along profile AA' and VES point (VES IV)' were also projected along profile BB'.

3.6 Field Problems

Some of the problems encountered during the field measurement are:

- i. Draining of the battery during the field measurement slows down the measurement and the battery has to be recharged before continue taken the measurements or an alternative battery should be provided.
- ii. Poor contact between the electrodes and ground when the electrodes were hammered vertically into the ground.
- iii. Animals such as goats, sheep and cow moving around the field sometimes disrupted the measurements.
- iv. The practical difficulty in moving great length of cables and electrodes around.

CHAPTER FOUR: FIELD RESULTS AND INTERPRETATION

4.1 Introduction

In electrical resistivity tomography (ERT), prior information about unknown parameters (such as resistivity values and depth of the layers) are of paramount importance for inversion processing (Cardarelli and Fischanger, 2006). As in all other geophysical methods, the interpretation of data from electrical imaging involves expressing in geological terms the information given by the measured apparent resistivity data. Such an interpretation demands, on the one hand, considerable practical experience with the method and, on the other hand, a sound knowledge of the geology of the region under consideration (Loke, 1999). In this work, all the available geological information on the project area was taken into consideration to constrain the interpretations.

4.2 Data Processing Procedure

The raw field data were processed using RES2DINV (Loke and Barker, 1996). This is a computer programme that automatically determines a two-dimensional (2-D) resistivity model for the subsurface for the data obtained from electrical survey. It is a window based programme. This method is based on the following equation:-

$$(\mathbf{J}^T \mathbf{J} + \mathbf{uF})\mathbf{d} = \mathbf{J}^T \mathbf{g} \quad (4.1)$$

where $\mathbf{F} = \mathbf{f}_x \mathbf{f}_x^T + \mathbf{f}_z \mathbf{f}_z^T$

\mathbf{f}_x = horizontal flatness filter

\mathbf{f}_z = vertical flatness filter

\mathbf{J} = matrix of partial derivatives

\mathbf{u} = damping factor

d = model perturbation factor

g = discrepancy vector

The forward problem is solved through a finite difference algorithm, whose main features are a versatile user defined discretization of the domain and a new approach to the solution of the inverse Fourier transform. The forward modelling subroutine is used to calculate the apparent resistivity values. The inverse procedure is based on an iterative smoothness-constrained least-squares algorithm. This computer programme uses a smoothness constrained non-linear least-squares optimization inversion technique to convert measured apparent resistivity values to true resistivity values and plot them in cross-sections. The inversion process removes geometrical effects from the pseudosection and produces an image of true depth and true formation resistivity. One advantage of this method is that the damping factor and flatness filters can be adjusted to suit different types of data. The programme creates a resistivity cross-section, calculates the apparent resistivities for that cross-section, and compares the calculated apparent resistivities with the measured apparent resistivities. The iteration continues until a combined smoothness constrained objective function is minimized. The depth of investigation cannot be determined by simple calculations and it depends on the acquisition geometry, the conductivity structures and data errors (Oldenburg and Li, 1999). However, they have demonstrated through various modelling exercises that there is a loss of reliability in the inverted resistivity values at the bottom and ends of resistivity images where the resistivity values are least constrained by the data.

A common method for presentation of 2-D resistivity data is in the form of pseudosection. A pseudosection is made by plotting the data points in a diagram, using the length axis for the distance along the surveying line and the depth axis for the electrode separations (ABEM

LUND Instruction Manual, 2010). The distance for the electrode configuration midpoint is thus plotted against the electrode separation for each measured data point, letting the latter reflect the measurement depth. The corresponding apparent resistivities for the plotted points are then used to contour the variation in apparent resistivity along the surveying line. The pseudosection thus obtained reflects the variation of resistivity in the ground in a qualitative way, and approximate structures and depths to layer interfaces may be estimated. It should be noted that the pseudosection is simply a 2-D equivalence of the plotted field data points in a linear depth scale.

The 2-D model used by the programme divides the subsurface into a large number of rectangular blocks, to determine the resistivity of the rectangular blocks that will provide an apparent resistivity pseudosection that agrees with the actual measurements. Figure 4.1a shows an arrangement of the blocks loosely tied to the distribution of the data points in the pseudosection. The distribution and the size of the blocks are automatically generated by the programme, so that the number of blocks usually does not exceed the number of data points. The depth of the bottom row is set to be approximately equal to the median depth of investigation (Edwards, 1977) of the data points with the largest electrode spacing. Figure 4.1b shows an alternative arrangement with blocks of uniform width extending to the ends of the survey line.

The measured apparent resistivity data files for all the resistivity imaging survey lines were downloaded from the ABEM ES464 Terrameter to a flash drive. The flash drive was uploaded on a computer in which ABEM file conversion (SAS4000 Utilities) and RES2DINV application software have been installed. The SAS4000 Utilities software was used to convert

the original data file (in .s4k format) to the appropriate (.DAT format) input file readable by the inversion software RES2DINV.

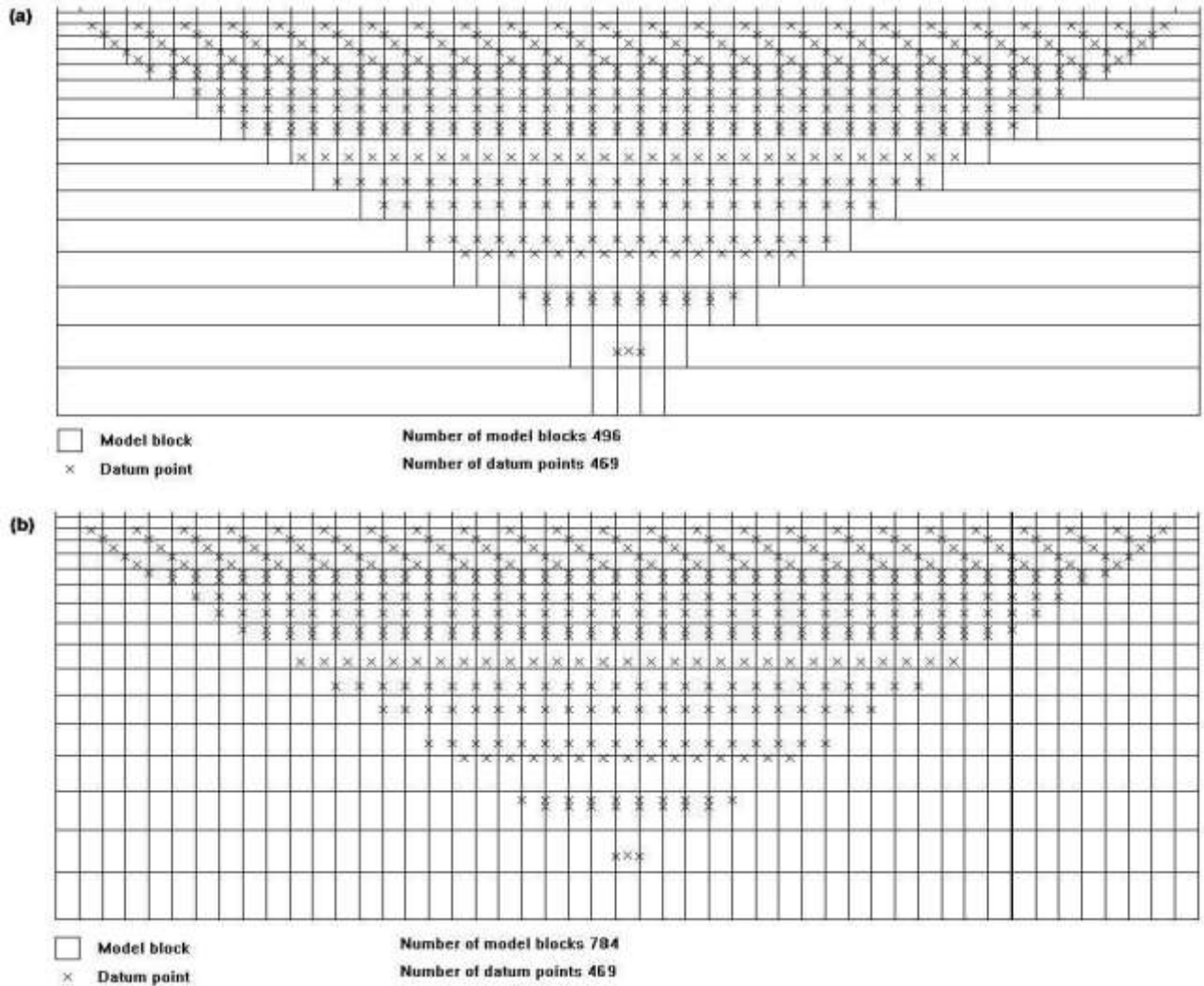


Figure 4.1: Two possible arrangements of the blocks used in a 2-D model together with the data points in the pseudosection (Edwards, 1977).

A total of seven files were converted. Each of the converted file represents a profile which was imported into the RES2DINV programme. It is worth noting that to get a good model, the data must be of equally good quality. Therefore the apparent resistivity data when viewed as a profile plot showing each data level were edited by eliminating or removing inherent (bad)

data points (example shown in Figure 4.2). Even though great care was taken during the survey, inherent bad data points were visible by their unique high or low values when compared to neighbouring data points. The bad data points might have been generated from sources such as; very poor ground contact at an electrode such that sufficient current could not be injected into the ground. Eliminating these data points were inevitable, otherwise they might influence the final output model. The inversion of the input data set for each profile was carried out (after satisfactory editing) with least-square inversion routine. The final outputs displayed after the inversion were the measured and calculated apparent resistivity pseudosections and the inverse model showing true depth and true formation resistivity.

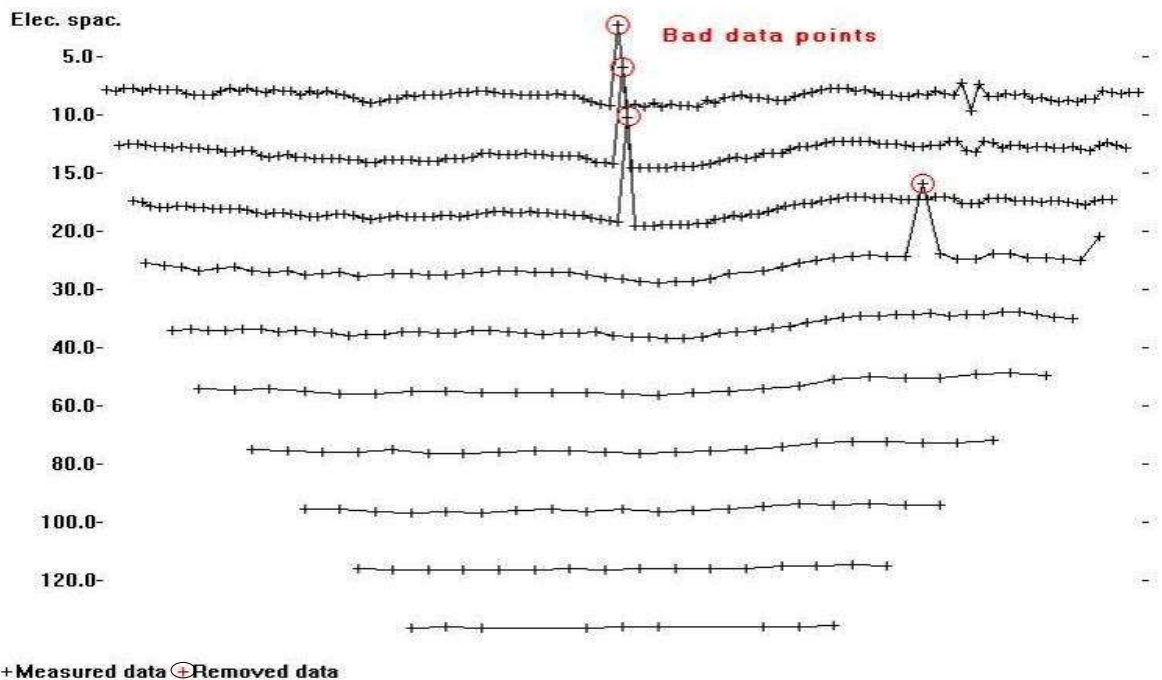


Figure 4.2 An example of a profile showing data set with a few bad data points.

4.3 Interpretation Technique

Interpretation of resistivity data consists of two steps: a physical interpretation of the measured data, resulting in a physical model, and a geological interpretation of the resulting physical

parameters (Dahlin, 2001). The large-scale VES data were interpreted with the state of the art interpretation technique, called the 2-D smoothed damped least-squares inversion algorithm. The results obtained based on 2-D inversion of field data and borehole information, were interpreted to determine the depth and extent of shallow bedrock, thickness of overburden, aquifer, *etc.* In interpreting LUND Imaging data, computer assistance is needed due to the large amount of data collected from the field.

4.4 Geological Control

A good knowledge and use of the geology of an area is very important for any meaningful interpretation of any geophysical data. Therefore, in this research work, informations obtained from previous works and borehole log within the area of survey were taken into consideration in the course of interpretation.

4.5 Geologic Section from Borehole Data

Boreholes are a necessary and reliable source of primary data and the electrical resistivity imaging interpretations provide secondary information. Although borehole log data provides good sample for a six-inch diameter vertical cylindrical volume, it can be a poor representation of the several square metres surrounding the borehole. Alternatively, electrical resistivity imaging provides block averages of resistivity. Also, borehole data can be a more expensive data acquisition method when compared to ERI survey. The 2-D inversion results of the survey were correlated with the lithology information obtained from the boreholes in Garaji village and Unguwar Nagamda. A complete set of borehole logs used in this research can be found at Rural Water Supply and Sanitation Agency (RUWASSA), Katsina State, Nigeria. The geological well-log (Figure 4.3) of Garaji village obtained from RUWASSA, shows that the topsoil in the village is dark brown sandy soil which may be up to 6m thick in

the area. The layer below this is about 13m thickness and consists of sandy clay. These two layers overlay the weathered basement rock, which consists of feldspar, quartz, with mica from the depth of about 19m to 37m, the fresh basement rock were not revealed by the borehole log.

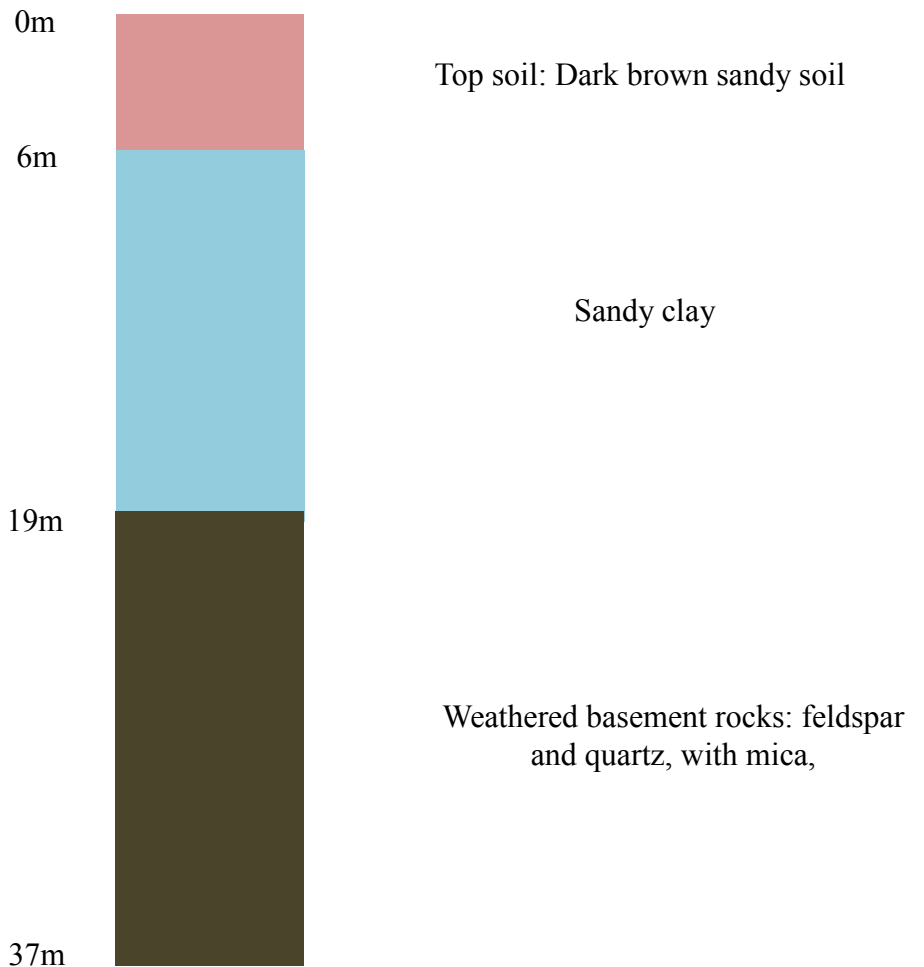


Figure 4.3: Geological Well-Log of Garagi (Kankara Local Government Area) obtained from RUWASSA, Katsina (2014).

The second of these logs is that of a borehole in Unguwar Nagamda obtained from RUWASSA (see Figure 4.4) and shows an overburden made up of two layers of 12m thick. The first layer is composed of light brown top sandy soil of 5m thick. The second layer is

made up of medium grained quartz grains and clay of about 7m thick. The weathered basement rock lies immediately beneath the overburden and it is from about 12m depth downwards to 43m, consisting of loose biotite-mica, feldspar and quartz. The fresh basement rock was not revealed by the borehole log.



Figure 4.4: Geological Well-Log of Unguwar Nagamda (Kankara Local Government Area) obtained from RUWASSA, Katsina (2014).

4.6 Typical Resistivity Values from Previous Work

Also resistivity values obtained from previous work close to the study area have been used to correlate the results of the present survey, and these are considered in this section.

Representative resistivity values of earth materials in the study area were derived from the work of Michael (1977). The representative resistivity values presented in Table 4.1 have been compiled as a guide for the present work.

Table 4.1 Typical Resistivity values compiled from previous work (Michael, 1977).

S/N	Rock type	Resistivity (Ωm)
1	Pure Kaolin	20 – 50
2	Kaolinite Clay (contaminated)	50 – 100
3	Micaceous clay and sand with some patches of Kaolinitic clay	120 – 150
4	Clay mottled micaceous clay (lateritic)	200 – 400
5	Mica schist	> 600

4.7 Field Results

The 2-D electrical resistivity images of the earth's subsurface along seven profiles were obtained for this research work within the study area. Five of them, profiles 2, 3, 4, 5 and 6, are along North to South moving in the west direction of the survey area while profiles 1 and 7 are along East to West direction of the survey area (see Figure 3.6). The inversion results depict the images of the geoelectric sections obtained from the processed data. The result shows three images for each profile. The upper image is a plot of the measured apparent resistivity pseudosection which is obtained by plotting the observed apparent resistivity data against the depth with colour infill instead of line contours. The middle image is the calculated apparent resistivity pseudosection obtained by plotting the calculated apparent resistivity data

against the depth with colour infill instead of line contours. The Third image is the resistivity model obtained after a definite number of iterations of the inversion programme. The resistivity model shows variation in the geologic properties of the subsurface, which is in relation to the measured resistivity with scales shown at the lower end of each, the side bar shows the depth below the subsurface with a maximum depth of about 39.4m and the lateral distance is shown above the section; each profile starts from 5m to 205m. In addition, Figure 4.5 shows the types of colours used in the interpretation of 2-D results.



Figure 4.5: Types of colours used in the interpretation of 2-D results.

4.7.1 Result of Profile One

Figure 4.6 shows the resistivity inversion results for profile 1 with 3 iterations and 2.7% absolute error. This shows measured apparent resistivity pseudosection (a), the calculated apparent resistivity pseudosection (b) and the inverse model resistivity section (c), of profile 1. The 200m long profile runs East to West direction. The inverse resistivity model shows a very thick layer with dark blue, blue and light blue colours having resistivity values ranging from about $17\Omega\text{m}$ to $147\Omega\text{m}$; the layer covers almost all the entire profile from the surface (1m) to a depth of about 35m around the centre of the profile. This layer is saturated with water consisting of the top sandy clay soil, clay and sandy clay. Also, within this layer dark blue colour emerges which reveals very low resistivity section from about $17\Omega\text{m}$ to $35\Omega\text{m}$. This section may indicate the presence of groundwater because of the low resistivity values. This profile shows a close correlation with the borehole log data obtained from Rural Water Supply and Sanitation Agency (RUWASSA, 2014).

Underneath the top layer, reveals the weathered basement rock consisting biotite-mica, feldspar and quartz having light blue, sky blue, green and dark green colours which occurred from a depth of 28.5m to 39.4m around the centre of the profile and extends between 90m to 129m along the profile, having resistivity values between $90\Omega\text{m}$ to $608\Omega\text{m}$. Underlying this layer is a zone with light green, yellow, tan, orange, red, dark red and plum colours which indicate high resistivity ranging from about $608\Omega\text{m}$ to $5129\Omega\text{m}$ and above between 114m to 125m horizontally along the profile and from the depth of 36m downwards, this zone indicates the fresh basement rock with high resistivity values.

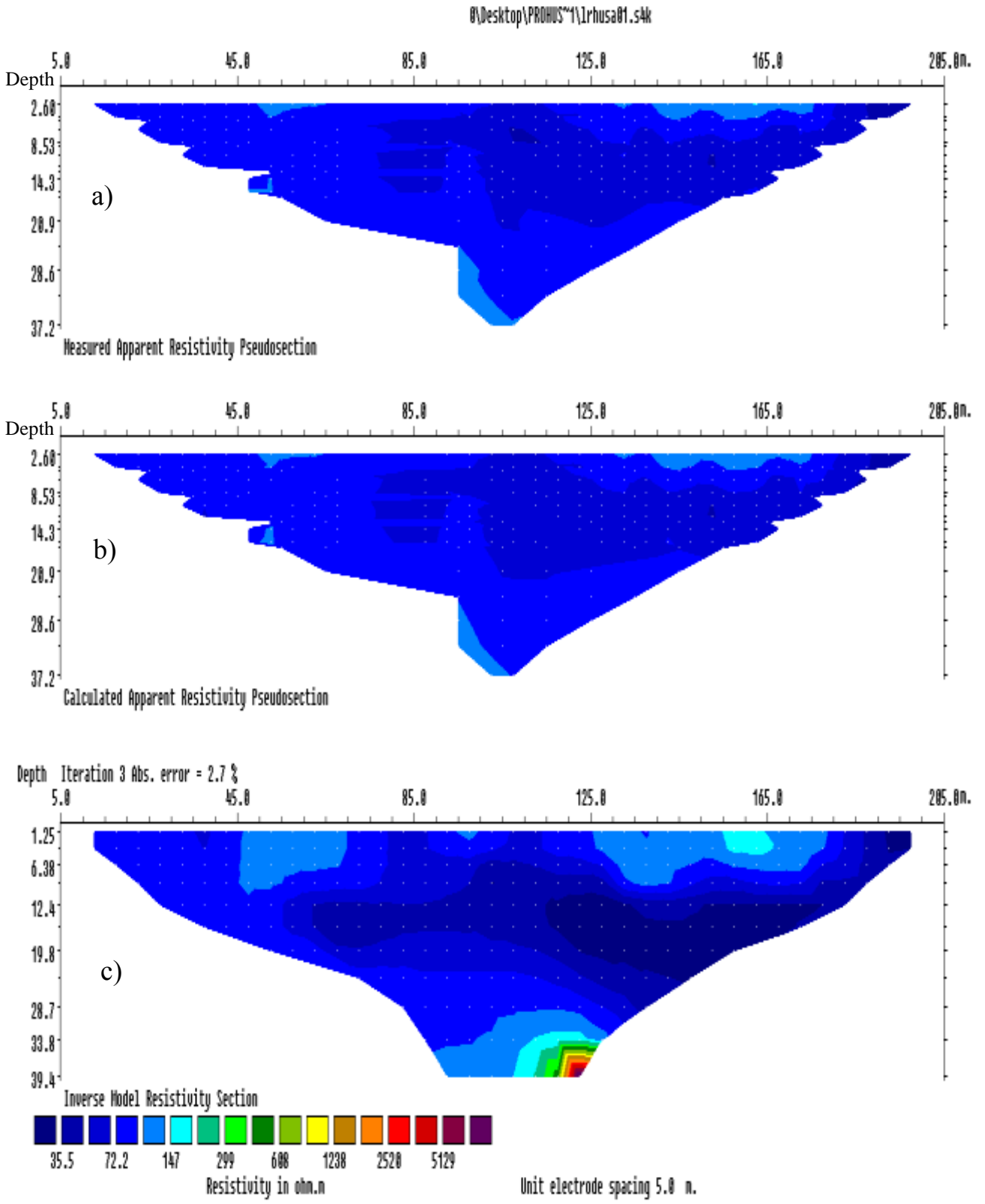


Figure 4.6: Result of 2-D inversion of the Wenner-Schlumberger array data along profile 1.

4.7.2 Result of Profile Two

Figure 4.7 shows the resistivity inversion results for profile 2 with 3 iterations and 5.6% absolute error. This shows measured apparent resistivity pseudosection (a), the calculated apparent resistivity pseudosection (b) and the inverse model resistivity section (c), of profile 2. The 200m long profile runs South to North direction and is perpendicular to profiles 1 and 7. The resistivity model shows a surface layer with resistivity ranging from about 76 Ω m to 270 Ω m with variable thicknesses from 4m to 16m having green, dark green, light green, yellow and tan colours. This consists of clay and sandy clay. Underneath this layer at the depth of 7m to 18m, between 47m to 73m along the profile, low resistivity values of 26 Ω m to 45 Ω m with blue and light blue colours was observed, this section may be saturated with water. Between 128m to 157m along the profile at the depth of about 16.5m downwards with dark blue and blue colours having low resistivity values ranging from about 6 Ω m to 35 Ω m, which indicates that, is the aquiferous layer dipping down and this information shows a close correlation with the borehole log data. Also, low resistivity stratum of 45 Ω m to 76 Ω m was encountered having sky blue and green colours with variable thickness dipping down and extending from about 38m to 173m along the profile. This stratum is very thick and likely to be white Kaolin and mottled Kaolin extending downwards with variable thicknesses.

Between 135m to 180 m along the profile from 1m to a depth of about 12m with red, dark red and plum colours having very high resistivity value from about 370 Ω m and above, this section represent void, with hole on the surface, because void is attributed with high resistivity value if it is not filled water (meaning it is filled with air). At the depth of 14m to 39m around the centre of the profile between 95m to 124m along the profile, weathered basement rock was encountered inform of an intrusion with green, dark green, light green and yellow colours

consisting biotite-mica, feldspar and quartz, having resistivity values between $76\Omega\text{m}$ to $218\Omega\text{m}$.

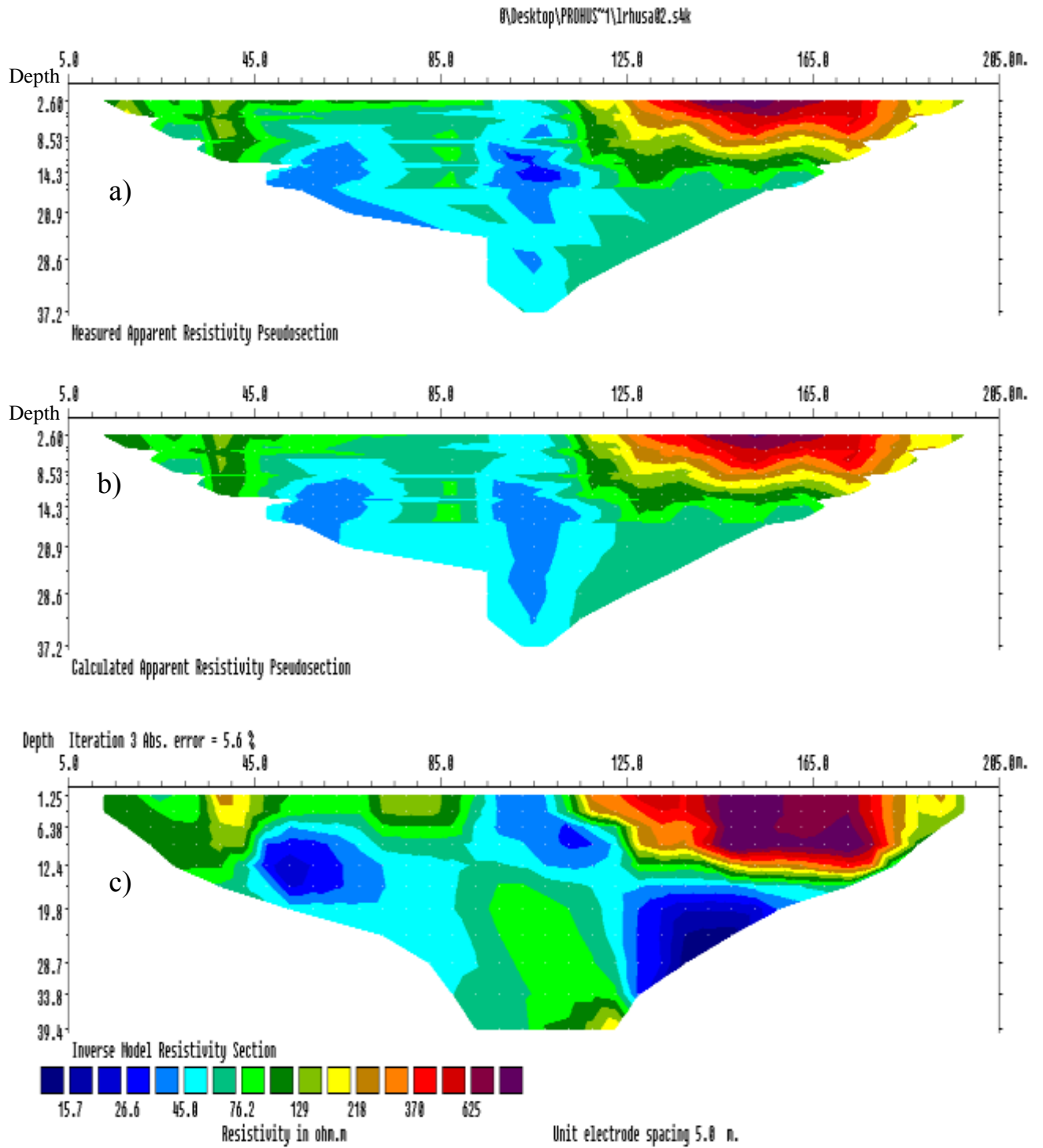


Figure 4.7: Result of 2-D inversion of the Wenner-Schlumberger array data along profile 2.

4.7.3 Result of Profile Three

Figure 4.8 shows the resistivity inversion results for profile 3 with 3 iterations and 10.3% absolute error. This shows measured apparent resistivity pseudosection (a), the calculated apparent resistivity pseudosection (b) and the inverse model resistivity section (c), of profile 3. The 200m long profile runs South to North direction with separation of 20m from profile 2. The resistivity model reveals a thick layer of high resistivity ranging from about 94 Ω m to 360 Ω m having green, dark green, light green and yellow colours from 25m along the profile to the end with variable thicknesses ranging from 11m to 14m from the surface. This layer consists of top soil, clay and dark brown sandy clay with some patches of laterite with yellow and tan colours below 38m, 80m, 103m and 125m marks along the profile. Underneath this stratum, there is occurrence of low resistivity section with sky blue and green colours having resistivity values ranging from about 48 Ω m to 94 Ω m between the distances 43m to about 160m along the profile with variable thicknesses from the depth of about 10m to 24m below 75m mark and from the depth of about 8m to 39m beneath 100m mark around the centre of the profile, the stratum become thin at the depth of 20m beneath 150m mark along the profile. This very thick layer is the mixture of white Kaolin, mottled weathered Kaolinite and mottled clay.

At the depth of 18m downwards, between 120m to 155m along the profile low resistivity zone was encountered having dark blue, blue and light blue colours bounded by resistivity values ranging between 6 Ω m to 48 Ω m, which reveals that is groundwater trapped in aquifer which extend downwards. This result shows a close correlation with the borehole log data. Also, between 133m to 180m along the profile to the depth of 16m from the surface, very high resistivity section with tan, orange, red and dark red colours was observed bounded by

resistivity values ranging from about $359\Omega\text{m}$ to $1362\Omega\text{m}$ and above, this section represent a void created by the local miners in search of Kaolin. Weathered basement was encountered in the form of an intrusion having green colour consisting of biotite-mica, feldspar and quartz at the distances 103m to 116m from a depth of 28.5m to 39.4m with resistivity values ranging from $94\Omega\text{m}$ to $140\Omega\text{m}$ was observed.

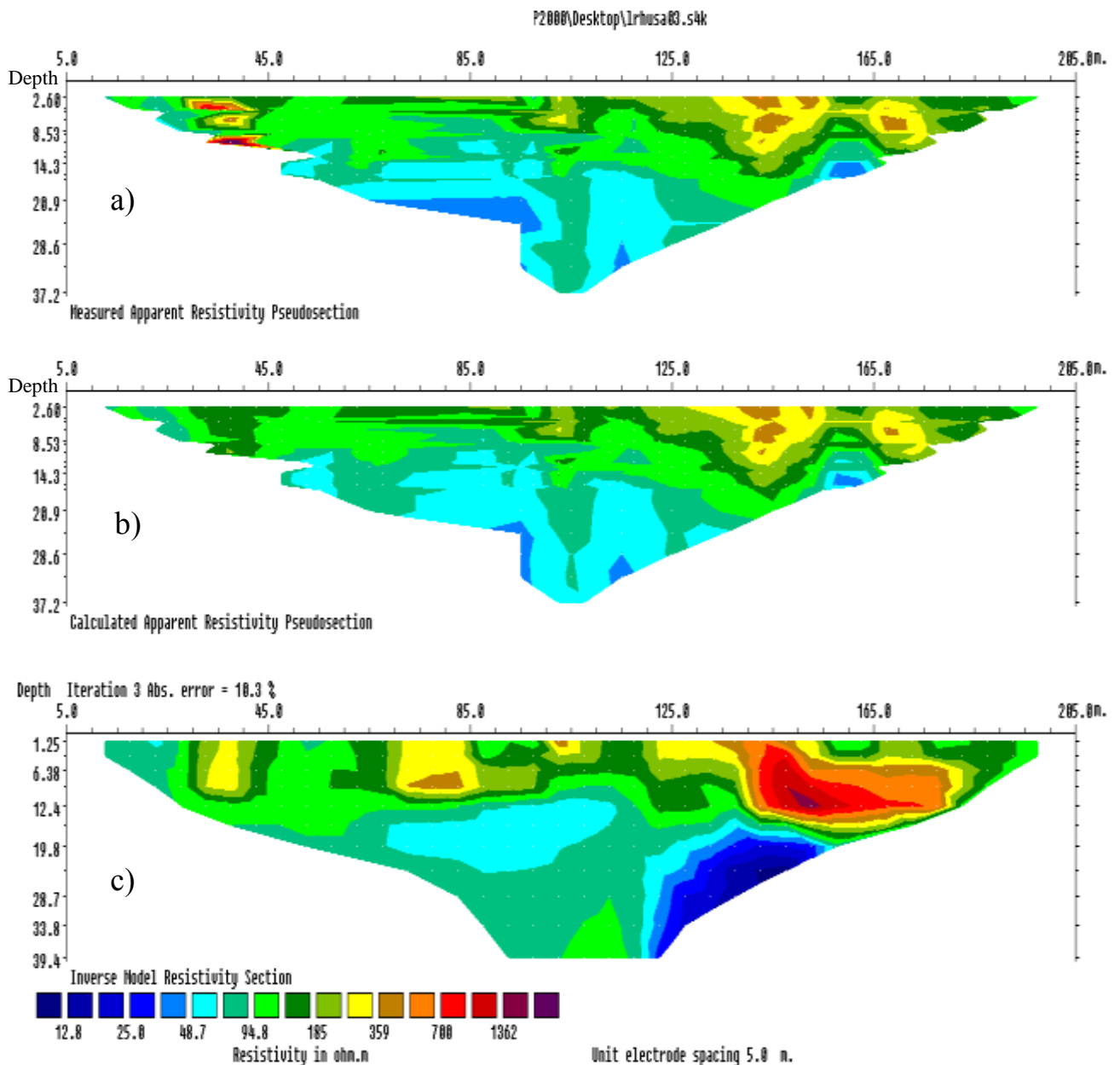


Figure 4.8: Result of 2-D inversion of the Wenner-Schlumberger array data along profile 3.

4.7.4 Result of Profile Four

Figure 4.9 shows the resistivity inversion results for profile 4 with 3 iterations and 5.0% absolute error. This shows measured apparent resistivity pseudosection (a), the calculated apparent resistivity pseudosection (b) and the inverse model resistivity section (c), of profile 4. The 200m long profile runs South to North direction with separation of 20m from profile 3. The resistivity model reveals a section having red, dark red and plum colours with high resistivity between 262 Ω m to 412 Ω m and above between 115m to 155m along the profile to depth of 13m from the surface interpreted as a void with hole on the surface. Green, dark green, light green, yellow and tan colours between 13m to 60m along the profile to a depth of 13m from the surface below 60m mark, emerge a high resistivity layer of about 66 Ω m to 190 Ω m, this layer is very thick ranging from the top of the profile and it extend to the end of the profile and dipping down to around the centre of the profile beneath 85m, 100m, 110m, 125m and 160m marks to 39.4m depth. This layer consists of dark brown top sandy clay, clay and saturated sandy clay. But, between 64m to 115m along the profile also high resistivity of 195 Ω m to 412 Ω m was observed having orange and red colours with thickness of about 9m from the surface consisting of top soil with laterite.

Also, dark blue, and light blue colours was observed between 117m to 153m along the profile from the depth of 12.5m downwards with low resistivity ranging from about 7 Ω m to 42 Ω m, this section of low resistivity extend downwards, which shows is the aquiferous layer. This result shows a close correlation with the borehole log data. There is an occurrence of low resistivity layer with sky blue and green colours between 26m to 103m along the profile from the depth of about 9.5m beneath 35m mark, the layer slopes down to around the centre of the profile with resistivity values ranging from 42 Ω m to 66 Ω m.

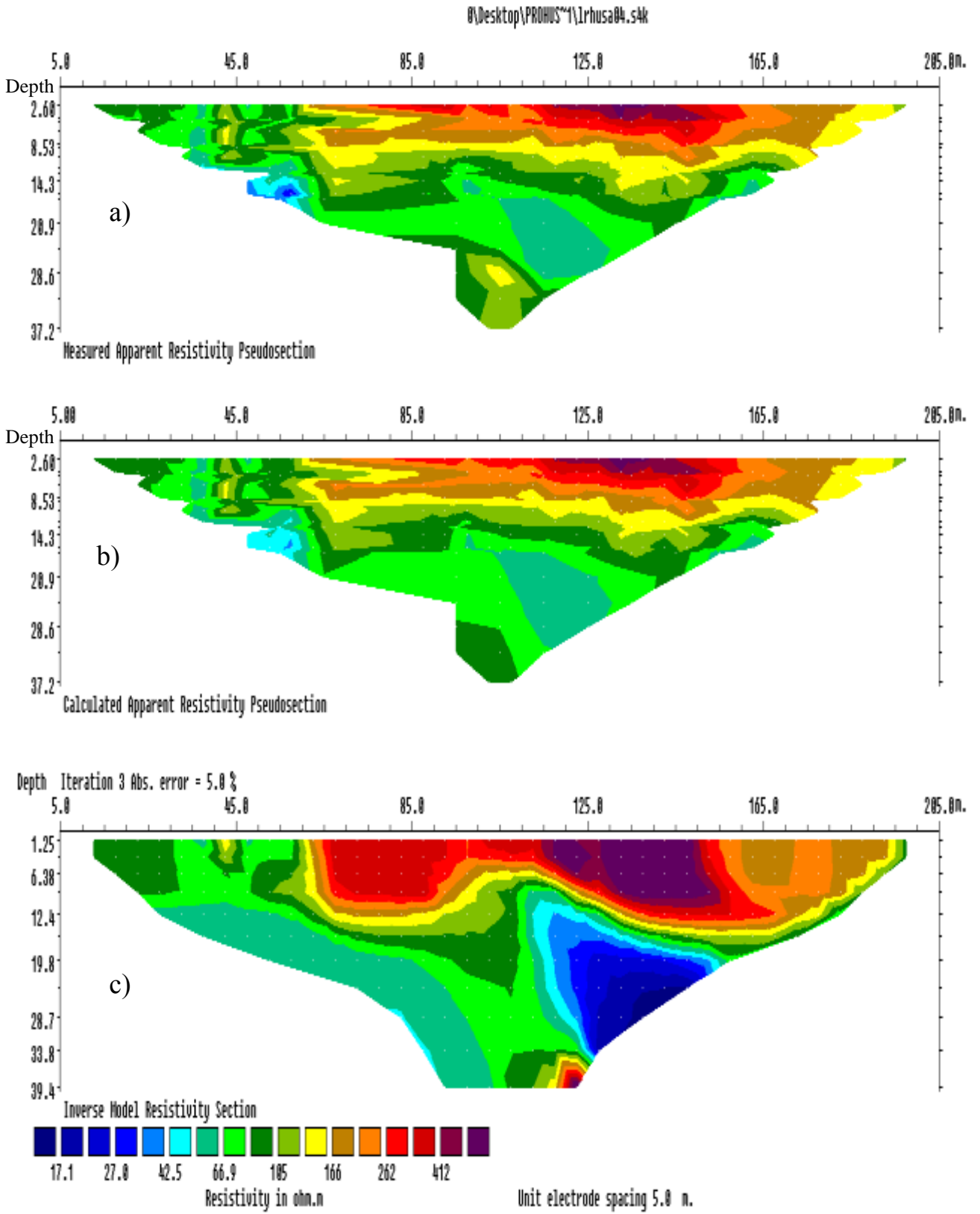


Figure 4.9: Result of 2-D inversion of the Wenner-Schlumberger array data along profile 4.

Also, another layer emerges in form of ring with the same resistivity values and colours (42 Ω m to 66 Ω m, sky blue and green colours) between 112m to 155m along the profile to the depth of about 33.8m below 125m mark. These two sections of layers consist of white Kaolin and mottled Kaolin.

High resistivity section having yellow, tan and orange colors was noticed with resistivity values from 135 Ω m to 262 Ω m from the depth of about 34.5m downwards, between 115m to 125m along the profile representing weathered basement rock. Whereby, beneath this section also, high resistivity was observed representing fresh basement rock extending downwards with resistivity values ranging from 262 Ω m to 412 Ω m and above between 119m to 124m from the depth of 35.5m, with red and plum colors.

4.7.5 Result of Profile Five

Figure 4.10 shows the resistivity inversion results for profile 5 with 3 iterations and 4.2% absolute error. This shows measured apparent resistivity pseudosection (a), the calculated apparent resistivity pseudosection (b) and the inverse model resistivity section (c), of profile 5. The 200m long profile runs South to North direction with separation of 20m from profile 4. The resistivity model reveals two sections with high resistivity anomaly ranging from about 200 Ω m and above having red, dark red and plum colours between 73m to 118m along the profile to the depth of 13m and between 138m to 183m horizontally along the profile to the depth of 13m again. These two sections with high resistivity indicate air filled voids.

Green, dark green, light green, yellow and tan colours was observed between 13m to 68m along the profile to the depth of 14.5m from the surface having resistivity values ranging from 60 Ω m to 160 Ω m, this thick layer which consists of top soil, dark brown sandy clay with intercalation of clay (between 48m to 64m marks to the depth of 6m from the surface and also between 122m to 133m marks along the profile to the depth of 5m from the surface with resistivity value between 35 Ω m to 60 Ω m, having light blue, sky blue and green colours), this layer also moves across the profile and below 85m mark from the depth of 13.5m, the layer also extend downwards to around the centre (up to 39.4m depth) of the profile and to the end of the profile too, with variable thicknesses beneath 120m, 135m and 190m marks along the profile. Patch of laterite with saturated sandy clay was observed having light green, yellow, tan and orange colours between 34m to 49m along the profile to the depth of about 9.5m from the surface with resistivity values between 110 Ω m to 200 Ω m.

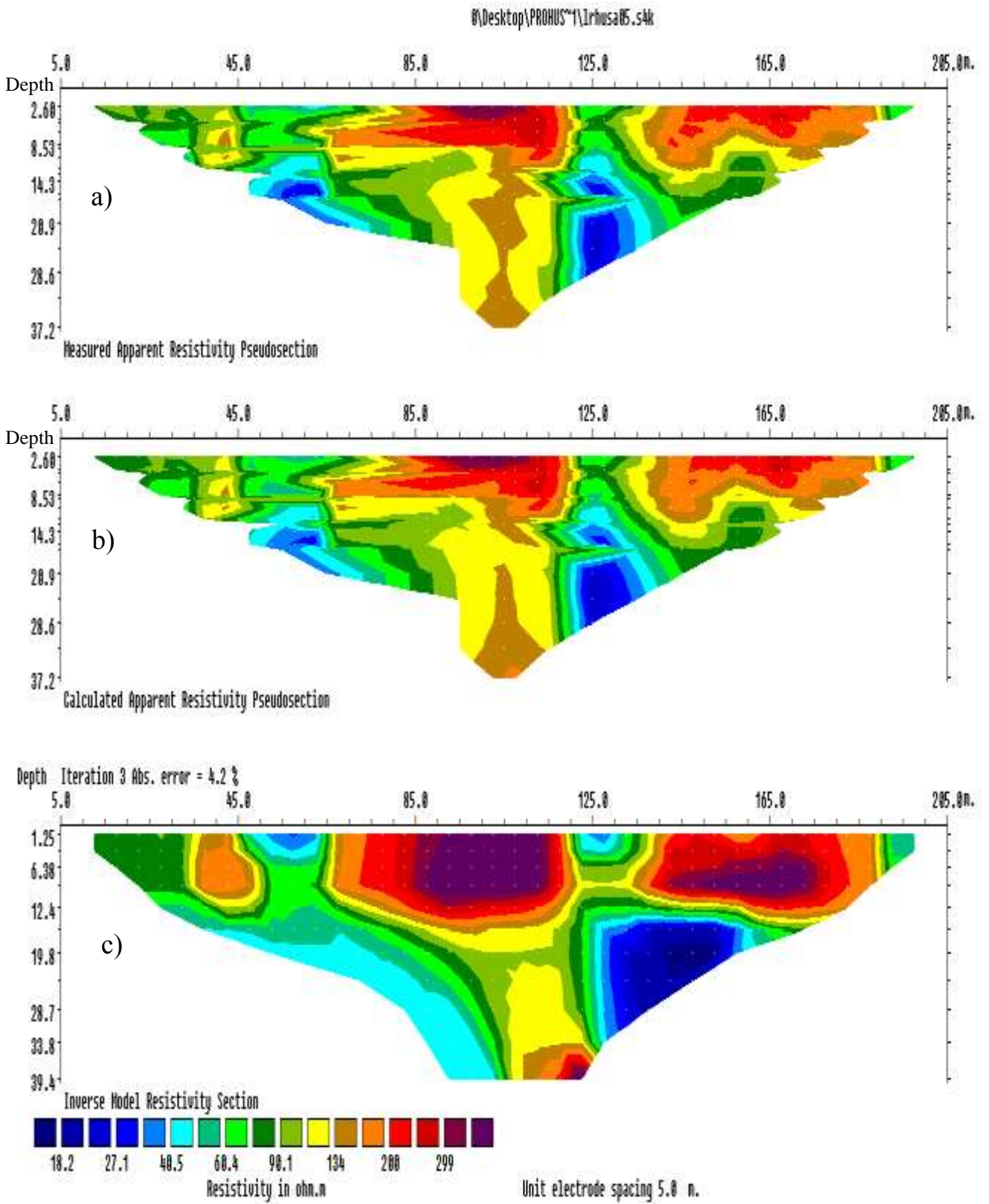


Figure 4.10: Result of 2-D inversion of the Wenner-Schlumberger array data along profile 5.

At the depth of 14m and below, between the distance 123m to 159m along the profile, dark blue, blue and light blue colours was observed with low resistivity values from about 5 Ω m to 40 Ω m. This low resistivity section dipping down is the aquiferous layer. This information shows a close correlation with the borehole log data. The model also, reveals a layer with sky blue and green colours bounded by resistivity values ranging from 40 Ω m to 60 Ω m between 28m mark from the depth of about 12m to 103m mark, this layer slopes down to 39.4m. Again, another layer appeared with the same resistivity values and colours (40 Ω m - 60 Ω m) between 124m to 165m marks along the profile with variable thicknesses in form of ring interpreted as Kaolin with mottled Kaolin strata.

Yellow, tan and orange colours represent weathered basement rock inform of an intrusion with resistivity values ranging from about 115 Ω m to 200 Ω m from the depth of 20m downwards below 110m mark. Beneath this layer is the fresh basement rock with red and plum colors from the depth of 35m downwards, between 117m to 124m along the profile, with very high resistivity anomaly ranging from 200 Ω m and above.

4.7.6 Result of Profile Six

Figure 4.11 shows the resistivity inversion results for profile 6 with 3 iterations and 4.0% absolute error. This shows measured apparent resistivity pseudosection (a), the calculated apparent resistivity pseudosection (b) and the inverse model resistivity section (c), of profile 6. The 200m long profile runs South to North direction with separation of 20m from profile 5. The inverse resistivity model reveals a layer having green, dark green, light green, yellow, tan and orange colours with high resistivity anomaly between $80\Omega\text{m}$ to $251\Omega\text{m}$ between 13m to the end of the profile with variable thicknesses ranging from 8m to 12m from the surface, the layer extend downwards to around the centre of the profile to the depth of 39.4m. This very thick layer consists of top soil, dark brown sandy clay, saturated sandy clay and clay. Two patches of laterite was observed having red colour between 63m to 95m marks along the profile to the depth of 7m from the surface and between 104m to 124m marks along the profile to the depth of 5m from the surface with resistivity values ranging from $251\Omega\text{m}$ to $367\Omega\text{m}$.

There is also an occurrence of small section of high resistivity between distances on the profile from about 148m to 165m from a depth of 4m to 10m; this high resistivity section indicate void, with red, dark red and plum colours bounded by resistivity value ranging from about $300\Omega\text{m}$ and above. There is also, a section representing blue and light blue with low resistivity values ranging from about $37\Omega\text{m}$ to $55\Omega\text{m}$, from the depth of 11m to 39m, this section extends along the profile and slopes down beneath 85m mark and below 100m mark to 39.4m depth around the centre of the profile. The low value of resistivity indicates that the layer is clay which is saturated with water.

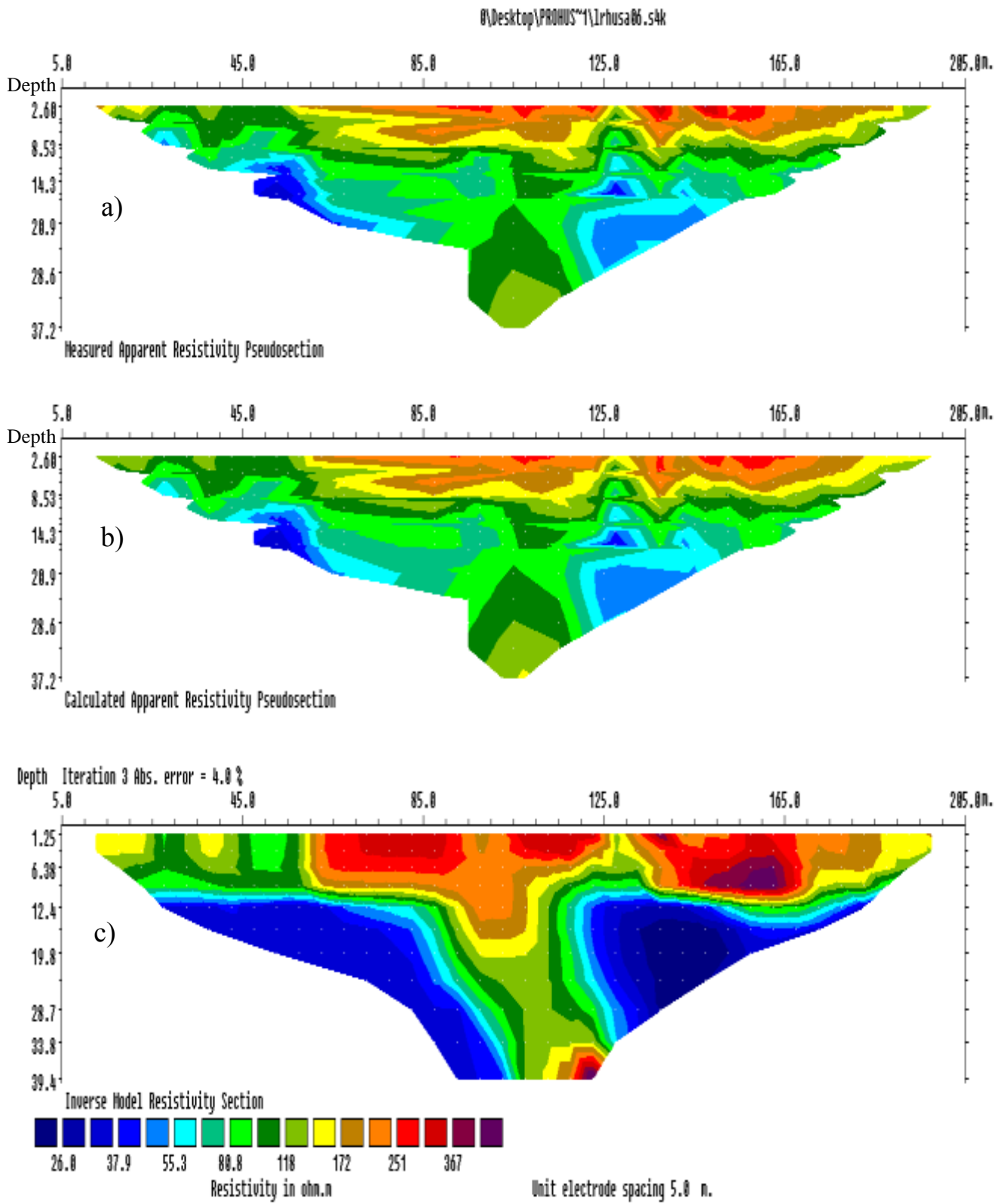


Figure 4.11: Result of 2-D inversion of the Wenner-Schlumberger array data along profile 6.

Between 123m to 184m along the profile from the depth of 11.5m downwards, low resistivity zone was observed with resistivity values ranging from 12 Ω m to 55 Ω m. This zone having dark blue and light blue revealed to be aquiferous layer extending downwards. This result shows a close correlation with the borehole log data. Above this section zone, there is a thin layer with sky blue and green colours having variable thicknesses bounded by low resistivity values ranging from 55 Ω m to 80 Ω m between 117m to 185m from the depth of about 10m below 120m mark. Also, another thin layer with the same resistivity values emerges from the depth of about 10m, between 24m mark along the profile extending to 85m mark and slopes down to 39.4m depth beneath 103m mark. These two sections with the same resistivity values consist of Kaolin and mottled Kaolin with variable thicknesses.

Yellow, tan and orange colors representing weathered basement rock emerges from the depth of 34m downwards between 118m to 125m along the profile consisting of biotite-mica, feldspar and quartz with resistivity values ranging from about 145 Ω m to 251 Ω m, beneath this layer is the fresh basement with resistivity values from 251 Ω m to 367 Ω m and above having red and dark red colours.

4.7.7 Result of Profile Seven

Figure 4.12 shows the resistivity inversion results for profile 7 with 3 iterations and 5.2% absolute error. This shows measured apparent resistivity pseudosection (a), the calculated apparent resistivity pseudosection (b) and the inverse model resistivity section (c), of profile 7. The 200m long profile runs East to West direction. The inverse resistivity model reveals a layer with high resistivity anomaly between $96\Omega\text{m}$ to $285\Omega\text{m}$ with green, dark green, light green and yellow colours between 13m to a distance of 144m along the profile with a thickness of 8.5m from the surface and at a distance of 155m to 174m along the profile with thickness of 6.5m from the surface which constitutes the overburden, this layer is made up of dark brown sandy clay, clay and some patches of laterite soil are seen at a distance of 37m to 63m and 19m to 28m with a thickness of 4.5m from the surface, with resistivity values from about $210\Omega\text{m}$ to $415\Omega\text{m}$.

Underneath this layer from the depth of about 7m to 15m below 55m mark, layer with sky blue and green colours was encountered with variable thicknesses and it extend from 21m to 194m along the profile bounded by resistivity ranging from $56\Omega\text{m}$ to $97\Omega\text{m}$. This layer indicates Kaolin with mottled Kaolin stratum. Underlying this stratum is a moderately low resistive layer with dark blue, blue and light blue colours from a depth of about 11m to 39m around the centre of the profile with resistivity values ranging from about $7\Omega\text{m}$ to $45\Omega\text{m}$. This reveals that, the layer is saturated with water and is an indication that is groundwater trapped in the aquifer around the centre of the profile and this information shows a close correlation with the borehole log data.

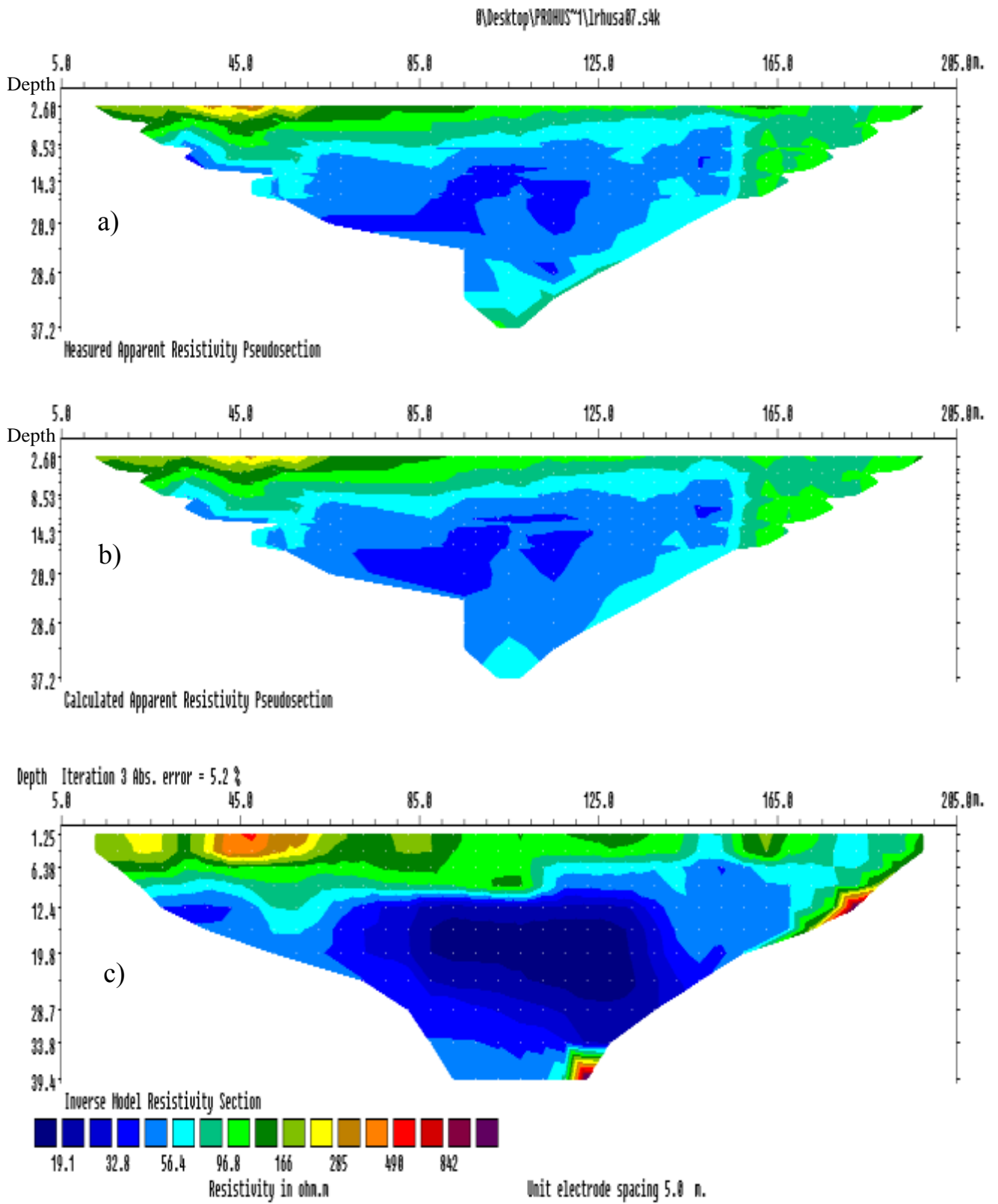


Figure 4.12: Result of 2-D inversion of the Wenner-Schlumberger array data along profile 7.

Underneath this stratum, between about 88m to 126m distance along the profile from the depth of 34m to 39m, zone having sky blue, green, dark green, yellow, tan and orange colours with resistivity anomaly ranging from 56 Ω m to 490 Ω m was observed. This zone is the weathered basement rock consisting feldspar, quartz and biotite mica. At the depth of 36.5m red and dark red colors was observed between 118m to 124m emerges fresh basement rock with very high resistivity values from 285 Ω m to 842 Ω m and above. This section extends downward to 39.4m depth and beneath.

4.7.8 Merging of the profiles for the detection of continuity of the subsurface structures

The resistivity model of the profiles laying in the east - west direction and those in the south - north direction are depicted in Figures 4.13 to 4.19 respectively. This is done to enable the check for continuity and strike of the subsurface structures.

4.7.8.1 Continuity of structures

It is assumed that structures or stratum cannot end abruptly within a basin of deposition, but must feather out, or extend across the width of the basin and terminate against older rocks. According to Nicolas Steno principle lateral of continuity “ It states that the principle of original lateral continuity proposes strata originally extended in all directions until they thinned to zero or terminated against the edges of their original basin of deposition.” This was the third of the principles of Nicolas Steno (Dott and Batten, 1976).

The resistivity models of all the 7 profiles are shown in Figures 4.13 to 4.19. Based on the interpretation of the data, the resistivity models have revealed that there is continuity of Kaolin layers from profiles 2, 3, 4, 5 and 6; the layers of Kaolin having resistivity values between 40 Ω m to 94 Ω m in these profiles are extending from east to west direction. But in case of profiles 1 and 7, revealed that there is continuity of Kaolin layers only on profile 7 which is

located in the northern part of the survey area with resistivity values between $56\Omega\text{m}$ and $96\Omega\text{m}$ having sky blue and green colours (see Figures 4.11 to 4.17 for more detailed view). This means that, in all the 7 profiles, the Kaolin layers having resistivity value ranging between $40\Omega\text{m}$ and $96\Omega\text{m}$ extends from east to west and in the north direction within the survey area but not in the south direction (profile 7).

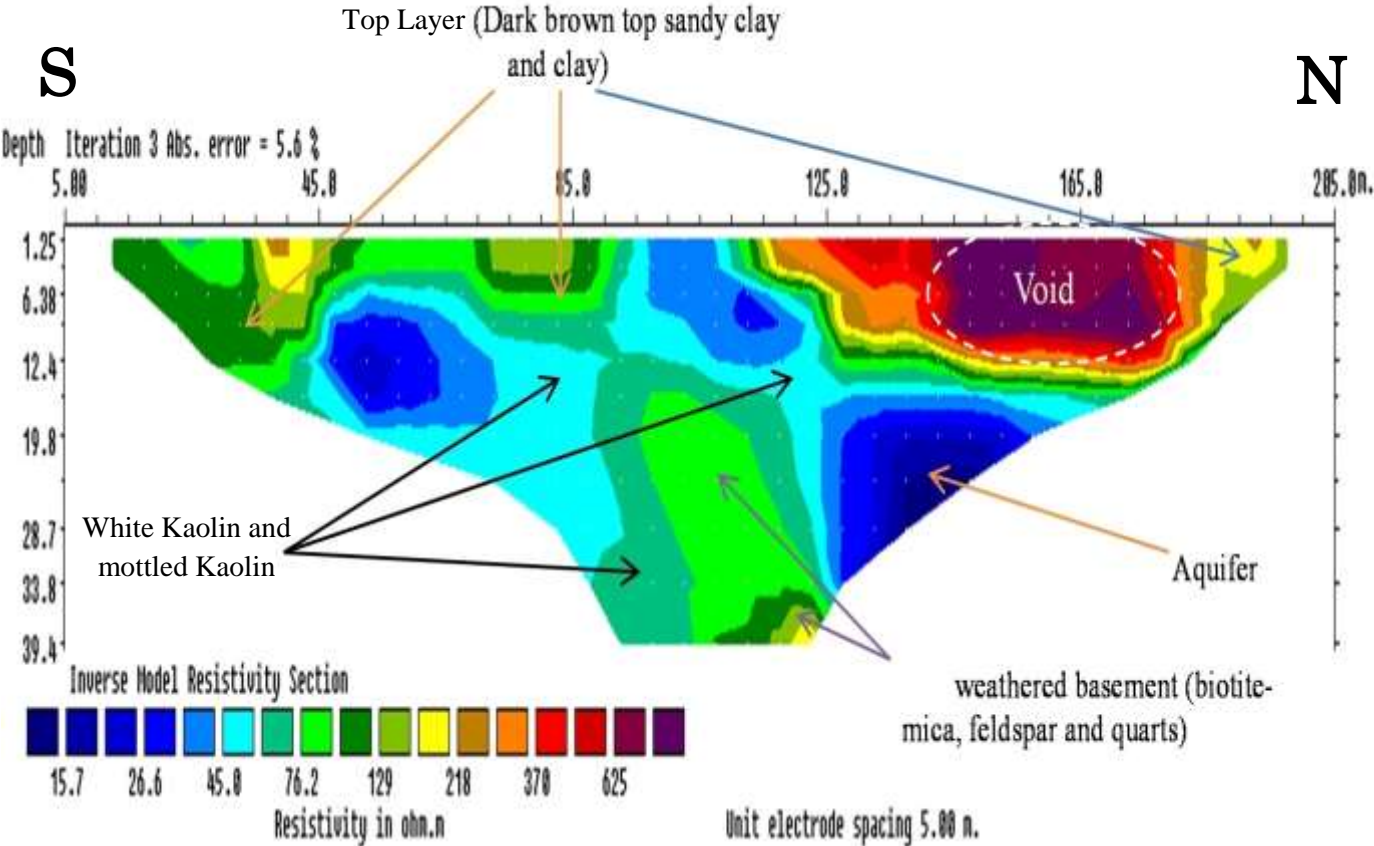


Figure 4.13: Inverse resistivity model of profile 2.

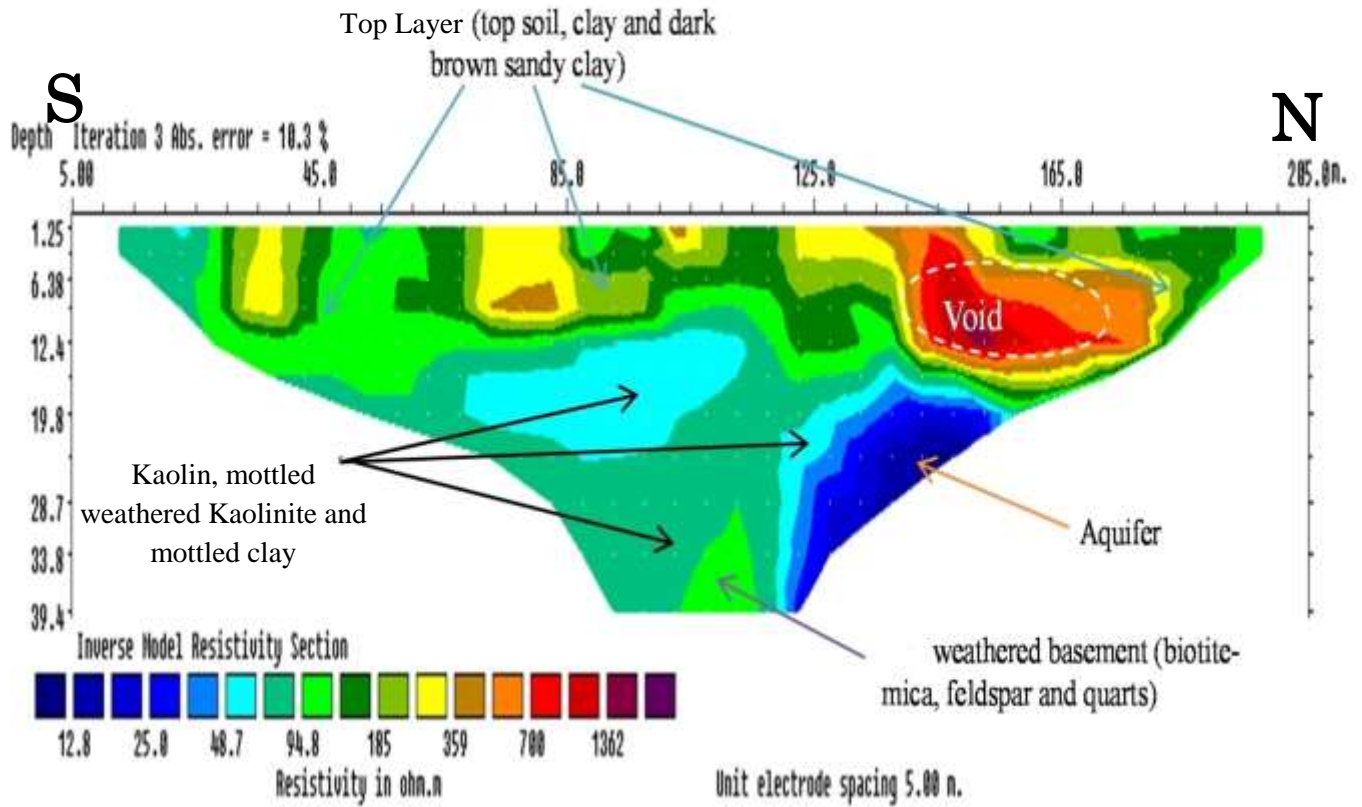


Figure 4.14: Inverse resistivity model of profile 3.

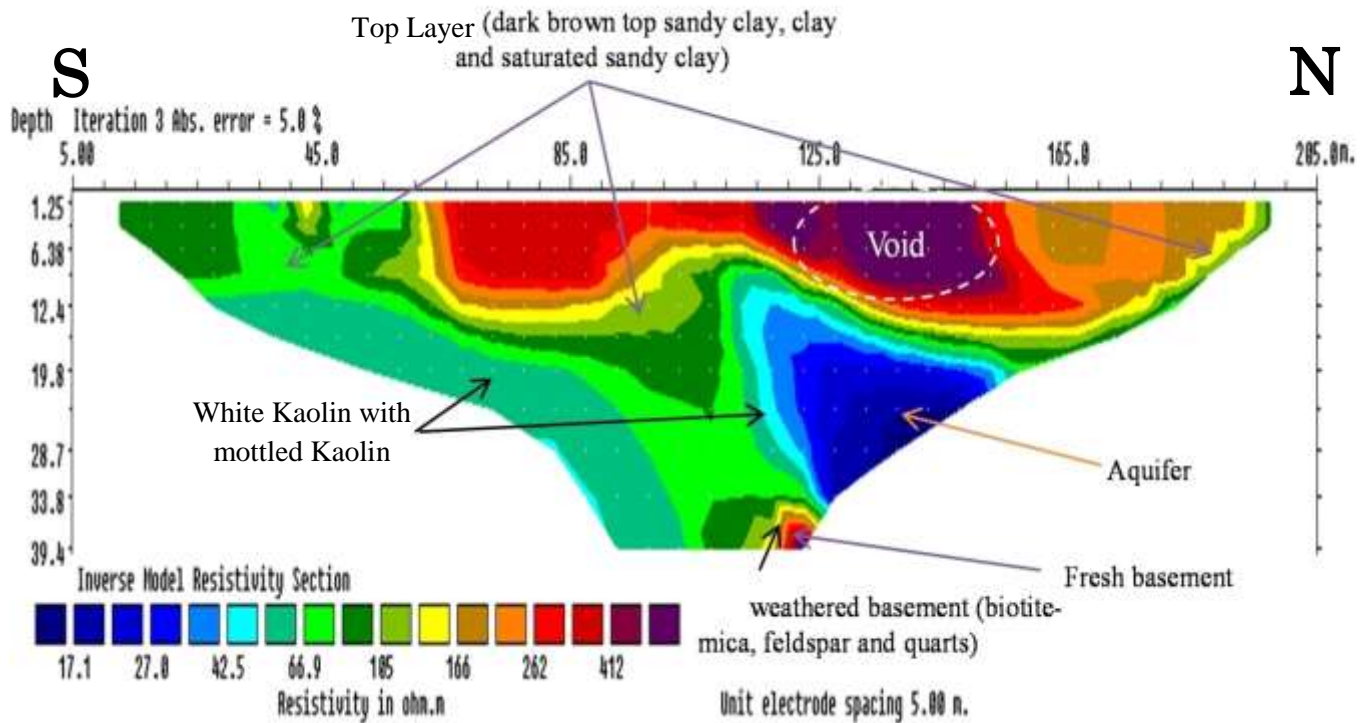


Figure 4.15: Inverse resistivity model of profile 4.

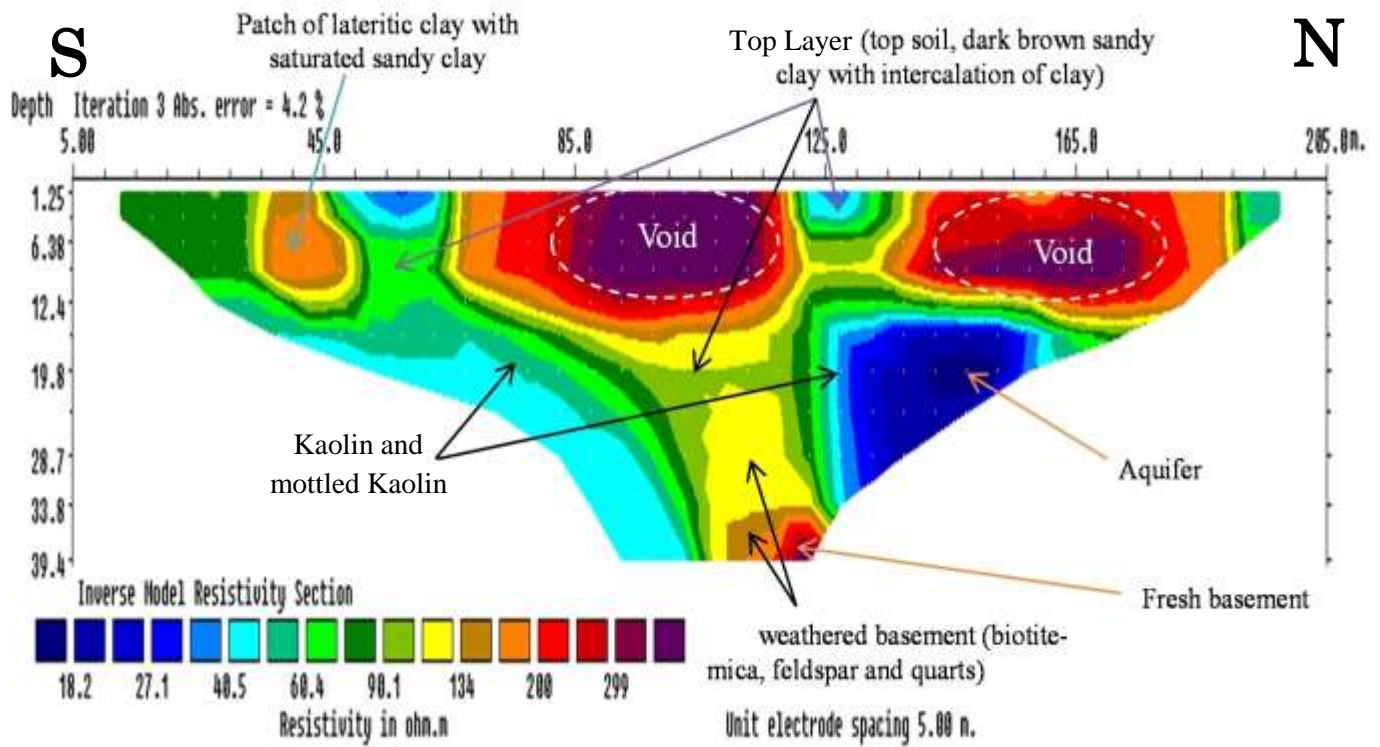


Figure 4.16: Inverse resistivity model of profile 5.

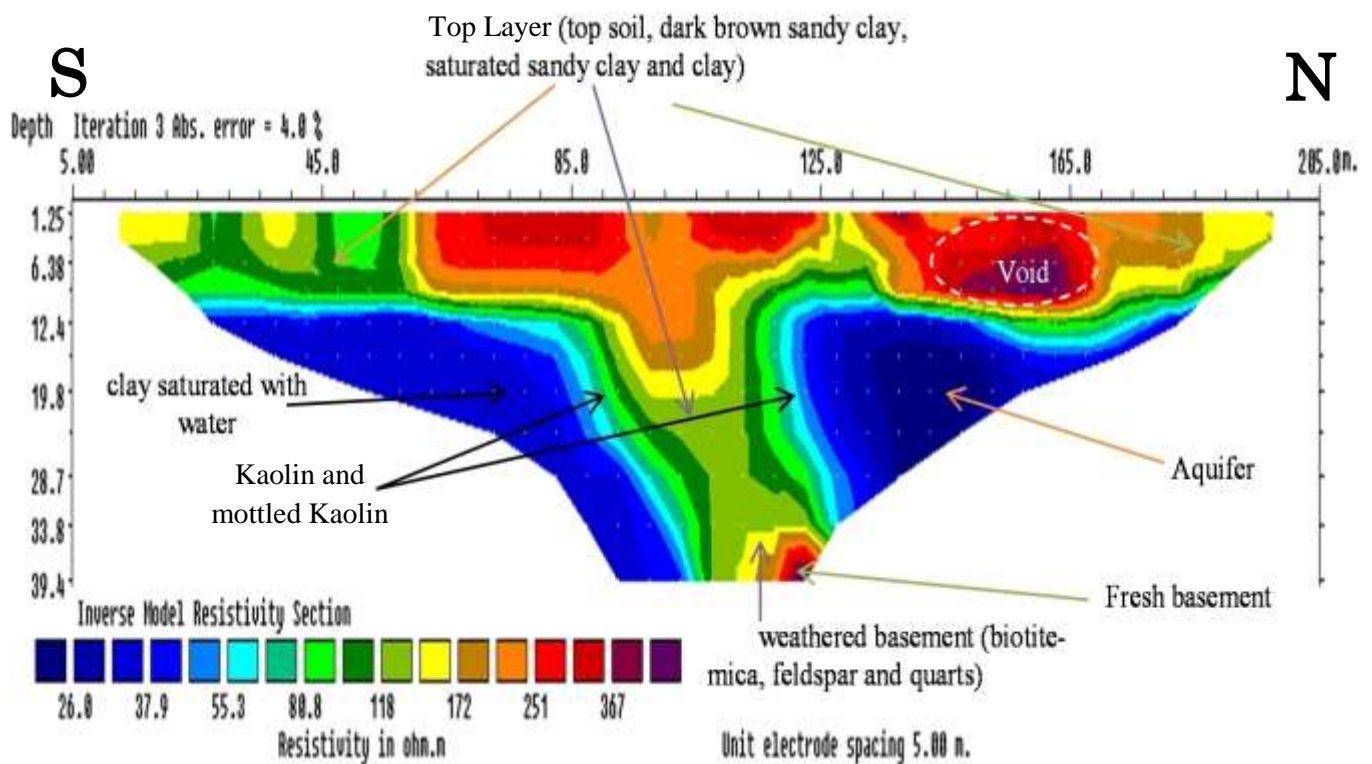


Figure 4.17: Inverse resistivity model of profile 6.

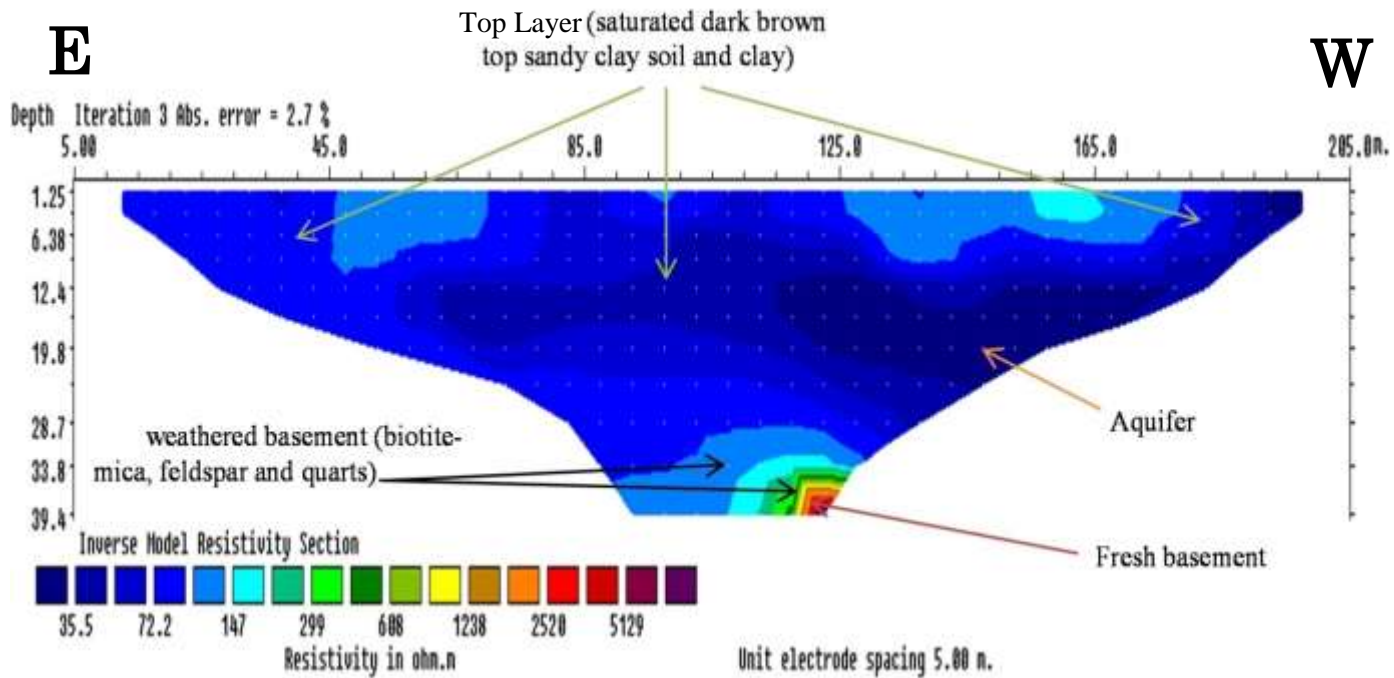


Figure 4.18: Inverse resistivity model of profile 1.

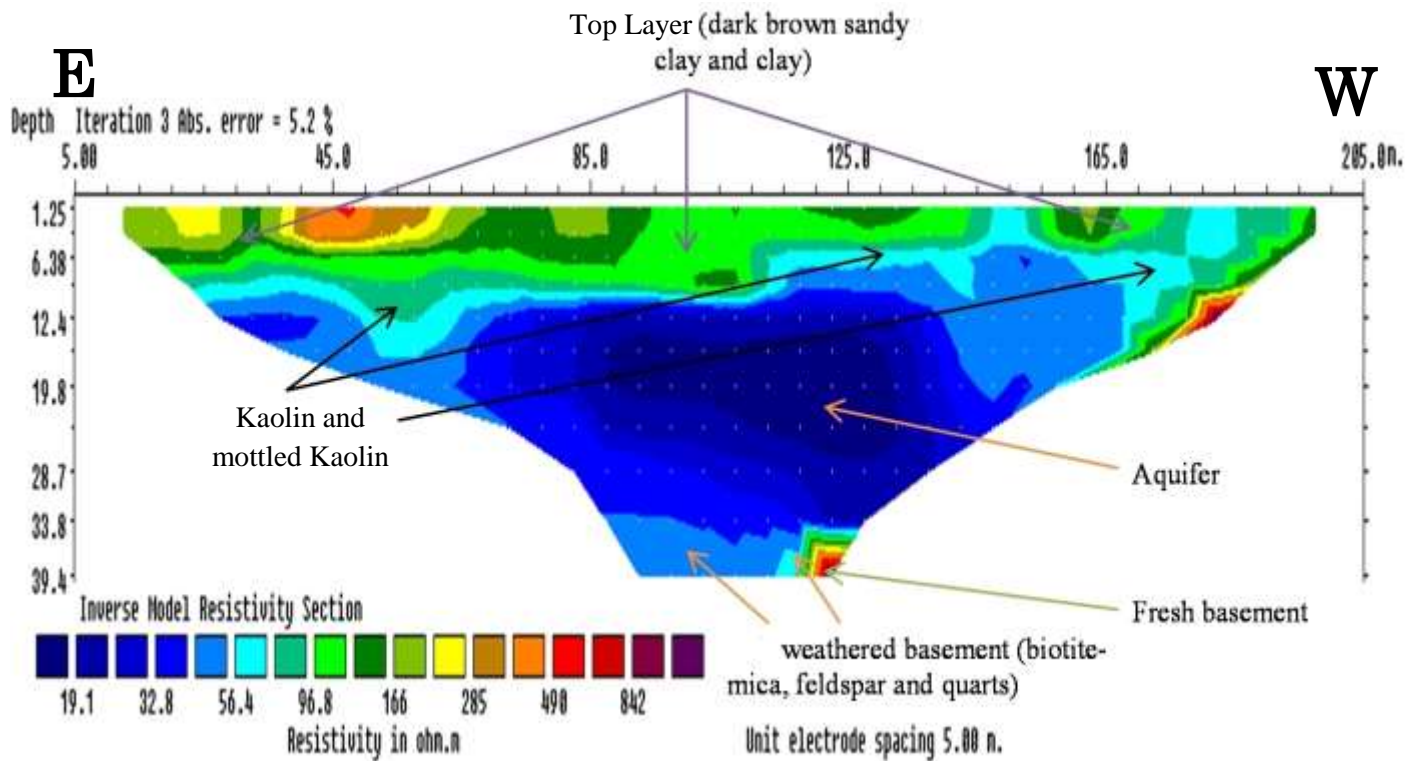


Figure 4.19: Inverse resistivity model of profile 7.

4.8 Vertical Electrical Sounding Results and Discussions

Seven vertical electrical soundings, randomly distributed, were conducted in the study area (Figure 3.6).

4.8.1 Result of VES I

VES I is HH curve type as shown in Figure 4.20, characterized by $\rho_1 > \rho_2 < \rho_3 > \rho_4 < \rho_5$; Table 4.2 shown VES I of result and interpretation with the top soil having 315 Ω m as the resistivity value and thickness of 1.52m; the second layer has a resistivity value of 203 Ω m with a thickness of 2.36m, with sand clay as a possible regolith material. The third layer has a resistivity value of 354 Ω m with a thickness of 6.02m at the depth of 9.90m, which is weathered basement. The fourth layer has a resistivity value of 30 Ω m which may be referred to as the aquiferous layer with thickness of 21.0m and the bottom layer represent the fresh basement with resistivity value of 6013 Ω m having infinite thickness.

Table 4.2: VES I result and interpretation

Layer number	Resistivity (Ω m)	Thickness (m)	Depth (m)	Inferred lithology
1	315	1.52	1.52	Top soil
2	203	2.36	3.88	Sandy clay
3	354	6.02	9.90	Weathered basement
4	30	21.0	31.0	Aquifer
5	949			Fresh basement

whereby,

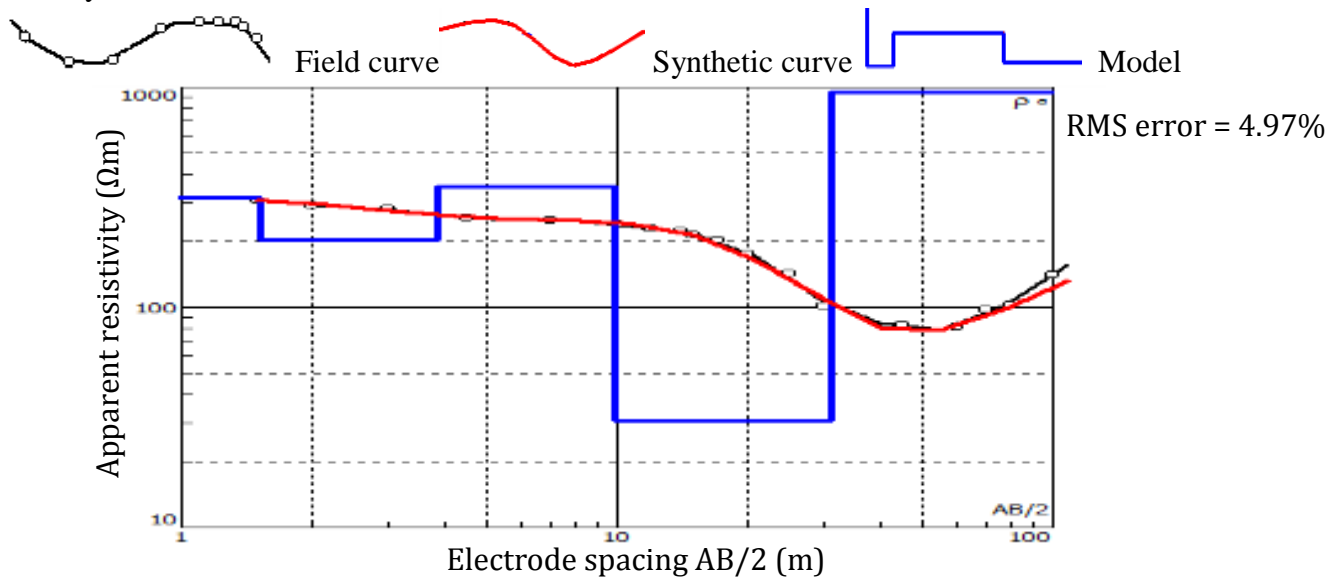


Figure 4.20: Computer iterated curve of VES I.

4.8.2 Result of VES II

VES II is HK curve type as shown in Figure 4.21, characterized by $\rho_1 > \rho_2 < \rho_3 < \rho_4 > \rho_5$; Table 4.3 shown VES II result and interpretation. The first layer having a resistivity value of 186Ωm and a thickness of 2.59m shows the top sandy clay soil; the second layer has a resistivity value of 135Ωm with a thickness of 9.11m at a depth of 11m and is considered as saturated sandy clay. The third layer is a Kaolin layer with a resistivity value of 14Ωm and a thickness of 15.30m and the fourth layer is the weathered basement with a resistivity value of 642Ωm with a thickness 13.20m and the last layer represent the fresh basement rock with infinite thickness.

Table 4.3: VES II result and interpretation

Layer number	Resistivity (Ωm)	Thickness (m)	Depth (m)	Inferred lithology
1	186	2.59	2.59	Top sandy clay
2	135	9.11	11.0	Saturated sandy clay
3	14	15.30	27.00	Kaolin
4	642	13.20	40.00	Weathered basement
5	492			Fresh basement

whereby,

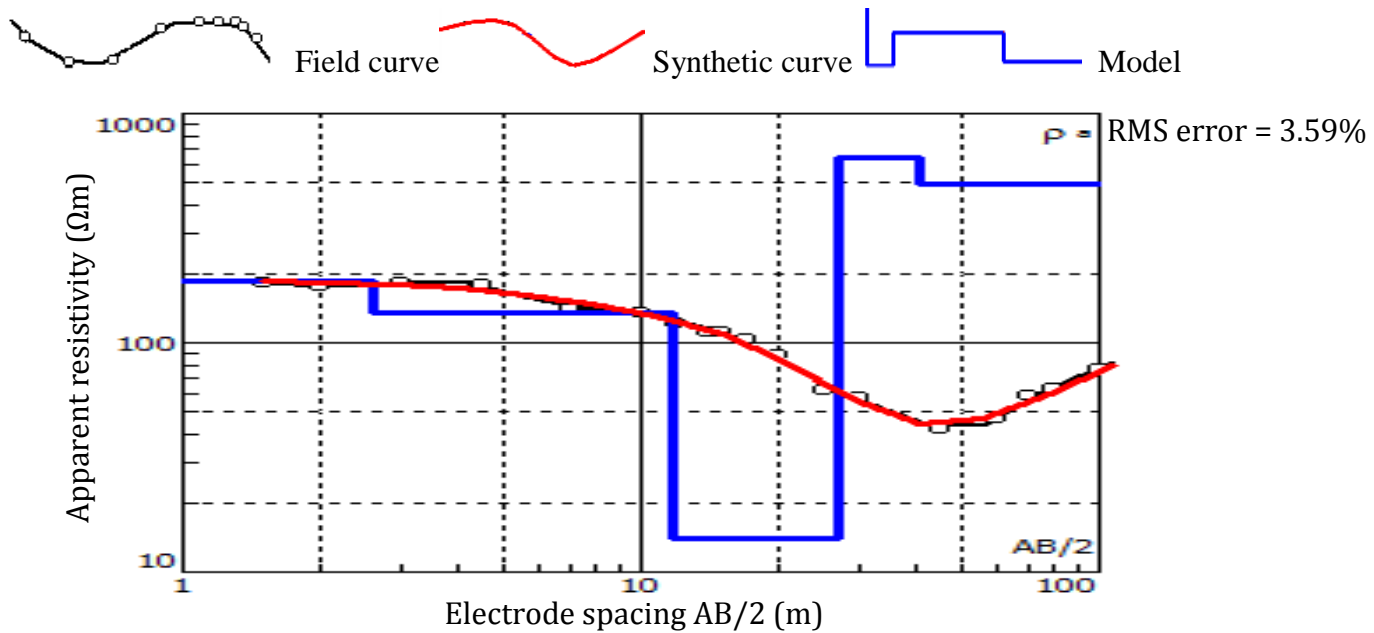


Figure 4.21: Computer iterated curve of VES II.

4.8.3 Result of VES III

VES III is HH curve type as shown in Figure 4.22, characterized by $\rho_1 > \rho_2 < \rho_3 > \rho_4 < \rho_5$ and Table 4.4 shown VES III result and interpretation with top soil being the first layer with resistivity value of 204Ωm and thickness of 1.43m; the second layer has a resistivity value of 156Ωm which shows saturated clayey sand material with a thickness of 2.66m at a depth of 4.09m. The third layer has a resistivity value of 272Ωm (showing a sandy clay material) and a thickness of 4.03m at a depth of 8.12m. The fourth layer has low resistivity value of 11Ωm at a depth 21.83m with thickness of 13.71m, which could be referred to as thick layer of Kaolin and the bottom layer represent the fresh basement rock with very high resistivity value of 925Ωm having infinite thickness.

Table 4.4: VES III result and interpretation

Layer number	Resistivity (Ωm)	Thickness (m)	Depth (m)	Inferred lithology
1	204	1.43	1.43	Top soil

2	156	2.66	4.09	Saturated clayey sand
3	272	4.03	8.12	Sandy clay
4	11	13.71	21.83	Kaolin
5	925			fresh basement

whereby,

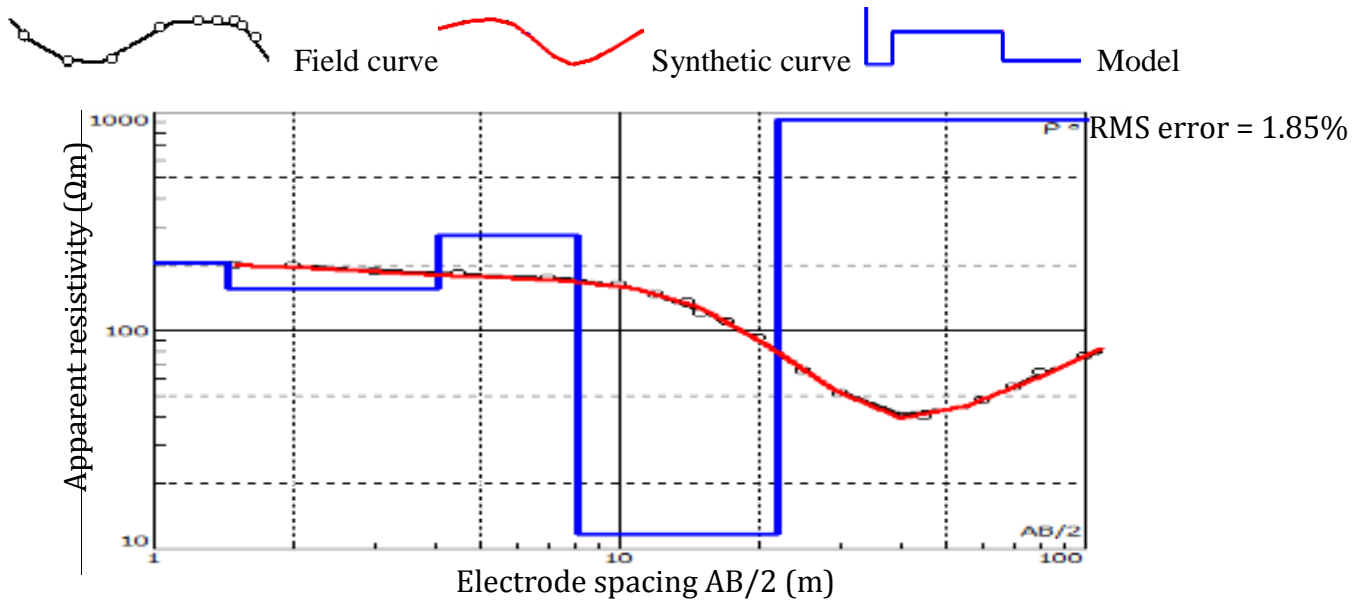


Figure 4.22: Computer iterated curve of VES III.

4.8.4 Result of VES IV

VES IV is HH curve type as shown in Figure 4.23, characterized by $\rho_1 > \rho_2 < \rho_3 > \rho_4 < \rho_5$, where Table 4.5 shown VES IV result and interpretation showing five regolith layers with the first layer being the top soil with a resistivity value of 409Ωm and relative thickness of 1.07m, the second layer with resistivity value of 141Ωm has 2.94m as its thickness and the third layer with resistivity value of 413Ωm, which is the weathered basement of thickness 4.35m. The fourth layer has a resistivity value of 16Ωm (aquiferous layer) with a thickness 16.50m and is good for underground water development. The bottom layer represent the fresh basement with resistivity value of 451Ωm having infinite thickness.

Table 4.5: VES IV result and interpretation

Layer number	Resistivity (Ωm)	Thickness (m)	Depth (m)	Inferred lithology
1	409	1.07	1.07	Top soil
2	141	2.94	4.01	Sandy clay
3	413	4.35	8.36	Weathered basement
4	16	16.50	24.90	Aquifer
5	451			Fresh basement

whereby,

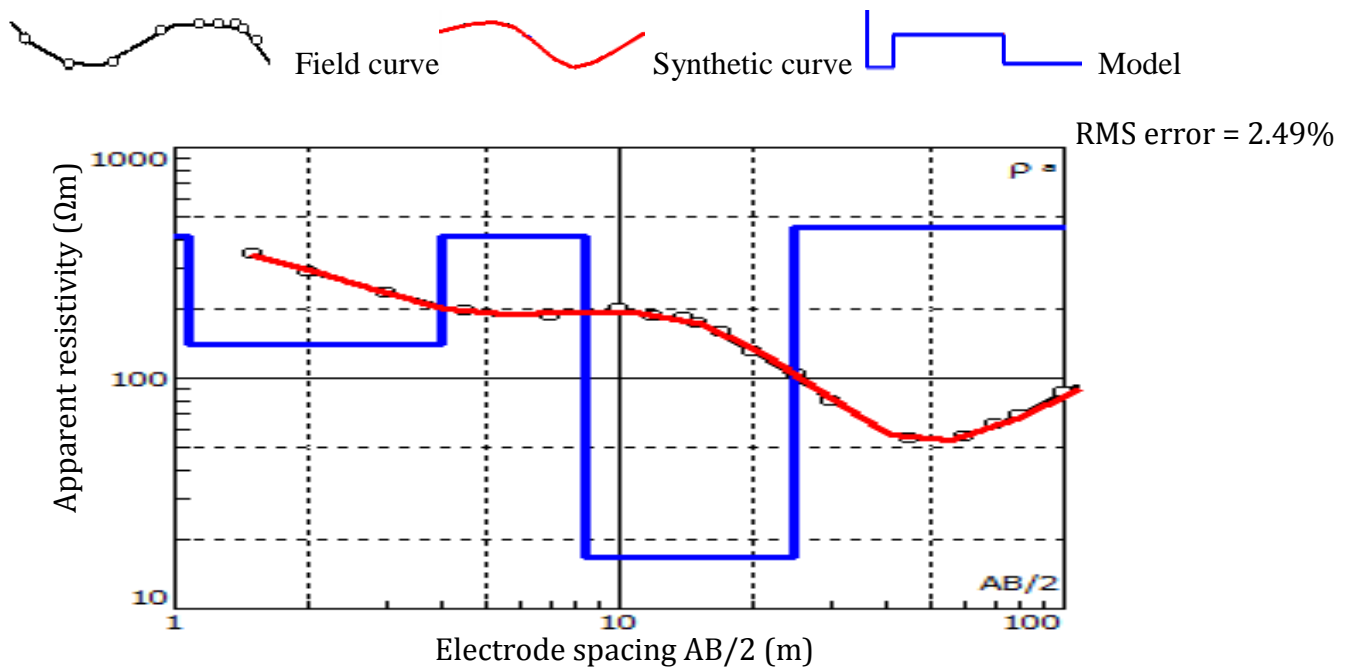


Figure 4.23: Computer iterated curve of VES IV.

4.8.5 Result of VES V

VES V is KAK curve type as shown in Figure 4.24, characterized by $\rho_1 < \rho_2 > \rho_3 < \rho_4 > \rho_5 > \rho_6$; The first layer is the top clay soil with a resistivity value of $4\Omega\text{m}$ and a thickness of 1.17m; the second layer has a resistivity value of $94\Omega\text{m}$ with a thickness of 1.15m at a depth of 2.31m; the third layer is a Kaolin, with a resistivity value of $74\Omega\text{m}$ and a thickness of 4.83m at a depth of 7.14m; the fourth layer is the aquiferous layer with a resistivity value of $83\Omega\text{m}$ with a

thickness of 23.10m. The fifth layer is the weathered basement, with a resistivity value of 93Ωm and a thickness of 9.49m at the depth of 30.20m and the bottom layer represent weathered saturated clay with resistivity value of 3Ωm having infinite thickness. Table 4.6 shown VES V result and interpretation.

Table 4.6: VES V result and interpretation

Layer number	Resistivity (Ωm)	Thickness (m)	Depth (m)	Inferred lithology
1	4	1.17	1.17	Top clay soil
2	94	1.15	2.31	Sandy clay
3	74	4.83	7.14	Kaolin
4	83	23.10	30.20	Aquifer
5	93	9.49	39.70	Weathered basement
6	3			Weathered saturated clay

whereby,

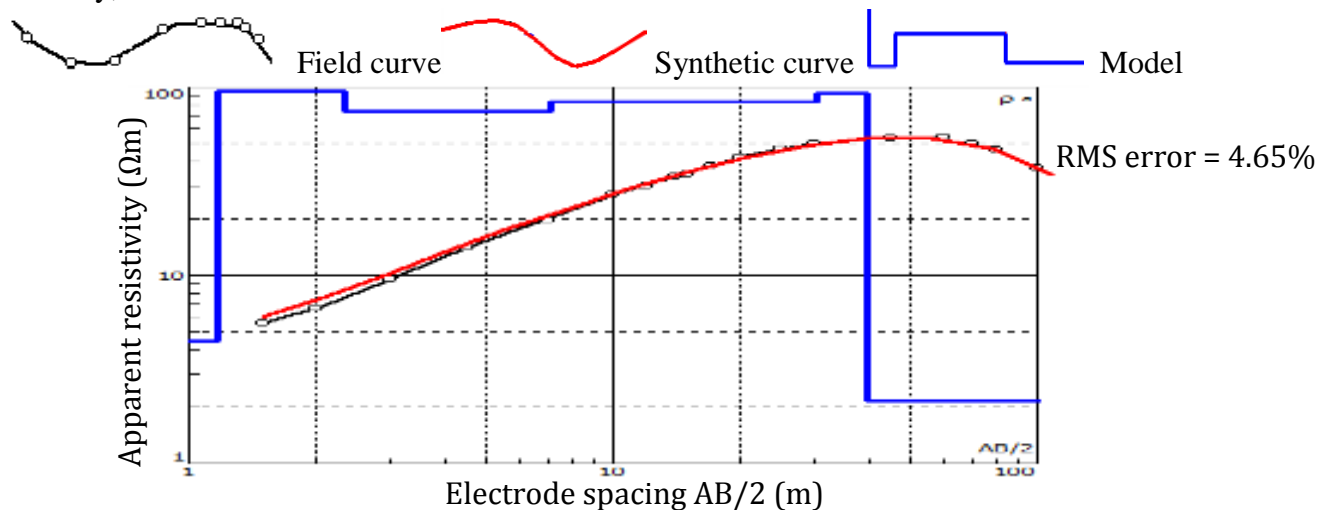


Figure 4.24: Computer iterated curve of VES V.

4.8.6 Result of VES VI

VES VI is HH curve type as shown in Figure 4.25, characterized by $\rho_1 > \rho_2 < \rho_3 > \rho_4 < \rho_5$; where Table 4.7 represent VES VI result and interpretation. The first layer is the top sandy clay soil with resistivity value of 142Ωm and thickness of 1.11m; the second layer with resistivity value of 50Ωm which shown Kaolin material with a thickness of 3.39m at the depth of 4.50m. The

third layer has a resistivity value of 280Ωm showing a weathered basement with a thickness of 3.66m at a depth of 11.80m. The fourth layer has low resistivity value of 30Ωm at the depth 27.50m with thickness of 15.70m, which could be referred to as aquiferous layer and is good for underground water development. The bottom layer represent the fresh basement with resistivity value of 780Ωm having infinite thickness.

Table 4.7: VES VI result and interpretation

Layer number	Resistivity (Ωm)	Thickness (m)	Depth (m)	Inferred lithology
1	142	1.11	1.11	Top sandy clay
2	50	3.39	4.50	Kaolin
3	280	7.32	11.80	Weathered basement
4	30	15.70	27.50	Aquifer
5	780			Fresh basement

whereby,

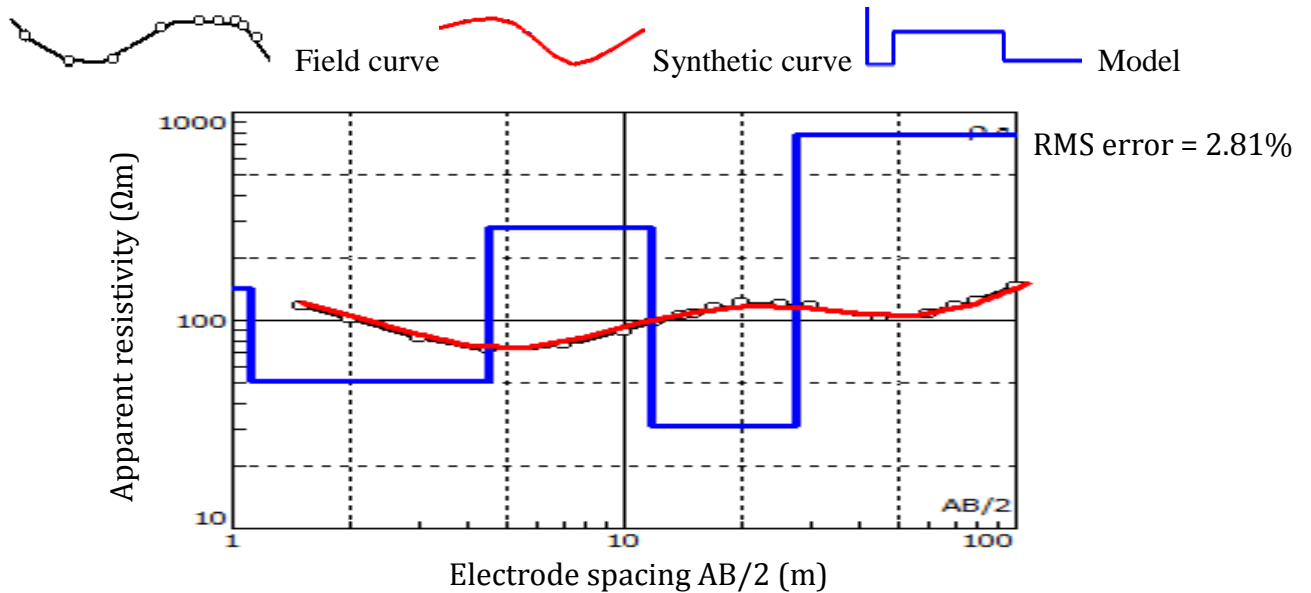


Figure 4.25: Computer iterated curve of VES VI.

4.8.7 Result of VES VII

VES VII is KKH curve type as shown in Figure 4.26, characterized by $\rho_1 < \rho_2 > \rho_3 < \rho_4 > \rho_5 < \rho_6$; where Table 4.8 represent VES VII result and interpretation. The first layer is the top sandy

clay soil with a resistivity value of $206\Omega\text{m}$ and a thickness of 1.17m ; the second layer has a resistivity value of $260\Omega\text{m}$ interpreted as lateritic clay with a thickness of 0.76m , the third layer is the Kaolin, with a resistivity value of $30\Omega\text{m}$ and a thickness of 4.86m at a depth of 6.62m ; the fourth layer is the weathered basement with a resistivity value of $652\Omega\text{m}$ with a thickness of 6.22m . The fifth layer is the aquiferous layer with a resistivity value of $144\Omega\text{m}$ and a thickness of 25.40m at the depth of 38.40m . The bottom layer represent the fresh basement with resistivity value of $702\Omega\text{m}$ having infinite thickness.

Table 4.8: VES VII result and interpretation

Layer number	Resistivity (Ωm)	Thickness (m)	Depth (m)	Inferred lithology
1	206	1.17	1.17	Top sandy clay
2	260	0.79	1.96	Lateritic clay
3	30	4.86	6.62	Kaolin
4	652	6.22	13.00	Weathered basement
5	144	25.40	38.40	Aquifer
6	702			Fresh basement

whereby,

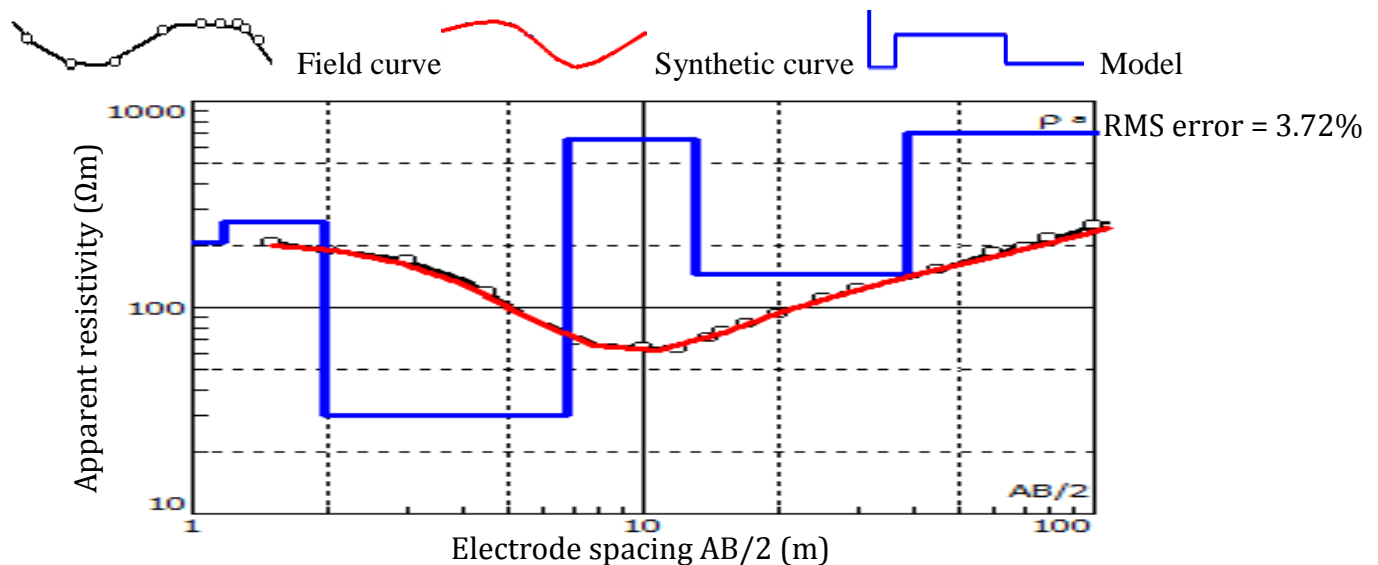


Figure 4.26: Computer iterated curve of VES VII.

4.9 Goelectric section along profile AA'

Figure 4.27 shows goelectric section along profile AA', the VES points in this profile are VES II, VES III, (VES VI)' and VES V. VES point (VES VI)' is projected along the profile AA' as shown by figure 4.27, so that to obtain clear goelectric section.

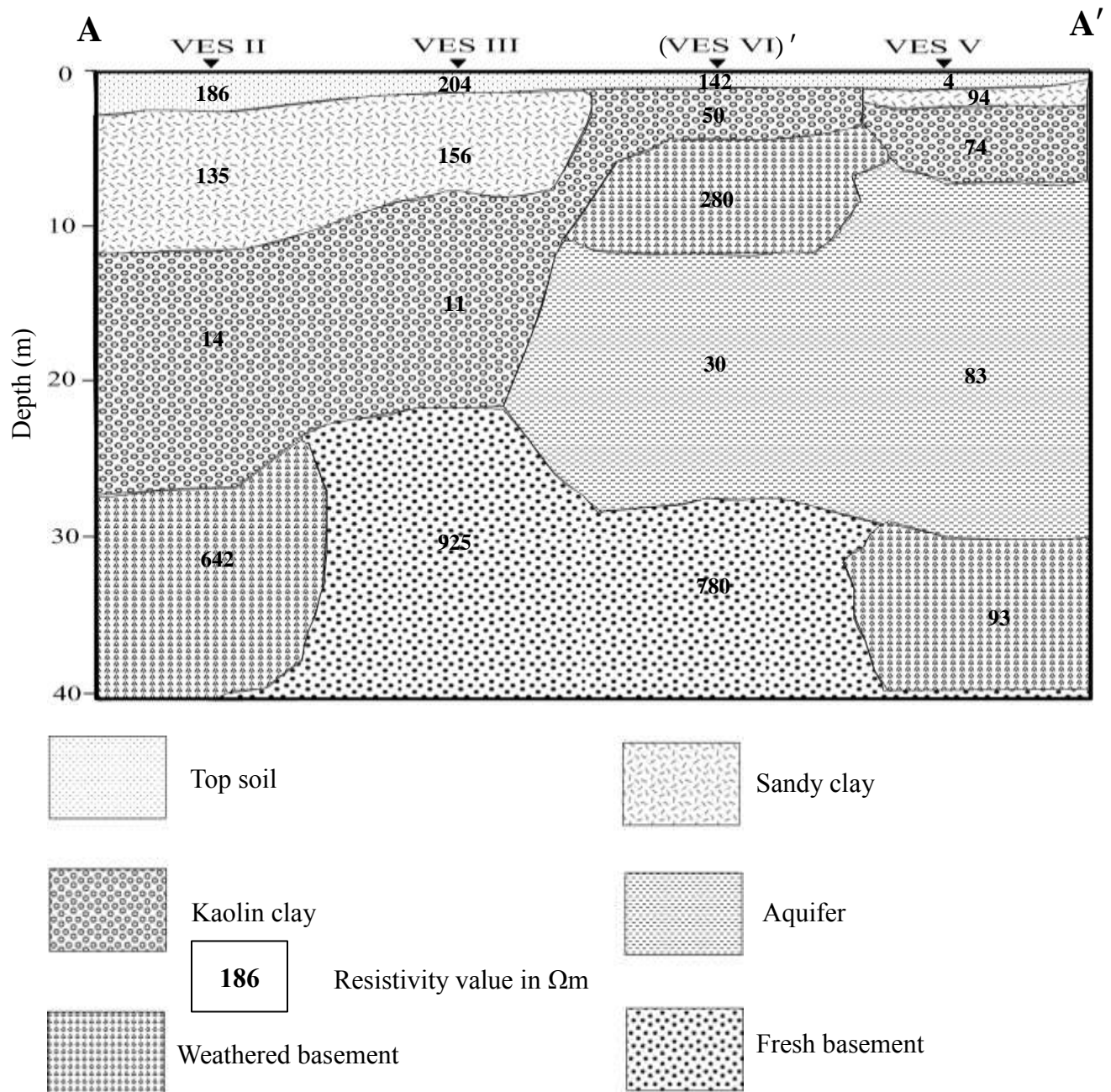


Figure 4.27: Goelectric section of Profile AA' beneath VES II, III, (VES VI)' and V

4.10 Geoelectric section along profile BB'

Figure 4.28 shows geoelectric section along profile BB', the VES points in this profile are VES I, (VES IV)' and VES VII. VES point (VES IV)' is projected along profile BB' as shown by figure 4.28, so that to obtain clear geoelectric section.

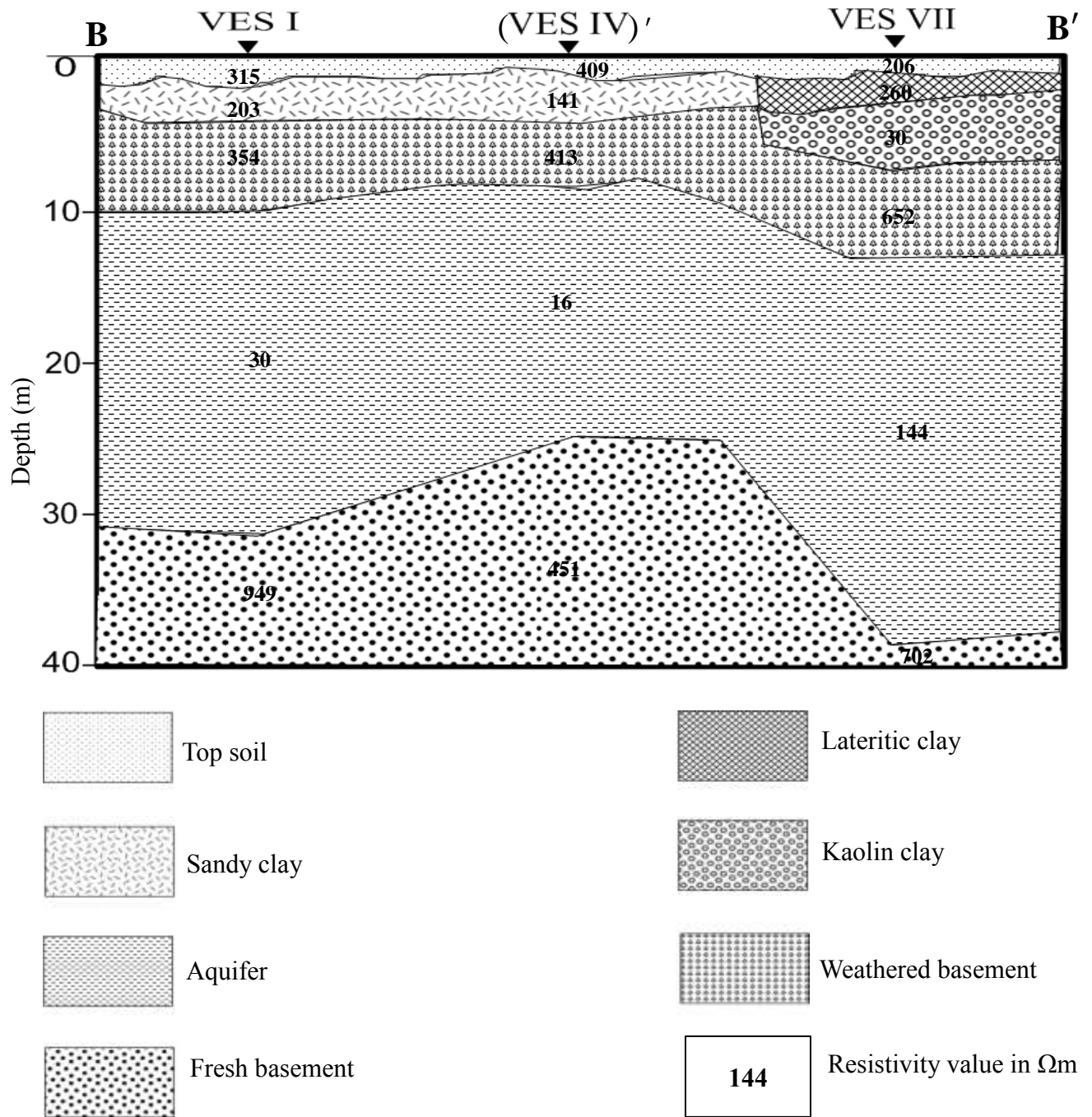


Figure 4.28: Geoelectric section of Profile BB' beneath VES I, (VES IV)' and VII

CHAPTER FIVE:

CONCLUSION AND RECOMMENDATIONS

5.1 Conclusion

A 2-D Electrical resistivity imaging has been successfully carried out at Dajin Gwamna, Kankara Local Government, Katsina State, Nigeria with the aim of delineating the Kaolin deposit. Considering the results of this research, the inversion results of almost the seven profiles revealed three distinct layers ranging from top layer which is made up of mainly dark brown sandy clay, clay, Kaolin and mottled Kaolin; Weathered basement rock which consists of biotite-mica, feldspar and quartz and the fresh basement rock as the third layer. The resistivity models have revealed that there is continuity of Kaolin layers from profiles 2, 3, 4, 5 and 6; the layers of Kaolin in these profiles are extending from east to west direction. But in case of profiles 1 and 7, the model has revealed that there is continuity of Kaolin layers only on profile 7 which is located in the northern part of the survey area. Profile 1 lies in the southern part of the survey area. This means that, the Kaolin layers are extending from east to west and in the north direction within the survey area but not in the south direction. In addition, the layers vary in vertical and horizontal directions with variable thicknesses between 1.25m to 39.40m within the study area with resistivity values between $41\Omega\text{m}$ - $97\Omega\text{m}$. But in case of VES, the results have shown that, the Kaolin which is buried under variable thicknesses at different layers has resistivity values between $11\Omega\text{m}$ - $74\Omega\text{m}$ with variable thicknesses ranging between 3.39m – 15.30m. The results of 2-D and that of VES were correlated, which depicts that Kaolin deposit within the surveyed area has resistivity values between $11\Omega\text{m}$ - $97\Omega\text{m}$. The study also revealed that, the delineated layers of Kaolin were extending from east – west and in the north direction, whereby layers were absent in profile 1 which is located in the southern part of the survey area. It was observed that the

exploration of Kaolin mineral should be targeted trending east, west and also in the northern part of the site. The results obtained from 2-D electrical resistivity imaging and vertical electrical soundings were correlated with the borehole data during interpretation.

5.2 Recommendations

Based on the result of this research, it is recommended that:-

- i. Further investigation based on 2-D resistivity survey should be carried out employing large number value of electrodes so as to have deeper probe of the subsurface (that is, to have clear image of fresh basement rock).
- ii. There is need to carry out 2-D resistivity survey using roll along over a larger area outside the present study area to ascertain the complete lateral extent of the kaolin deposit.
- iii. Self potential (S.P.) and Very Low Frequency (V.L.F.) geophysical methods should be employed massively, because they are cheaper in terms of cost compared to 2-D electrical resistivity imaging.
- iv. A 3-D electrical resistivity survey will give a better image of the volume of the deposit.

REFERENCES

- ABEM Instrument AB. (2010). *Terrameter SAS1000/4000 LUND Imaging System Instruction Manual*. Retrieved from <http://www.abem.se>
- Acworth, R. I. (1987). The Development of Crystalline Basement Aquifers in a Tropical Environment. *Quarterly Journal of Engineering Geology and Hydrogeology*, 20(4): 265-272.
- Adefila, J. O. (2014). Pattern of Agricultural Development in Southern Parts of Katsina State, Nigeria: Notion for Rational Planning, *Journal of Agriculture and Veterinary Science*, 7(1):14-20.
- Adeoye, A. F. (2000). *The Geology and Geochemistry of Ironstone and Kaolin Deposits in Sheet 85 (Udubu), Bauchi State*. An Unpublished M.Sc. Thesis, Department of Geology, Ahmadu Bello University, Zaria.
- Aderiye, J. (2014). Kaolin Mineral Materials for Automobile Ceramic Brake pad Manufacturing Industry. *International Journal of Technology Enhancement and Emerging Engineering Research*, 2: 84-88.
- Adindu, C. I., Moses, J., Thaddeus, C. A., and Tse, D. T. (2014). Exploring Ceramic Raw Materials in Nigeria and their Contribution to Nation's Development. *American Journal of Engineering Research*, 3(9): 128-131.
- Aggarwai, N. (1983). *Application of Geophysical Methods to Delineate Kaolin Deposits and Survey for Groundwater Potentialities at Minjibir, Kano State*. An Unpublished M.Sc. Thesis, Department of Physics, Ahmadu Bello University, Zaria.
- Ajibade, A. C. (1976). *Provisional classification and correlation of the schist belts of northwestern Nigeria*. In: Kogbe C. A. (ed.), *Geology of Nigeria*, Elizabethan Publishing Company, Lagos. pp. 85-90.
- Akhirevbulu, O. E. and Ogunbajo, M. I. (2011). The Geotechnical Properties of Clay Occurrences Around Kutigi, Central Bida Basin, Nigeria. *Ethiopian Journal of Environmental Studies and Management*, 4(1): 25-35.
- Atanda, P. O., Oluwole, O. O., and Oladeji, T. A. (2012). Electrical Porcelain Production from Selected Kaolin Deposit in Southwestern Nigeria Using Slip Casting. *International Journal of Materials and Chemistry*, 2(3): 86-87.
- Ayoade, J. O. (2004). *Introduction to Climatology for the Tropics*. Spectrum Books. Ibadan, pp. 220-230.
- Badmus, B. S., Olurin, O. T., Ganiyu, S. A. and Oduleye, O. T. (2013). Evaluation of Physical Parameters of Various Solid Minerals within Southwestern Nigeria Using Direct Experimental Laboratory Methods. *American International Journal of*

Contemporary Research, 3(3): 152-161.

- Badmus, B. S., and Olatinsu, O. B. (2009). Geophysical Evaluation and Chemical Analysis of Kaolin Clay Deposit of Lakiri Village, Southwestern Nigeria. *International Journal of Physical Sciences*, 4(10): 592-606.
- Benea, M., and Gorea, M. (2004). *Mineralogy and Technological Properties of Some Kaolin Used in the Ceramic Industry*. Studia Universities Babes-bolyai, Geologia, XLIX, pp. 33-39.
- Barker, R. D. (1996). *The Application of Electrical Tomography in Groundwater Contamination Studies*. EAGE 58th Conference and Technical Exhibition Extended Abstracts, P082.
- Batayneh, A. T. (2006). Resistivity Tomography as an Aid to Planning Gas-pipeline Construction, Risha Area, North-East Jordan. *Near Surface Geophysics*, 4: 313-319.
- Bowers, T. S., Jackson, K. J. and Helgeson, H. C. (1984). *Equilibrium Activity Diagrams*. Springer-Verlag Berlin, pp. 397.
- Brindley, G.W. (1951). *The X-Ray Identification and Crystal Structures of Clay Minerals*. Chapter 11, Mineralogical Society, London.
- Cardarelli, E. and Fischanger, F. (2006). 2D Data Modelling by Electrical Resistivity Tomography for Complex Subsurface Geology. *Geophysical Prospecting*, 54: 121-133.
- Christensen, N. B. and Sorensen, K. I. (1994). *Integrated use of Electromagnetic Methods for Hydrogeological Investigations*. Proceedings of the Symposium on the Application of Geophysics to Engineering and Environmental Problems, March 1994, Boston, Massachusetts, pp. 163-176.
- Commission, E. (2007). *Ceramic Manufacturing Industry*. Reference document on Best Available Techniques in the Ceramic Manufacturing Industry, European Commission, Institute for Prospective Technological studies, Seville, August 2007.
- Dahlin, T. (1996). 2D Resistivity Surveying for Environmental and Engineering Applications. *First Break*, 14: 275-284.
- Dahlin, T. (2001). The Development of Electrical Imaging Techniques, *Computers and Geosciences*, 27(9): 1019-1029.
- Dott, R. H. and Batten, R. L. (1976). *Evolution of the earth*, Second edition, McGraw-Hill, ISBN 0070176191, New York, pp. 504.

- Dahlin, T. and Owen, R. (1998). *Geophysical Investigations of Alluvial Aquifers in Zimbabwe*. Proceedings of the IV Meeting of the Environmental and Engineering Geophysical Society (European Section), September 1998, Barcelona, Spain, pp. 151-154.
- Edwards, L. S. (1977). A Modified Pseudosection for Resistivity and Induced Polarization. *Geophysics*, 42: 1020-1036.
- Egbai, J. C. (2011). Vertical Electrical Sounding for the Investigation of Kaolin Deposits in Ozanogogo Area of Ika South Local Government Area of Delta State, *Nigeria. Journal of Emerging Trends in Engineering and Applied Sciences*, 2(1): 147-151.
- Egbai, J. C. (2013). Kaolin Quantification in Ukwu Nzu and Ubulu Uku using Electrical Resistivity Method. *International Journal of Review in Applied and Social Sciences*. 14: 692-693.
- Elueze, A. A., Bakare, C. A., and Bolarinwa, A. T. (2004). Mineralogical, Industrial and Chemical Characteristics of Residual Clay Occurrences in Iwo and Ijebu Districts, Southwestern Nigeria. *Journal of Mining & Geology*, 40(2): 119-126.
- Griffiths, D. H. and Barker, R. D. (1993). Two-Dimensional Resistivity Imaging and Modelling in Areas of Complex Geology. *Journal of Applied Geophysics*, 29: 211-226.
- Johansson, S. and Dahlin, T. (1996). Seepage Monitoring in an Earth Embankment Dam by Repeated Resistivity Measurements. *European Journal of Engineering and Geophysics*, 1(3): 229-247.
- Kankara, I. A. and Farouk, H. A. (2015). Provisional Dating of Metasedimentary Rocks in South Katsina State, Northwestern Nigeria: Studies in Proterozoic Crustal Evolution. *Journal of Physical Science and Environmental Studies*, 1(4): 55-61.
- Kaolin Uses, Benefits and Dosage (2010). Retrieved from <http://www.drugs.com>
- Kean, W. F., Muriel, J. W. and Richard, L. H. (1987). Monitoring Moisture Migration in the Vadose Zone with Resistivity. *Groundwater*, 25(5): 562-571.
- Keller, G. V. and Frischknecht, F. C., (1966). *Electrical Methods in Geophysical Prospecting*. Pergamon Press, London.
- Konta, J. (1995). Clay and Man: Clay Raw Minerals in the Service of Man. *Applied Clay Science. Elsevier*, 10(4): 269-335.
- Koefoed, O. (1979). *Geosounding Principles, 1: Resistivity Sounding Measurements*. Elsevier Science Publishing Company, Amsterdam.

- Lohva, J. and Lehtimäki, J. (2005). Geophysical Investigation of Kaolin and Ilmenite Deposits in Finland. *Geological Survey of Finland, Special Paper 39*, pp. 147-154.
- Loke, M. H. (1999). *Electrical Imaging Surveys for Environmental and Engineering Studies; A Practical Guide to 2-D and 3-D Surveys*. Self Published Note Book, pp. 15-57.
- Loke, M.H. (2001). *Tutorial: 2-D and 3-D Electrical Imaging Surveys*. Retrieved from <http://www.geotomosoft.com>
- Loke, M. H. (2004). *Tutorial: 2-D and 3-D Electrical Imaging Surveys*. Retrieved from <http://www.goelectric.com>
- Loke, M.H. (2014). *Tutorial: 2-D and 3-D Electrical Imaging Surveys*. Retrieved from <http://www.geotomosoft.com>
- Loke, M. H. and Barker, R. D. (1996). Rapid Least-Squares Inversion of Apparent Resistivity Pseudosections Using a Quasi-Newton Method. *Geophysical Prospecting*, 44: 131-152.
- Malu, S. P., and Babson, A. (2007). Producing Insulating Refractory Bricks with Kaolin and Sawdust. *Journal of Engineering and Applied Sciences*, 2(12): 1697-1699.
- McGinnis, L. D. and Jensen, T. E. (1971). Permafrost-hydrogeologic Regimen in Two Ice-free Valleys, Antarctica, from Electrical Depth Sounding. *Quaternary Research*, 1(3): 389- 409.
- Michael, E. E. (1977). *Geophysical Exploration for Buried Kaolin Mineral near Kankara, Katsina Province, Katsina State, Nigeria*. Unpublished M. Sc. Thesis, Department of Physics, Ahmadu Bello University, Zaria.
- Mode, A. W., and Amobi, J. O. (2006). Geochemistry of Clays and their Applications in the Ceramics Industry. *Ashaku Journal of Ceramics*, 3: 85 - 96.
- Mosuro, G. O., Bayewu, O. O., and Oloruntola, M. O. (2011). Application of Geophysical and Geostatistical Methods in the Estimate of Clay Deposit Reserve of Idofe and Environs, Southwestern Nigeria. *Mineral Wealth*, 160: 41-48.
- Murray, H. H. (2010). Industrial Application of Kaolin. *Tenth National Conference on Clays and Clay Minerals*. New Jersey: Georgia Kaolin Company, pp. 233-295.
- Obaje, N.G. (2009). *Geology and Mineral Resources of Nigeria*, Lecture Notes in Earth Sciences, Springer-Verlag Berlin Heidelberg, New York, pp. 144-148.
- Ogundana A.K., Olutomilola O. O., Okunade A., and Aladesanmi A.O.(2015). Geophysical Evaluation of Lateral Continuity of some part of Ikere Kaolin Deposit, Southwestern Nigeria. *The International Journal of Engineering And*

Science, 4(11): 71-79.

Oldenburg, D.W. and Li, Y. (1999). Estimating Depth of Investigation in D.C. Resistivity and IP surveys. *Geophysics*, 64(2): 403- 416.

Oyeka, A. N. (1976). Report on Kankara Kaolin deposits, Kankara, Katsina Province, North Central State with notes on Marble Occurrence. *Geological Survey of Nigeria*, Unpublished Report No. 1529.

Pazdirek, O. and Blaha, V. (1996). *Examples of Resistivity Imaging Using ME-100 Resistivity Field Acquisition System*. 58th Conference and Technical Exhibition Extended Abstract Amsterdam, pp. 5-20.

Pfannkuch, H. (1969). On the Correlation of Electrical Conductivity Properties of Porous Systems with Viscous Flow Transport Coefficients. In Inter-national Association of Hydraulic Research, ed., *Fundamentals of Transport Phenomena in Porous Media*, 1972. *Elsevier*, pp. 45-54.

Reynolds, J. M. and Paren, J. G. (1980). Recrystallization and the Electrical Behaviour of Glacier Ice. *Nature*, 283(5742): 63- 64.

Reynolds, J. M. and Paren, I. G. (1984). Electrical Resistivity of Ice from the Antarctic Peninsula. *Journal of Glaciology*, 30(106): 289-295.

Reynolds, J. M. (1987). The Role of Surface Geophysics in the Assessment of Regional Groundwater Potential in Northern Nigeria. In: Cuishaw, M.G., Bell, F.G., Cripps, J.e. and O'Hara, M. (eds), *Planning and Engineering Geology*, Geological Society Engineering Group Special Publication no. 4: 185-190.

Ritz, M., Parisot, J. C., Diouf, S., Beauvais, A. and Dione, F. (1999). Electrical Imaging of Lateritic Weathering Mantles over Granitic and Metamorphic Basement of Eastern Senegal, West Africa. *Journal of Applied Geophysics*, 41: 335-344.

Runge, I. C. (1996). *Mining Economics and Strategy*. Edited by Andrew Mular, Doug Halbe and Derek Barratt, Society for Mining, Metallurgy and Exploration Inc. (SME), Littleton USA, New York, USA.

Rural Water Supply and Sanitation Agency (RUWASSA), Katsina State (2014). National Borehole Reporting Format. Borehole Number, E-18, E-20.

Talabi, A.O., Ademilua, O.L., and Akinola, O. O. (2012). Compositional Features and Industrial Application of Ikere Kaolinite, Southwestern Nigeria. *Research Journal in Engineering and Applied Sciences*, pp. 328-329.

Telford, W. M., Geldart, L. P. and Sheriff, R. E. (1990). *Applied Geophysics*, Second Edition, Cambridge University Press, London, pp. 522-525.

Udo, R. K. (2001). *Geographical Regions of Nigeria*. Oxford University Press, Ibadan.

Vogley, A. W. (1985). *Economics of the Mineral Industries*. American Institute of Mining, Metallurgical and Petroleum Engineers, Inc., New York, USA.

Zoltan, A., Fodor, J., and Williams, R. B. (2005). *Environmental Health Criteria for Bentonite, Kaolin, and Selected Clay Minerals*. International Labour Organization, and the World Health Organization. Library Cataloguing-in-Publication Data, pp. 23-25.